מכון ויצמן למדע
WEIZMANN INSTITUTE OF SCIENCE

Thesis for the degree
Doctor of Philosophy

חבור לשם קבלת התואר
דוקטור לפילוסופיה

By
Javier G. Groshaus

מאת
חביאר גרוסהאוס

ספקטרום הבליעה של מערכת אלקטרונים דו-מימדית בשדה מגנטי בטמפרטורות נמוכות

Low Temperature Absorption Spectroscopy of a 2D Electron System in Magnetic Field

Regular Format

Advisor:
Prof. Israel Bar-Joseph

מנחה:
פרופ' ישראל בר-יוסף

March 2006

אדר תשס"ו

Submitted to the Scientific Council of the
Weizmann Institute of Science
Rehovot, Israel

מוגש למועצה המדעית של
מכון ויצמן למדע
רחובות, ישראל

Abstract

In this work we develop a photocurrent technique in order to study the low temperature optical interband absorption spectrum of a two dimensional electron system in back-gated GaAs quantum wells in perpendicular magnetic fields.

Focusing on the absorption spectrum in the lowest Landau Level around filling factor $\nu = 1$, we find that the spectrum consists of bound electron-hole excitonic states, trion and exciton like. We show that their oscillator strength is a powerful probe of the 2DES spatial correlations. We present a quantitative model in order to explain the results. The analysis shows that near $\nu = 1$ the ground state of the electron system consists of Skyrmions of small size (a few magnetic lengths).

When focusing on the spectra in the range $0 < \nu < 1$ at very low temperatures in a dilution fridge, we find that the oscillator strength of the peak associated with the singlet trion is very sensitive to the temperature, the density and the filling factor. We propose that the oscillator strength of this absorption, and in particular the dichroism of the trion absorption can be used to probe the spin polarization of the 2DES. We present a quantitative model that relates the dichroism of the trion absorption to the spin polarization. The analysis of the dichroism leads to the following conclusions: as ν is increased above 1/3, the system undergoes a spin depolarization, and a partially spin-polarized phase develops around $\nu = 2/3$. This phase is observed for a range of magnetic fields of over 2 Tesla, and it is possibly due to the formation of spacial magnetic domains.

תקציר

בעבודה זו, אנו מפתחים שיטה על בסיס פוטו-זרם על מנת לחקור את ספקטרום הבליעה של מערכת אלקטרונים דו-מימדיים בשדה מגנטי בטמפרטורות נמוכות.

בהתמקד על ספקטרום הבליעה ברמת לנדאו הנמוכה בסביבת גורם המילוי $\nu=1$, נמצא כי הספקטרום מורכב מצבים קשורים לחור דמויי טריאון ואקסיטון. אנו מראים כי חוזק הבליעה שלהם מהווה למעשה חיישן רב עוצמה הרגיש ליחסי הגומלין המרחביים בין האלקטרונים. אנו מציגים מודל כמותי על מנת להסביר את התוצאות. האנליזה מראה שבסביבת $\nu=1$, מצב היסוד של מערכת האלקטרונים מורכב מסקירמיונים מגודל זעיר (כמה פעמים אורך המגנטי).

בהתמקד על ספקטרום בתחום $0<\nu<1$ בטמפרטורות נמוכות מאוד במקרר חמהיל, נמצא כי חוזק הבליעה של הפיק המזוהה עם הטריאון הסינגלט הוא מאוד רגיש לטמפרטורה, לצפיפות האלקטרונים ולגורם המילוי. אנו מצעים כי ניתן להשתמש בדיכרויזם הבליעה של הטריאון לצורך מדידת קיטוב הספין של האלקטרונים. אנו מציגים מודל כמותי המקשר בין דיכרויזם הבליעה של הטריאון לקיטוב הספין של האלקטרונים. האנליזה מובילה למסקנות הבאות: כאשר ν גדל מעל 1/3, מידת קיטוב הספין קטנה, ובסביבת $\nu=2/3$ מתפתחת פזה בעלת קיטוב חלקי. פזה זו נצפתה עבור תחום של שדות מגנטיים המשתרע על 2.25 Tesla. ייתכן כי פזה זו מאופיינת ע"י אזורים מגנטיים מרחביים.

Acknowledgments

I would like to thank foremostly my advisor Prof. Israel Bar-Joseph for his guidance, support, for his all encompassing teachings, his involvement, his readiness to offer advice and untired availability for discussion, for introducing me to an exciting branch of condensed matter physics, to the community, to people and great opportunities, for his help with his insight and in the practical daily work in the experimental and theoretical research and in the organizational, financial, logistic and interpersonal coordination domains, and for his help with the preparation of all reports and manuscripts including this thesis. I would like to thank also my collaborators in the department for their help and advice, including staff members and students whose collaboration consisted mainly in contributing to the great atmosphere of community in the department. Here is only a partial list of them, in an order fairly chronological (not by merit): Maxim Khodas, Prof. Moti Heilblum, Prof. Eli Zeldov, Prof. Alexander Finkelstein, Go Yusa, Yossi Yayon, Michal Avinun, Hadas Shtrikman, Vladimir Umansky, Michael Rappaport, Michael Shneidermann, Olga Raslin, Diana Mahalu, Yoram Rotblat, Yossi Rolnik, Roby Tsabary, Mira Parente, Tomer Hansen, Merav Dolev, Eran Ginossar, Rafi Bistritzer, Eytan Grosfeld, Eran Sela, Eros Mariani, Oren Zarchin, Jens Martin, Soenke Groth, Hadar Steinberg, Prof. Yehoshua Levinson, Michael Stern, Paulina Płochocka, Tali Dadosh and Yoav Gordin. I would like also to thank my collaborators in Lucent Bell-Labs: Brian Dennis, Loren Pfeiffer, Ken West and Aron Pinczuk. I also would like to thank people that reminded me there is an outside world outside the department, to my supporting and loving family, my parents and sister, and also my dear friends. I close by thanking my beloved wife Dvira Segal for her love and support, and for her fruitful collaboration with the creation operator and time propagator of our beloved son Arbel.

Contents

Chapter 1

Introduction

1.1 Motivation

In this research, we study the low temperature optical interband absorption spectrum of a two dimensional electron system (2DES) in GaAs quantum wells (QWs) in a perpendicular magnetic field (B). Since the discovery of the Fractional Quantum Hall Effect (FQHE) [Stormer *et al.*, 1999, Tsui *et al.*, 1982], it became clear that the Coulomb interactions between the electrons play a major role in the macroscopic properties of this system. Theses interactions are manifested not only in the transport properties, but also in the optical spectrum. The absorption spectrum can be a powerful tool to probe the ground state of the 2DES that is present in the system prior to illumination. Indeed, the electron-electron spacial correlations and the average spin polarization of the system, $\mathcal{P}$, have been probed by absorption spectroscopy [Aifer *et al.*, 1996, Astakhov *et al.*, 2000, Huard *et al.*, 2000, 1998, Lematre *et al.*, 2000, Plochocka *et al.*, 2004, Yusa *et al.*, 2000].

The electron-electron Coulomb interactions play a major role in determining $\mathcal{P}$. This is most readily seen in the regime where the Landau degeneracy exceeds the number of electrons, namely in the filling factor range $\nu \leq 1$, where there is no phase space limitation on occupying only lowest Zeeman states, $|\uparrow\rangle$, in the lowest Landau level. In this regime, in an independent

particle picture the ground state of the system is fully spin-polarized: it consists of electrons occupying states only at the lowest Zeeman level $|\uparrow\rangle$ in the lowest Landau Level (LLL). On the other hand, in the presence of interactions the ground state of the 2DES is a result of minimizing the Coulomb (direct and exchange terms) and Zeeman energies. The exchange term favors a spatially antisymmetric wavefunction, and thus a fully polarized ground state. However, such antisymmetric wavefunction may not constitute in general an optimal spatial electron distribution that minimizes the direct term [1]. Hence, if the Zeeman energy is small enough, the ground state may include a spatially symmetric component, resulting in spin depolarization.

An example of a system where $\mathcal{P}$ is dominated by the interactions is the 2DES near $\nu = 1$, i.e. $\nu = 1 - \epsilon$. In this regime, experiments have shown that the 2DES exhibits a strong depolarization as ν is tuned away from 1 [Aifer *et al.*, 1996, Barrett *et al.*, 1995, Schmeller *et al.*, 1995]. This behavior is understood [Fertig *et al.*, 1994, Sondhi *et al.*, 1993] as due to the formation of spin-textures or Skyrmions. The depolarization is due to electrons flipping their spins in order to minimize their energy.

The suitability of absorption spectroscopy techniques for probing $\mathcal{P}$ can be understood as follows. In the interband absorption process, an optical transition connects the 2DES initial ground state to a final state in which a photoexcited valence hole and a conduction electron are added to the 2DES. Since photon absorption is an instantaneous process, it can provide information on the states of the system before any relaxation process takes place. According to the Fermi Golden Rule, the probability for absorption is proportional to the phase space available in the final state [2]. In brief, the result is that the absorption is weak when the final states are highly occupied, and is strong when this states are empty. Therefore the absorption provides straightforward information on the states occupation. Hence, by studying the circular dichroism of the absorption we can probe different spin-levels and obtain the spin polarization of the ground state of the 2DES.

Application of the Fermi Golden Rule within a simplified picture of non-interacting electrons fails to account for the strong interactions of the electrons with the valence hole. At low electron

[1] This somewhat simplified explanation should be understood within the context of the Hartree-Fock mean field picture.

[2] The formalism of the absorption in the Fermi Golden Rule framework will be explained in more detail in Section 1.2.3.

densities ($n_e < 10^{10}$ cm^{-2}), it is well established that the spectrum is dominated by a neutral exciton (X) and a negatively charged exciton or trion (T) [Kheng *et al.*, 1993], [Finkelstein *et al.*, 1995, Wojs and Hawrylak, 1995, Wojs *et al.*, 2000, Yusa *et al.*, 2001] [3]. In this work, we have developed an approach that allows us to model and interpret the absorption spectrum in the Quantum Hall Effects regimes. Our model takes into account the Coulomb interactions between the electrons and the valence hole and also between the electrons in the initial ground state and final states (namely, the states prior to absorption, and photoexcited states, respectively).

Current techniques for measuring absorption present several difficulties [4]. We have developed an alternative approach for obtaining the absorption spectrum by measuring the photocurrent (PC) spectrum. We measure the PC flowing between a single QW and a back gate. This allows a background-free, low noise measurement. This also allows measurement at very low illumination intensity (of the order of $\sim 10^{-6}$ μW/cm^2), which is a great advantage specially when measuring in dilution refrigerators where heating should be minimized. Another advantage is that by using a gate, we can not only tune the magnetic field but also the density of electrons.

1.2 Optical properties and hole bound excitonic complexes

In this section, we review the interband optical properties of the 2DES, with emphasis on the effect of Coulomb interactions on the spectrum.

1.2.1 The optical spectrum in the presence of a 2D Fermi sea of electrons at zero magnetic field (B=0)

Interband optical absorption spectra from undoped, direct gap semiconductor hetero-structures are characterized by two thresholds: a discrete excitonic feature due to excitation of a bound electron-hole pair, and a well-defined step-like continuum edge shifted up in energy from the

[3] The subject of excitonic complexes will be expanded in more detail in sections 1.2.
[4] See Chapter 2.

bound state by the exciton binding energy. In contrast, in the presence of a high density of free carriers the spectra exhibit only a single threshold that typically appears as a step like edge with a pronounced enhancement at the threshold. This enhancement, which is called the Fermi-edge singularity (FES), results from the many-body response of the mobile two dimensional electrons to the photo-excited valence hole. The FES problem was addressed more than three decades ago by Mahan [Mahan, 1967] and others [Nozieres and de Dominicis, 1969] in the context of the X-ray absorption in metals. It was subsequently observed in semiconductor quantum wells (QWs) [Skolnick *et al.*, 1987].

The evolution of the absorption between the exciton dominated regime at very low density to the 2DEG dominated line-shape at higher density has been actively researched in recent years. These studies were triggered by the observation of the trion. It has been shown [Finkelstein *et al.*, 1995, Kheng *et al.*, 1993] that in the case of semiconductor hetero-structures containing a low excess 2D carrier density, a neutral exciton, X_0, can bind an extra electron causing the formation of a negatively charged exciton, also referred to as trion. In GaAs QWs, the trionic feature appears ~ 1 meV lower in energy than the X_0. The observation of the trion strongly supports earlier calculations of the absorption spectrum in presence of a 2DEG by Hawrylak [Hawrylak, 1991], which predicted that there should be three thresholds in the absorption spectrum. They should correspond to occupancy of the bound state by two, one, and zero electrons. Physically, the first threshold corresponds to excitation of an electron into a trion with the second electron provided by the Fermi sea. The second threshold corresponds to the creation of an exciton, and the third to creation of unbound electrons. Huard and co-workers [Huard *et al.*, 2000] measured in CdTe QWs the evolution of the absorption line-shape as the electron density, n_e, increases. They found that at low density the X_0 peak is dominant, and as n_e increases, the lower lying trion peak becomes dominant and evolves into the FES. Interestingly, they observed that the X_0 peak shifts towards higher energies with increasing n_e. The picture drawn was that the injection of a hole into a 2DEG creates a bound electronic state below the conduction band edge, even at high n_e. In the ground state this bound state is occupied by two electrons with anti-parallel spins.

This doubly occupied state evolves smoothly from the trion of the low n_e spectrum. The

second threshold related bound level is singly occupied only. In this view, the exciton is just an ionized trion, and the energy difference between them defines the minimum energy for removing one electron from the trion. This energy separation is the sum of the binding energy and the Fermi energy, as predicted by [Brum and Hawrylak, 1997, Hawrylak, 1991] and confirmed by [Huard *et al.*, 2000, Yusa *et al.*, 2000].

1.2.2 The optical spectrum of 2D electrons in magnetic field

Evolution from Landau to excitonic transitions in photoluminiscence

Most of the research into the optical properties of a 2DEG in a perpendicular magnetic field has been done by photoluminescence (PL) spectroscopy. In high density 2DEGs ($> 10^{11}$ cm^{-2}) when a magnetic field is applied, this emission band breaks up into relatively sharp transitions between Landau levels (LLs) of holes and electrons. Each level is further split according to the spin orientation (Zeeman split). The LL energy measured from the band bottom is $(n^e + \frac{1}{2})\hbar\omega_c^e$ for electrons and $(n^h + \frac{1}{2})\hbar\omega_c^h$ for holes, where $\omega_c^{e,h}$ is the appropriate cyclotron frequency, and $n^e, n^h = 0, 1, 2\ldots$ (for allowed transitions $n^e = n^h$). The density may be thus expressed in terms of how many of the levels are filled by means of the filling factor $\nu = n_e\phi_0/B$, where $\phi_0 = 4.137 \times 10^{-11}$ T-cm^2 is the quantum magnetic flux.

In the regime of high ν, the Landau levels (LLs) peaks retain an envelope reminiscent of the FES [Skolnick *et al.*, 1987], a feature which has raised much theoretical interest [H. Westfahl *et al.*, 1998]. The transition energy varies nearly linearly with B, as expected theoretically if the Coulomb interaction of the electrons is neglected. However, it has been observed [Gakhtman *et al.*, 1996, Kheng *et al.*, 1993, Yoon *et al.*, 1997] that the B dependence of the lowest transition (i.e., the $0-0$ LL transition) changes abruptly, at a certain critical field, to approximately quadratic. For fields above this critical value, the emission energy is very close to the transition from the singlet negative trion state observed in the same QW at low electron density. This changeover from linear (LL-like) to quadratic (trion-like) occurs always at the field at which the lowest electron LL is just filled; i.e., the field at which the electron filling factor is $\nu = 2$. It has been argued that this behavior is not a coincidence, but is a consequence of the hidden symmetry

inherent in 2DEG systems in strong magnetic fields [Dzyubenko and Lozovik, 1991]. In this picture, in a strictly two dimensional system in infinite magnetic fields, the energy of an exciton created in the presence of a 2DES is not affected by interactions with the surrounding electrons. The requirement of a strict 2D would explain why this effect is observed in symmetrical QWs and not in asymmetrical ones [Rashba and Sturge, 2000]. The 'infinite field' condition would explain why the transition is excitonic only below $\nu = 2$, where the state can be described within the lowest Landau level (LLL) approximation.

Singlet and triplet state

The study of the excitonic ground state at low ν has been an active field of research. Studies of the light (circular) polarization of the trions at $\nu < 1$ allowed a study of the spin states of the trion [Shields *et al.*, 1995]. The Pauli exclusion principle requires systems with two identical fermions to be anti-symmetric upon exchange of the particles. This results in the two-electron system arranging into an anti-symmetric singlet state of zero total spin ($S = 0$) or a triplet with total spin quantum number $S = 1$. It was shown that, like in the case of the hydrogen ion H^-, the ground state at $B = 0$ is the singlet and the triplet is unbound [Finkelstein *et al.*, 1996a].

Several theoretical works predicted that at large magnetic fields the triplet, with its anti-symmetrical spatial wave- function which minimized the electrostatic repulsion of electrons, will be the ground state [Palacios *et al.*, 1996, Whittaker and Shields, 1997, Wojs and Hawrylak, 1995]. This prediction was not confirmed experimentally and stood for some years as a serious open question. Recently, by calculating the energy spectra of a dilute 2DEG system [Wojs *et al.*, 2000] it was found that two different triplet states should be bound at high magnetic fields. These states are distinguished by their angular momentum. While one of them decays radiatively by a direct transition ('bright' triplet), the other decays only by a scattering assisted process, and is termed the 'dark' triplet. The dark triplet indeed does not appear in absorption measurements [Sanvitto *et al.*, 2002, Schüller *et al.*, 2004a,b, 2003], but is present in PL, where it was found to become the ground state at high field [Yusa *et al.*, 2001].

Inter-Landau levels second order processes

Another excitonic effect that has been observed in the absorption spectrum of CdTe QWs in a perpendicular field [5], is the so called combined exciton cyclotron resonance (combined ExCR) [Yakovlev *et al.*, 1997]. It was demonstrated that there is a new three particle optical resonance. In this case, an incident photon creates not only an exciton, but, in addition, excites a background electron from one Landau level to another. This effect has a counterpart in the emission spectra, the shake-up process [Finkelstein *et al.*, 1996b, 1997]. In this case, a trion may recombine while the remaining electron is excited to some higher lying LL.

Filling factor signatures

The trion was realized to be a useful probe into the understanding of the spectrum in the fractional quantum Hall effect (FQHE) regime. It was shown that the optical spectrum at this regime could be interpreted in terms of a trion which weakly interacts with the surrounding electrons. The emission intensity of the triplet was found to be maximal at fractional filling factors [Yusa *et al.*, 2001]. The dependence of excitonic features on ν, i.e. the ratio between n_e and B, rather than on any of them independently, is a signature of the ability of the excitonic complexes to probe the 2DES. Further evidence in this direction is the observation in the absorption spectra obtained from transmission measurements in CdTe QWs, that the trion absorption peak intensity maximum occurs at $\nu = 1$ for a range of densities and fields [Lovisa *et al.*, 1997].

1.2.3 Models for interpreting the absorption

In this section we review several models that have been used to interpret the absorption spectrum in terms of the initial and final states in the transition. They are formulated within the Fermi Golden Rule, and second order processes, such as the ExCR effect discussed above, are neglected.

[5] The techniques included photoluminescence excitation (PLE) and deriving the absorption from reflectivity measurements

The Fermi Golden Rule

According to the Fermi Golden Rule, the rate of the optical interband transition as function of the photon energy ω (where $\hbar = 1$) transitions is is given by

$$W(\omega) = 2\pi \sum_f |\sum_\alpha w_\alpha(\omega) \langle f| c_\alpha^\dagger h_\alpha^\dagger |i\rangle|^2 \delta(E_f - E_i - \omega) \tag{1.1}$$

where $|i\rangle$ and $|f\rangle$ are the initial and final many-body states of the 2DES respectively [6], and E_i, E_f are the corresponding energies. Here $e_\alpha^\dagger$ and $h_\alpha^\dagger$ are the creation operators of an electron in the conduction band and a hole in the valence band, respectively, in a state labeled by α . The label α can include several quantum numbers such as angular or linear momentum, Landau level and spin. The summation over α should be over a complete basis of orthonormal states labeled by this index. $w_\alpha(\omega)$ is the matrix element of the dipole operator.

This expression can be further simplified by the usual so called *envelope approximation*. In this approximation, it is assumed that the dipole operator is determined only by the Bloch wavefunctions, and thus is a property of the bands involved in the transition and does not depend on the envelope wavefunctions. Therefore, for all transitions between a valence band (say the heavy-hole band HH) and the conduction band, the dipole moment $w_\alpha(\omega)$ will be regarded as a constant w [7]. As a result we obtain

$$W(\omega) = 2\pi w^2 \sum_f |\langle f| \sum_\alpha c_\alpha^\dagger h_\alpha^\dagger |i\rangle|^2 \delta(E_f - E_i - \omega) \tag{1.2}$$

In practice, the absorption peaks have a finite width, and the oscillator strength I should be taken as the integral of the peak around the energy $\omega = E_f - E_i$, and the summation of the finals states f should be only over those states with energy within the peak width. This is

[6] The states $|i\rangle$,$|f\rangle$ are actually the *envelope* wavefunctions functions. In the context of Bloch theorem [Ashcroft and Mermin, 1976], the initial and final states can be expressed as a product between a Bloch wavefunction that is periodic in the lattice parameter of the crystal, and an envelope wavefunction that changes smoothly over such small scales. In the presence of a high magnetic field, the length scale of the *envelope* wavefunction is the magnetic length l_B. In the electron-hole creation operator $c_\alpha^\dagger h_\alpha^\dagger$, the fact that the same α appears for both particles comes from the fact that the photon linear momentum is negligible, and that the angular momentum of $\pm$ 1 is taken by the difference in angular momentum of the Bloch functions of the valence and conduction bands (see section 'Selection Rules')

[7] In the case of band mixing, namely, the case where the final states are a superposition of states if different bands, each component should keep its matrix element w_α.

expressed as

$$I = \int W(\omega)d\omega = 2\pi w^2 \sum_{f,\alpha} |\langle f|c_\alpha^\dagger h_\alpha^\dagger|i\rangle|^2 \tag{1.3}$$

In particular, if the light is circularly polarized, the integral can be taken over the peak corresponding to transitions to a given Zeeman level, i.e.

$$\begin{aligned} I^+ &= \int W_\uparrow(\omega)d\omega \\ &= 2\pi w^2 \sum_{f,\alpha} |\langle f|c_{\alpha,\uparrow}^\dagger h_{\alpha,\uparrow}^\dagger|i\rangle|^2 \\ I^- &= \int W_\downarrow(\omega)d\omega \\ &= 2\pi w^2 \sum_{f,\alpha} |\langle f|c_{\alpha,\downarrow}^\dagger h_{\alpha,\downarrow}^\dagger|i\rangle|^2 \end{aligned} \tag{1.4}$$

These expressions are still quite untractable because one needs to know the actual many-body eigenstates (both final and initial) in terms of the single particle operators. In the following I describe some simplifying approaches that have been taken in an experimental context in order to interpret the results of absorption in terms initial and final states.

Single-particle model

The eigenstates of a non-interacting 2DES are given by the so called many-body Fock states. Fock states are those that can be described by the occupation number of each single particle orbital alone. In the case of fermions, this occupation number can be only 0 or 1, and hence the fermionic Fock state can be expressed by a single Slater determinant. A Fock state for the initial state $|i\rangle$ (without valence holes) can be written in general as:

$$|i_\Omega\rangle = \prod_{\alpha\in\Omega} c_\alpha^\dagger|0\rangle \tag{1.5}$$

where Ω is the set of occupied orbitals (α has to belong to this set), and $|0\rangle$ is the vacuum state. Similarly, a final Fock state $|f\rangle$ with one valence hole at state α_h can be written as

$$|f_{\Omega',\alpha_h}\rangle = h^{\dagger}_{\alpha_h} \prod_{\alpha\epsilon\Omega'} c^{\dagger}_{\alpha}|0\rangle. \tag{1.6}$$

Note that in a transition $|i_\Omega\rangle \longrightarrow |f_{\Omega',\alpha_h}\rangle$, an electron-hole pair is created. As a result, the set of occupied electron orbitals in final state, Ω', is not very different from the initial set Ω. The new set Ω' just includes one additional electron. Examining Eq. 1.4, it is evident that for Fock states the only terms contributing to the oscillator strength I are those in which the electron is created in the same orbital α_h as the valence hole. As a result, the final states can be expressed in terms of the initial one as follows:

$$|f_{\Omega',\alpha_h}\rangle = h^{\dagger}_{\alpha_h} c^{\dagger}_{\alpha_h}|i_\Omega\rangle. \tag{1.7}$$

In quantizing magnetic fields, the single particle states states α are labeled by the Landau level index n, the spin $s = \uparrow, \downarrow$ and the momentum of Landau orbitals, which in case of the symmetric gauge, it is given by the angular momentum m. For example, at $\nu = 1$, the eigenfunction is

$$|\Psi_{\nu=1}\rangle = \prod_{m=0}^{N_\phi - 1} c^{\dagger}_{n=0,m,\uparrow}|0\rangle \tag{1.8}$$

where N_ϕ is the degeneracy of the Landau level, and $\uparrow$ denotes the lowers Zeeman level. [8]

At zero temperature and for $\nu \leq 2$, all the electrons are expected to be in the lowest Landau level with index $n = 0$. If in addition we consider transitions between lowest Landau levels of holes and electrons for a given Zeeman level, then all initial and final states then all electrons and holes are degenerate in energy. In such case, the summation should include all the states α in the lowest Landau level, and summation will be over the orbitals labeled by the angular momentum m. Hence inserting the states of Eq. 1.5 and 1.7 into Eq. 1.4, and replacing the label α by the the quantum numbers of the LLL orbitals, angular momentum m and spin s, we obtain

[8] Incidentally, this is also the wavefunction of the interacting 2DES. This is only true at exactly $\nu = 1$. If an electron of some angular momentum m_0 is removed from the system, ν will be decreased infinitesimally, i.e. $\nu = 1 - \epsilon$, and the non-interacting Fock state would be $|\Psi_{\text{Fock},m_0,\uparrow}\rangle = c_{n=0,m_0,\uparrow}|H_{\nu=1}\rangle$. As will be seen in a later section, the above is not an eigenstate of the interacting 2DES.

$$
\begin{aligned}
I^{+} &= 2\pi w^2 \sum_{m_h,s} |\langle i| h_{m_h,s} c_{m_h,s} \sum_{m=0}^{N_\phi - 1} c^{\dagger}_{m,\uparrow} h^{\dagger}_{m,\uparrow} |i\rangle|^2 \\
&= 2\pi w^2 \sum_{m_h,s,m} |\langle i| c_{m_h,s} \sum_{m=0}^{N_\phi - 1} c^{\dagger}_{m,\uparrow} \delta_{m_h,m} \delta_{s,\uparrow} |i\rangle|^2 \\
&= 2\pi w^2 \sum_{m=0}^{N_\phi - 1} |\langle i| c_{m,\uparrow} c^{\dagger}_{m,\uparrow} |i\rangle|^2 \\
&= 2\pi w^2 \sum_{m=0}^{N_\phi - 1} (1 - n_{m,\uparrow}) \\
&= 2\pi w^2 (N_\phi - N_\uparrow) \qquad (1.9)
\end{aligned}
$$

where $n_{m,\uparrow} \equiv \langle i| c^{\dagger}_{m,\uparrow} c_{m,\uparrow} |i\rangle$ is the occupation number of the orbital m in the lowest Landau level, and $N_\uparrow$ is the total number of electrons in $\uparrow$-states. [9] A similar expression can be derived for I^{-}:

$$
I^{-} = 2\pi w^2 (N_\phi - N_\downarrow) \qquad (1.10)
$$

The meaning of these equations is intuitive. The oscillator strength (OS) is proportional to the volume of single-particle phase-space available at each Zeeman level.

Such a model has been used by Aifer and co-workers [Aifer *et al.*, 1996, Manfra *et al.*, 1996] to obtain the average spin polarization, $\mathcal{P}$, of the initial state. The spin polarization is defined as follows

$$
\mathcal{P} = \frac{N_\uparrow - N_\downarrow}{N} \qquad (1.11)
$$

where $N = N_\uparrow + N_\downarrow$ is the total number of electrons. Using this model one can obtain relating

[9] The delta function in the derivation come from the the fact that the initial state doesn't include any valence hole, and the only hole is the system is the one created by the photon. Note also that the power of two was dropped because the occupation numbers $n_{m,\uparrow}$ in a many-body Fock state can only take the values of 0 or 1. As a result $(1 - n_{m,\uparrow})^2 = 1 - n_{m,\uparrow}$.

the spin polarization $\mathcal{P}$ to the integral of the absorption peaks I^+, I^-. Inserting Eq. 1.10 and Eq. 1.9 in Eq. 1.11 we obtain

$$\mathcal{P} = \left(\frac{2-\nu}{\nu}\right) \frac{\widetilde{I}^- - \widetilde{I}^+}{\widetilde{I}^- + \widetilde{I}^+} \tag{1.12}$$

where the filling factor is given by $\nu = N/N_{\phi_0}$, and $\widetilde{I}^{-,+}$ are the values of $I^{-,+}$ normalized by their band matrix w^2.

This expression was derived assuming that both initial and final states are Fock, non-interacting states. In fact, the derivation leading to Eq. 1.12 can be extended to allow interactions within the Landau level approximation (LLL) by noting that the initial and final states can be constructed from linear superpositions of orbitals in the LLL. Nevertheless, in what follows we will present alternative approaches that served as a basis to the new approach presented in this work.

Huard model

Huard and coworkers found that the absorption peak that is lowest in energy in CdTe QWs in strong magnetic fields has a singlet trion character [Huard *et al.*, 1998]. They modeled the oscillator strength (OS) of the trion-like peak taking into account that in a singlet trion the two electrons have opposite spins. They modified slightly Eqs. 1.9 and 1.10 to have the OS proportional not only to the single-particle phase-space available for photoexcitation of an electron, but also proportional to the number of electrons with opposite spin already present in the initial state. This is expressed as

$$\begin{aligned} I^- &\propto (1-n_\downarrow)n_\uparrow \\ I^+ &\propto (1-n_\uparrow)n_\downarrow \end{aligned} \tag{1.13}$$

where $n_{\uparrow(\downarrow)}$ is the average occupation number of the corresponding spin level. This approach also restricts the Hilbert space to the LLL. Using the notation described above, the occupation

numbers can be written as

$$\begin{aligned} n_\downarrow &= (1/N_\phi) \sum_{m=0}^{N_\phi - 1} \langle i | c^\dagger_{m,\downarrow} c_{m,\downarrow} | i \rangle \\ n_\uparrow &= (1/N_\phi) \sum_{m=0}^{N_\phi - 1} \langle i | c^\dagger_{m,\uparrow} c_{m,\uparrow} | i \rangle \end{aligned} \tag{1.14}$$

The resulting relation between the spin polarization, $\mathcal{P}$, and the OS is different from that in Eq. 1.12. Our approach will be similar to Huard's approach, except that we will take into account also the existence of *spacial correlations* between the electrons. This is to say that the instead of multiplying average occupation numbers, we would rather multiply *local occupation numbers*. This will be explained in more detail in Chapter 4.

1.3 The interacting 2DES ground state

The problem of the interacting 2DES in high magnetic field is exceedingly complex. While this complexity has hindered the progress in the advance in the theoretical description, the complexity also opens up a wealth of interesting phenomena, such as the Fractional Quantum Hall effect (FQHE) [Laughlin, 1983, Sarma and Pinczuk, 1997, Stormer *et al.*, 1999, Tsui *et al.*, 1982]. In spite of this complexity, some approximate solutions for the ground state of the system have been found for some specific cases. In this section we review briefly the theories of Skyrmions and of Composite Fermions (CFs).

1.3.1 Skyrmions

As explained in the introduction, electron-electron interactions play an important role in determining the ground state of a 2DES, and its spin polarization. In particular, at $\nu = 1$ the interactions favor a ferromagnetic order (full spin polarization) even in the absence of a Zeeman spin gap, E_Z. Furthermore, it was suggested that if this spin gap is sufficiently small, the ground state around $\nu = 1$ consists of charged spin textures excitations known as Skyrmions [Fertig *et al.*, 1994, Sondhi *et al.*, 1993]: neighboring electrons tend to align their spin in parallel

to minimize the exchange energy, creating a smooth texture of the spin field, in which many electrons participate. The projection of the spin along the magnetic field direction, S_z, varies gradually from the center of the texture towards the edges, with the total integrated charge being $-|e|$ for $\nu > 1$ (Skyrmion) and $+|e|$ for $\nu < 1$ (anti-Skyrmion). It has been realized that as the spin gap increases, such a large size structure becomes very costly in energy. Less electrons find it energetically favorable to flip their spin, and the Skyrmion size shrinks. Theoretical estimates for GaAs set the Skyrmion size at $B = 8$ T to be about two magnetic lengths only [Fertig *et al.*, 1994]. The experimental evidence for the Skyrmion theory comes primarily from NMR measurements [Barrett *et al.*, 1995], tilted magnetic field transport experiments [Schmeller *et al.*, 1995], optical absorption spectroscopy [Aifer *et al.*, 1996, Manfra *et al.*, 1996] and photoluminescence [Kukushkin *et al.*, 1997a,b, 1999]. In these measurements the average spin polarization $\mathcal{P}$ of the 2DES was determined and was shown to fall abruptly at both sides of $\nu = 1$, as predicted by the theory.

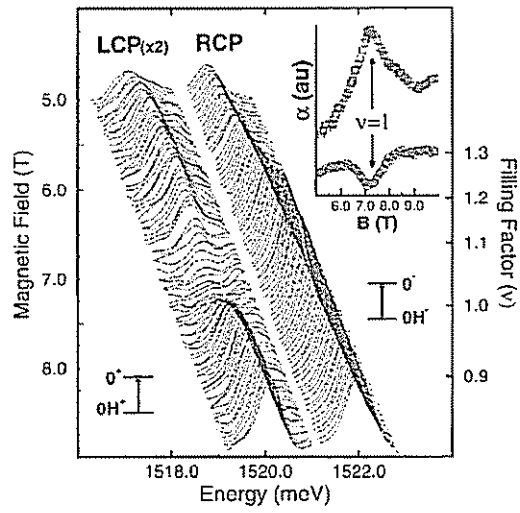

Figure 1.1: After Ref. [Manfra *et al.*, 1996]. Absorption spectra in the left and right handed circular polarization (LCP and RCP, respectively) as a function of magnetic field at $T = 1.5$ K. The RCP spectra are offset by 11 meV for clarity. The main optical transitions to the two lowest electron spin states are shown alongside the spectra. The inset displays the peak absorption coefficient α in the vicinity of $\nu = 1$

It is relevant to review here the results of [Aifer *et al.*, 1996, Manfra *et al.*, 1996] and to show

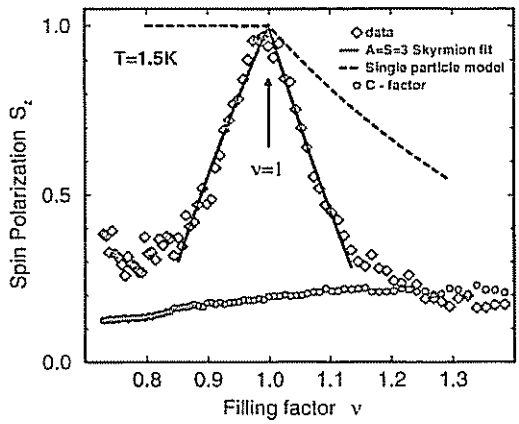

Figure 1.2: After Ref. [Manfra *et al.*, 1996]. Spin polarization plotted vs. filling factor (diamonds), calculated using Eqs. 1.9 and 1.10. The data is compared with both a single particle and Skyrmion-based model.

how the single-particle model based on the Fermi Golden Rule that was discussed in a previous section (see Eqs. 1.9 and 1.10) has been applied in order to measure the spin polarization $\mathcal{P}$. In Fig. 1.1, it is shown that indeed at $\nu = 1$ the absorption into the lower Zeeman level is quenched, and is maximal for transitions into the upper one. This is because the lowest Zeeman level is full and the upper is empty at this filling factor. As ν is tuned away from 1, the absorption coefficients at both Zeeman levels tend to approach each other, indicating that there is a loss of polarization at both sides of ν, as seen if Fig. 1.2. This is in agreement with Skyrmion. A single- particle ground state would have been fully polarized for $\nu < 1$ and the depolarization as ν is increased above 1 would have been more gradual. The single-particle model polarization is indicated by the dashed line in Fig. 1.2.

1.3.2 Composite Fermions

Recent studies have searched for signatures of composite fermions in the optical spectrum [Kukushkin *et al.*, 1999, 2002, Yusa *et al.*, 2001]. Composite fermions (CFs), electrons that are dressed with magnetic flux quanta pointing opposite to the applied magnetic field, were identified as quasi-particles that simplify our understanding of the fractional quantum Hall effect (FQHE). They are quasi-particles that can be regarded as weakly interacting, as opposed to

the electrons that are strongly interacting. They precess, like electrons, along circular cyclotron orbits, but with a diameter determined by a reduced effective magnetic field. The frequency of their cyclotron motion was measured by enhanced absorption of microwaves and the composite fermion effective mass was inferred to vary from 0.7 to 1.2 times that of the free electron mass as their density is tuned from 0.6 to 1.2×10^{11} cm^{-2} [Kukushkin *et al.*, 2002].

The composite fermion (CF) picture, initally proposed by J. Jain [Jain, 1989, 1990, 1994], has been motivated by the complex phenomenology of the FQHE. The CF picture considerably simplifies our understanding by mapping the FQHE of electrons to an integer quantum Hall effect (IQHE) of CF quasi-particles.

According to CF theory, the electrons minimize their Coulomb energy by attaching an even number ($2m$) of vortices of the wave-function [Lopez and Fradkin, 1991], creating a *correlation-hole* around the electrons. Vortices are characterized by a phase-change of 2π over a closed loop around them. This effect can be described as the Berry-phase effect accumulated around a magnetic flux quantum ϕ_0 in the Aharonov-Bohm effect. Therefore, the electrons are described as *dressed* with magnetic field quanta and experiencing an effective magnetic field $B^* = B - 2mn_e\phi_0$, where B is the applied applied magnetic field and n_e is the electron density. As a result, the filling factor of the CF's is given by $\nu_{CF} = n_e\phi_0/B^*$. Thus, the relation between the filling factor for electrons and that for CF is

$$\nu = \frac{\nu_{CF}}{2m\nu_{CF} \pm 1} \tag{1.15}$$

where the minus sign correspond to the case of negative B^*. It can be readily seen that when CF's exhibit the IQHE, namely when ν_{CF} is an integer, the electron filling factor ν is fractional. This amounts to explain the FQHE of electrons in terms of the IQHE of CFs.

An alternative description of the same theory can be stated as follows. The ground state at a fractional $\nu = p/q$ (p and q are integers) is described in terms of quasiparticles, CFs, with fractional charge e/q (e is the charge of the electron) and integer filling factor $\nu_{CF} = p$.

Spin polarization of composite fermions

The spin polarization, $\mathcal{P}$, of the 2DES in the FQHE regime has been measured by photoluminiscence [Kukushkin *et al.*, 2000, 1997b, 1999] and NMR techniques [Freytag *et al.*, 2002, 2001] and results have been described in terms of CF quasiparticles.

Consider, for example, the ground state at $\nu = 1/3$. It can be described as composed of CF of charge $e/3$ and filling factor $\nu_{CF} = 1$, where the CF fill the lowest Zeeman level of the LLL of the CF (CF-LLL) and thus the state is fully polarized, i.e. $\mathcal{P} = 1$. It was proposed that, in analogy to the situation around $\nu = 1$, the 2DES would depolarize as ν sways away from $\nu = 1/3$ due to the formation of CF Skyrmions, originated from residual interactions between the quasi-particles [Dethlefsen *et al.*, 2005, Kamilla *et al.*, 1996, Leadley *et al.*, 1997].

Another ground state of interest occurs at $\nu = 2/3$, for which $\nu_{CF} = 2$. In an independent CF model, $\mathcal{P}$ is expected to be determined by an interplay between the Zeeman and CF cyclotron energy. At low B, the Zeeman gap, which is linear in B, is lower than the CF cyclotron gap, which is proportional to $\sqrt{B}$. As a result, both spins states of the CF-LLL, $|\uparrow\rangle$ and $|\downarrow\rangle$, should be filled, and thus $\mathcal{P} = 0$. At high B, the $|\uparrow\rangle$ states of the second CF Landau level are lower in energy than $|\uparrow\rangle$ states of the CF-LLL, and hence $\mathcal{P} = 1$. As a result, when B is increased above a critical value B_c while keeping $\nu = 2/3$ constant, there should be a transition from $\mathcal{P} = 0$ to $\mathcal{P} = 1$. Such a transition has been predicted and observed in transport and optical experiments for several filling factors of the form $\nu = 2/q$, [Eisenstein *et al.*, 1989, Kukushkin *et al.*, 2000, 1999, Sarma and Pinczuk, 1997, Smet *et al.*, 2001]. An example of such transition can be seen in Fig. 1.3. A similar transition has been also consired for interacting electrons at $\nu = 2$ [Brey and Tejedor, 2002].

From the above description, the transition at $\nu = 2/3$ should be fairly abrupt. Experiments, however, show a more complex picture. In transport measurements [Smet *et al.*, 2001] the transition is sharp, extending over the relative narrow range of magnetic fields ~ 0.1 T . On the other hand, optical [Kukushkin *et al.*, 1999] and NMR measurements [Freytag, 2001, Freytag *et al.*, 2002, 2001] [10] have found a much larger broadening of the transition, which can can be over 1 T, and that it includes a plateau of constant partial polarization. Thus, an intermediate

[10] For a review on NMR measurements see Ref. [Horvatic and Berthier, 2002]

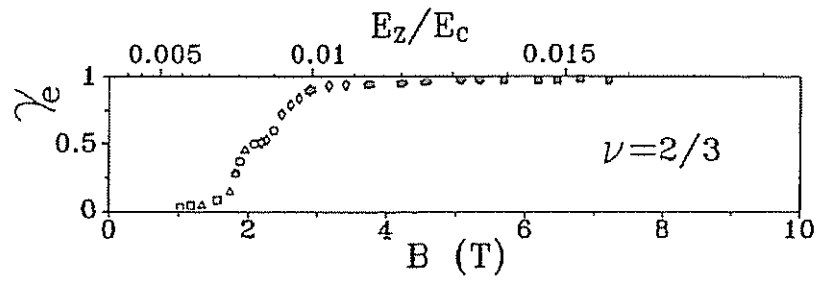

Figure 1.3: After Ref. [Kukushkin *et al.*, 1999]. Magnetic field dependence of the electron spin polarization ge measured in the FQHE regime at $\nu = 2/3$ in an heterostructure measured by photoluminiscence. E_Z/E_C is the ratio between the Zeeman and Coulomb energy

phase of $0 < \mathcal{P} < 1$ was shown to exist. The NMR results can be seen in Fig. 1.4. The states of partial spin polarization has been of much theoretical [Kamilla *et al.*, 1996, Mariani *et al.*, 2002, Murthy, 2000, Vyborny and Pfannkuche, 2004] and experimental [Schulze-Wischeler *et al.*, 2004, Stern *et al.*, 2004] interest recently. The proposed explanations include the effect of residual CF-CF interactions, disorder, spin-orbit coupling, the effect of the crystal periodic potential, and the existence of magnetic domains.

1.4 Layout

This work is organized as follow. In Chapter 2 we present the experimental techniques. In Chapter 3 we show the evolution of the measured spectra as a function of the 2DES density and the magnetic field. We find that at $\nu = 1$ the absorption peaks splits and a new lines appear. We identify the absorption lines as related to the known excitonic complexes. In Chapter 4 we present a quantitative model in order to explain the results. We find that several experimental results can be understood in terms of Skyrmions present in the 2DES. In Chapter 5 we present the measured spectra in a dilution fridge. Empirically, we find that the oscillator strength of the peak associated with the singlet trion is very sensitive to the temperature, the density and the filling factor. We propose that the oscillator strength of this absorption, and in particular the dichroism of the trion absorption can be used to probe the spin polarization of the 2DES. We present a quantitative model that relates the dichroism to the spin polarization,

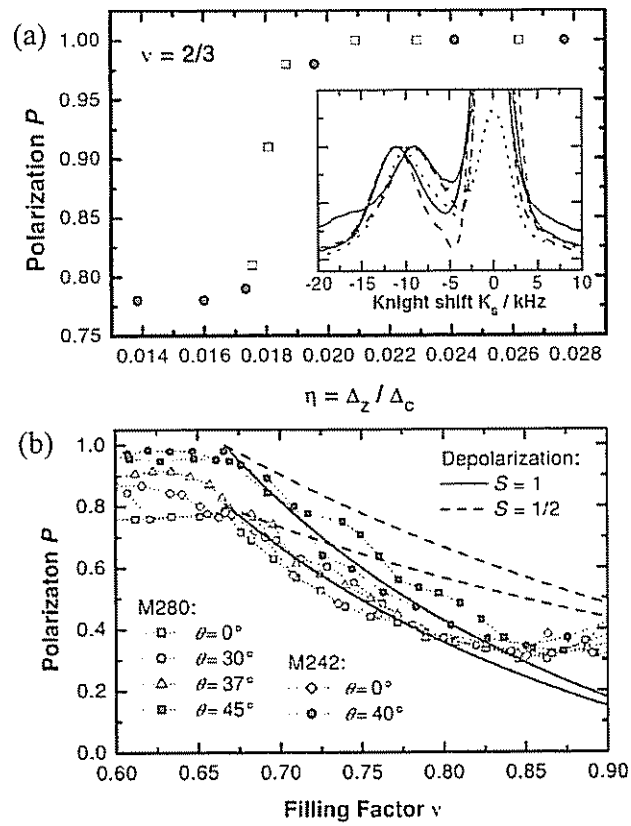

Figure 1.4: After Ref. [Freytag *et al.*, 2001]. (a) The phase transition of the $\nu = 2/3$ state as revealed by the dependence of the spin polarization on the ratio of Zeeman and Coulomb energies η of samples M280, a QW 30 nm wide denoted by black circles), and M242, a QW 25 nm wide denoted by empty squares, at temperatures below 100 mK. η was varied by changing the angle θ between the magnetic field direction and the normal to the 2D plane. The transition occurs at $\eta_c = 0.0185$, corresponding to a critical field of $B_c^{M280} = 6.7$ T and $B_c^{M242} = 8.9$ T. The inset shows the NMR spectra corresponding to the points for M280. (b) The filling factor dependence of the polarization for samples M280 and M242 at 100 mK and various tilt angles θ. The solid (dashed) lines correspond to a model assuming a depolarization of two (one) spin flips per removed flux quantum.

and interpret the experimental results in terms of a partially spin-polarized 2DES ground state around filling factor $\nu = 2/3$.

Chapter 2

Methods

2.1 Samples

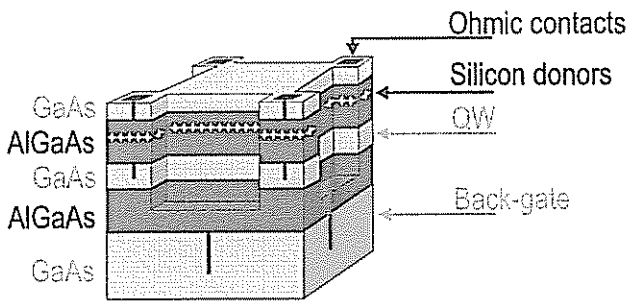

Figure 2.1: Sketch of the sample structure.

Several samples with the same general structure were investigated (see: Fig. 2.1), all consisting of a single 20 nm GaAs modulation-doped quantum well (QW) grown on top of a a thick $Al_xGa_{1-x}As$ barrier layer. The barrier layer separates the QW from the back-gate layer. Details of the structure can be found in Appendix A. The wafers were processed to a mesa structure with selective ohmic contacts to the 2DES and to the back-gate. Applying a voltage between the 2DES and the back gate we could tune the electron density n_e continuously.

2.2 Characterization

The ability of the gate to tune the density was initially verified by observing the evolution of the photoluminescence (PL) spectrum at zero magnetic field, $B = 0$, as the gate voltage, V_g, was tuned. In Fig. 2.2(a) it can be seen that the width of the spectrum increases with Vg. It has been shown [Pinczuk *et al.*, 1984] that this width is a measure of the chemical potential, and thus the density of electrons, n_e, can be extracted at each V_g. Fig. 2.2(b) shows the n_e obtained in this way as a function of V_g.

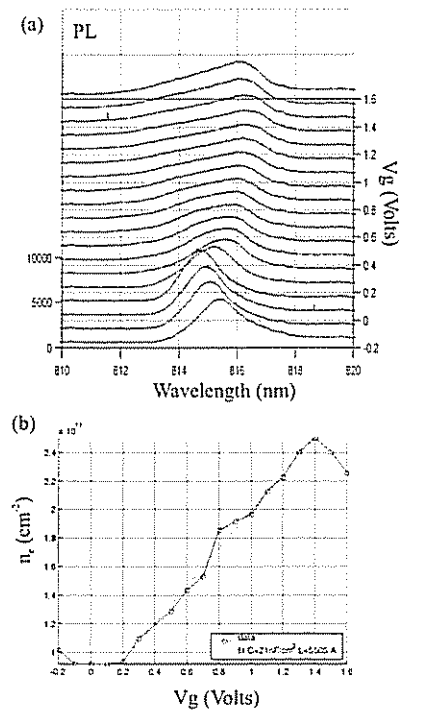

Figure 2.2: (a) Evolution of the photoluminescence (PL) spectrum at zero magnetic field, $B = 0$, as the gate voltage, V_g, was tuned. It can be seen that the width of the spectrum increases with Vg. (b) The electron density at each V_g, extracted following the method in Ref. [Pinczuk *et al.*, 1984]. The fitted capacitance is in agreement with the calculations for this sample. The temperature is 4 K, and the sample is CBE1057.

The sample is modeled as a capacitor where the QW and the back-gate play the role of the capacitor plates. From the slope of the graph the effective capacitance of the sample, C, can

be obtained, and the effective distance between the capacitor plates, L, can be calculated. The resulting distance of ~ 0.5 μm is in agreement with the actual width of the insulating AlGaAs barrier.

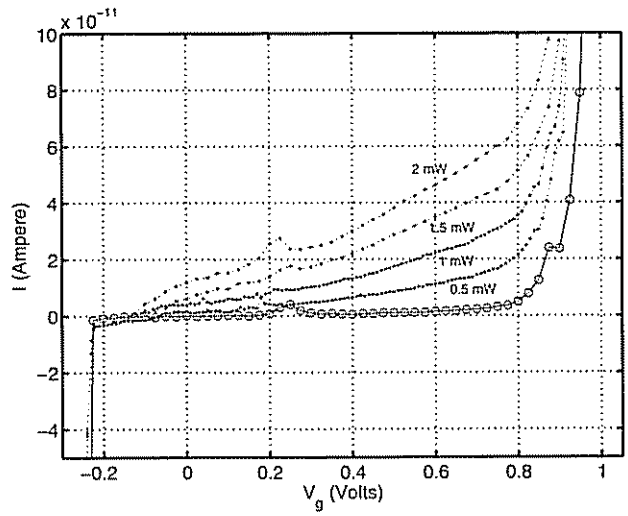

Figure 2.3: Current-voltage characteristic between the QW and the back-gate in darkness (open circles) and under illumination at a wavelength of 809 nm (DC mode). The temperature is 4 K, and the sample is CBE1057.

An important issue is the current leak between the back-gate and the quantum well. In Fig. 2.3 it can be seen that as V_g is pushed too far from 0, there is a strong leak current, even in darkness. This limits the range of densities available, as the device fails to work as a capacitor when the leak current is too large. In order to avoid this leak current, for the samples with the smallest insulating barrier (~ 0.5 μm), the alloying of the contacts to the 2DES had to be minimal, about one second at the eutectic melting point of the ohmic alloy used. The optimal time and temperature parameters of the alloying varied among different alloying setups (rapid thermal alloying machine or carbon-strip configuration) and even in the same setup over time, reflecting the uncertainty in the temperature control. The resistivity of the contacts was typically of the order of $k\Omega$. It can be seen in Fig. 2.3 that the leak current increases as the QW is illuminated with a wavelength above the absorption gap. This will be the basis of the photocurrent technique, explained in next section. The quantum efficiency of

this photocurrent, namely the number of electrons flowing per photon absorbed in the well, varied significantly among devices, and with the gate voltage. Assuming that only about 1% of the photons are actually absorbed in the well, the maximal efficiency that could be achieved in a given sample was in the range of 10^{-5} to 10^{-2} electrons per absorbed photon.

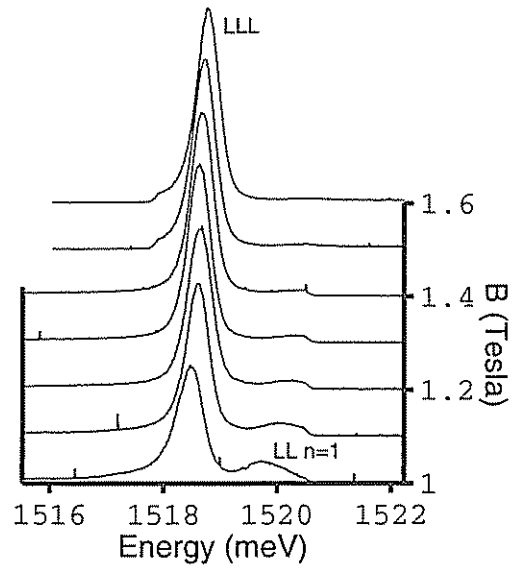

Figure 2.4: Photoluminescence spectra for different magnetic fields B at constant gate voltage, $V_g = -0.8$ V. At low B the filling factor ν is larger than 2, and we observe transitions corresponding to both the lowest Landau level (LLL) and the next Landau level ($n = 1$ LL). As B is increased, the degeneracy of each level increases and the population of the $n = 1$ LL is transferred to the LLL, and the corresponding PL vanishes. From the value of B for which $\nu = 2$, we obtain the density of the 2DES, n_e. The temperature is 75 mK, and the sample is Bell1.

An second method of measuring the density of the 2DES, n_e, is by PL measurements in magnetic fields. In the presence of such fields, the electrons occupy orbitals in quantized degenerate energy levels, namely, the known Landau levels (LL). Each Landau level (neglecting the Zeeman splitting in energy due to the spin) can be populated by a maximum density of $2B/\phi_0$, where $\phi_0 = 4.137\text{x}10^{-11}$ T-cm^2 is the flux quanta. The filling factor, defined as $\nu \equiv n_e\phi_0/B$, is equal to 2 when the density is such that both spins states in the lowest Landau level (LLL) are fully occupied, and the next LL is empty. Figure 2.4 shows PL spectra for different magnetic fields B at constant gate voltage. The strongest peak corresponds to

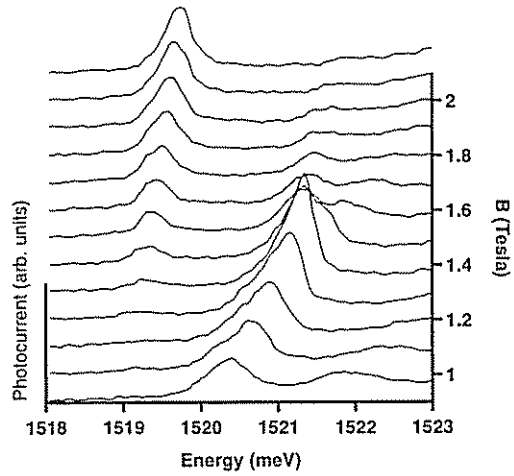

Figure 2.5: Photocurrent spectra for different magnetic fields B at constant gate voltage, $V_g = -0.5$ V. At low B the filling factor ν is larger than 2, the lowest Landau level (LLL) is full, and no absorption is possible. As B is increased, the degeneracy of the LLL increases as well and new empty orbitals become available. As a result, absorption becomes possible at $\nu < 2$. The temperature is $4K$, and the sample is Bell1.

transitions between lowest Landau level (LLL) in the the heavy hole (HH) valence band, to the LLL in the conduction band. At low B, ν is larger than 2, and a higher energy peak is present, corresponding to the next Landau level (LL $n = 1$). As B is increased, the degeneracy of each level grows and the population of the $n = 1$ LL decreases to zero, and the corresponding PL vanishes. From these measurements, an onset field, B_o, corresponding to $\nu = 2$ can be established at each gate voltage. The density of the 2DES can be obtained from the following expression:

$$n_e = \frac{2B_o}{\phi_0} \tag{2.1}$$

A third method to obtain the 2DES density is based on a similar argument as the explained above. As in the previous method, the procedure consists in determining the field B_o at which $\nu = 2$, and then obtaining n_e by Eq. 2.1. The difference lies in that now B_o is not given by the onset of the PL in the LL with $n = 1$, but by the onset of the absorption in the LLL. Indeed,

when $\nu \geq 2$, the LLL is full and Pauli principle prevents any further absorption into this level. As B is increased, the degeneracy of the LLL increased and new orbitals in the LLL become available. Hence, B_o is the field at which an onset for absorption into the LLL occurs. The absorption was measured by the photocurrent technique, as explained later in this chapter. Figure 2.5 shows spectra at constant gate voltage as B is scanned. It is seen that indeed the LLL peak (the lowest in energy) is not present at low B, and appears as B is increased [1].

2.3 Photocurrent measurement technique

Present techniques for measuring absorption present several difficulties. The most commonly used is photoluminescence excitation (PLE), where the spectrum obtained depends on energy dependent relaxation processes and thus may be not faithful to the true absorption. The technique of optical transmission presents several difficulties: Firstly, the absorption of a single quantum well (QW) is very weak (few percent), and thus the noise in the background light gets amplified in the signal. To circumvent this issue, it is possible to measure several QWs simultaneously. This introduces the problem of inhomogeneous broadening in the spectrum and also does not allow gating the samples. In addition to this, the transmission geometry presents the technical difficulty of illuminating and collecting the light from each side of the samples. In GaAs, the need to remove the opaque substrate adds another difficulty, and it may result in strained samples.

In this work we obtain the absorption spectrum by measuring the photocurrent (PC) flowing between the 2DES and a back-gate. We stress that the PC flows parallel to B and is thus not affected by the quantized resistivity of the 2DES, in contrast to in-plane photo-conductivity measurements [von Klitzing, 1980]. This technique have been previously demonstrated in obtaining the absorption spectrum of a 2DES at $B = 0$ using a front gate[Yusa *et al.*, 2000]. Using a front gate presented the difficulty that a spectrally broad large photocurrent originated between the well and the front-gate, possibly due to surface states, adding noise to the signal.

[1] More measurements around the onset field are shown together with the experimental results in Chapter 3. See for example Fig 3.1. As can be seen from Fig. 2.4 and 2.5, the nature of the onset may be not abrupt, and this introduces some uncertainty in the determination of the exact onset field B_o, specially at low densities.

With the use of a back-gate, we find that the photocurrent signal essentially occurs at laser energies above the fundamental gap of the well and at resonance with Landau Levels, resulting in low background spectra and confirming that the PC is indeed originated in absorption in the well. Furthermore, measurements of transmission [Plochocka, 2005] and photoluminescence excitation results in similar spectra, which gives us confidence that the measured PC spectrum indeed reflects the quantum well absorption spectrum.

Measurements were done in both DC and AC mode. In the DC mode, the sample is illuminated continuously at constant power at each wavelength. The current measured includes the photocurrent component, which varies with the wavelength, and a dark leak current which is a constant at each V_g, and can be substracted from the spectrum. In the AC mode, light intensity is modulated at a constant frequency by an optical chopper or by acousto-optic modulator. The acousto-optic modulator yields an illumination intensity that is changing smoothly in time from a maximum to a minimum value in a rather sinusoidal-shape. The minimal intensity was about 5% of the maximal.

The current is detected by an Ithaco trans-impedance amplifier. The amplifier was modified in order to get rid of unwanted 50 Hz from the power line, and have as power source large capacitance low-noise chemical battery. The output signal of the amplifier was registered by a DC volt-meter in the case of DC mode, and by a lock-in amplifier in the case of the AC mode. The frequencies used in AC mode were in the range of 1 to 10^4 Hz. This frequencies are low respect to the electron relaxation and electron-hole recombination time scales, and are essentially a way to measure the DC photocurrent signal, while improving the signal to noise ratio. In some devices it was found that other time scales exist that are comparable to the above range of frequencies. For example, some devices presented long rise times of the photocurrent signal. As a result, the frequencies were chosen taking into account the trade-off between several factors such as minimizing 1/f noise, maximizing the signal amplitude, avoiding frequencies near noise sources, avoiding frequencies at which the spectra shape becomes sensitive to this frequency due to the spectral dependence of the raise time [2].

[2] It was found that the spectral dependance of the signal time scales allows to measure the energy of the absorption lines by noting changes in the phase of the signal detected by the lock-in as a function of the laser wavelength. The resulting energies were in excellent agreement with the energies found from the amplitude of the signal.

2.4 Normalization by the photocurrent efficiency

Since the efficiency of the photocurrent depends on V_g we divide the signal by the value of the photocurrent I_0 measured at a photon energy much larger than the Fermi energy ϵ_F at each V_g. It is assumed that the absorption at this energy does not depend on the density, therefore I_0 yields a measure of the photocurrent efficiency. Normalizing the photocurrent by the efficiency allows a comparison of the absorption between different spectra.

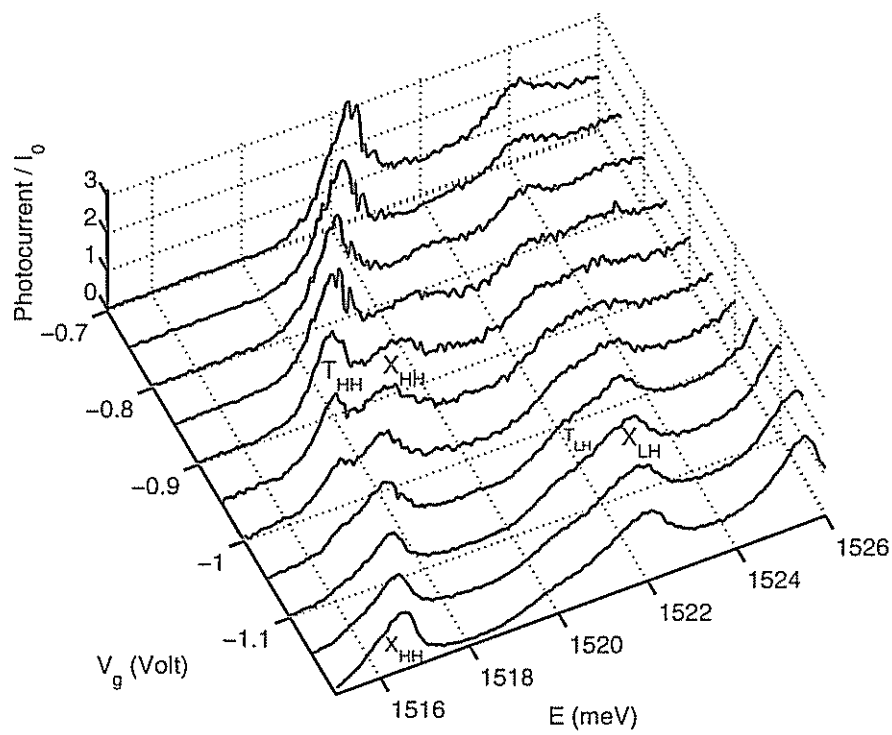

Figure 2.6: Spectra at $B = 0$ as for different gate voltages (V_g) at 85 mK.

As a qualitative validation for the normalization method, we show in Fig. 2.6 the evolution of the normalized photocurrent signal versus the photon energy at constant V_g for several values of V_g at $B = 0$. It is seen that at the lowest V_g (dilute limit), the lowest energy region of the

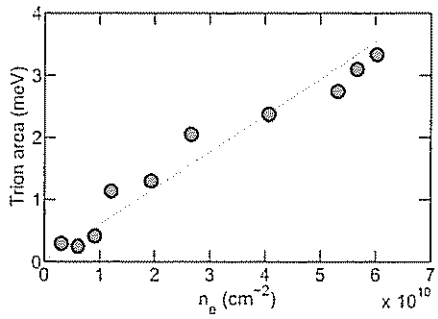

Figure 2.7: The heavy hole trion area versus the 2DES density,n_e, at $B = 0$ at 85 mK in sample Bell1. The dotted line is a linear fit. n_e was obtained by the method of PL in magnetic field, as explained the previous section.

spectrum is dominated by the neutral exciton peak, corresponding to the bound state of the photo-created HH- electron pair (X_{HH}). As V_g is increased toward 0, the increased n_e opens up the possibility of creating a trion, where the HH-e pair bind an additional electron from the 2DES (T_{HH}). At the same time, the 2DES screens the hole, causing a decrease in the oscillator strength of the exciton. A similar behavior is observed for the LH exciton and trion (X_{LH} and T_{LH} respectively).

To extract the oscillator strength, the trion and exciton were fitted by the sum of two gaussians. The area under the trion peak versus electron density is shown in Fig. 2.7 and is found to increase approximately linearly with the density n_e. Indeed, the trion oscillator strength is expected to increase linearly with the electron density. This has been predicted and observed for both trion emission and absorption spectra, for example in the Refs. [Esser, 2001, Rapaport *et al.*, 2000, Yayon, 2003]. This validates the reasonability of our normalization procedure. It must be stressed, however, that the normalization used is mostly for graphical purposes and that the conclusions and results in this work are not dependent on the normalization procedure.

2.5 Selection Rules

In the presence of an external magnetic field, all energy bands quantize into discrete Landau levels. Every LL splits into two Zeeman energy levels. In GaAs, absorption from LLL of both

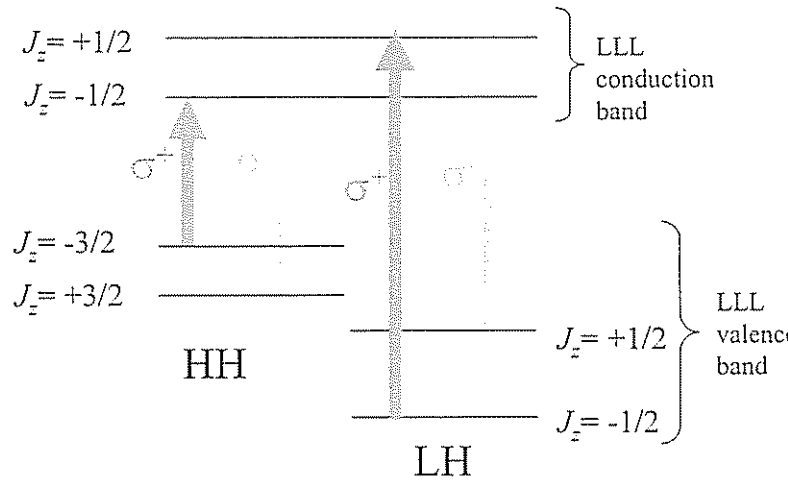

Figure 2.8: Sketch of the allowed transitions between the lowest Landau levels (LLL) of the valence band and LLL of the conduction band.

LH and HH bands into the lowest Landau level (LLL) of the conduction band is restricted by selection rules. According to these rules, the electrons do not change Landau level nor spin during the transition. Each level includes two spin-levels characterized by the J_z quantum number, namely, the projection of the total angular momentum on the axis perpendicular to the 2DES plane. Circularly polarized light incident along this axis amounts to photons with angular momentum $J_z = \pm 1$, corresponding to $\sigma^{\pm}$ polarization. Therefore, conservation of angular momentum restrict the transitions to those schematized in Fig. 2.8.

The sense of the polarization is only relevant in relation to the magnetic field direction. Therefore, the polarization can be switched between σ^+ and σ^+ either by by actually rotating the optical elements, or by keeping the polarizaton respect to the labaratory frame of reference, but inverting the direction of the magnetic field. In this work, the convention adopted is that a negative field, $B < 0$, corresponds to σ^+, and $B > 0$ corresponds to σ^-.

Figure 2.9 shows the photocurrent spectrum at each light polarization obtained in a dilution fridge with optical windows. The energy range shown includes LLL transitions for both HH and LH. Since the 2DES is mostly spin polarized, the dominant transition should be into the upper Zeeman level in the conduction band, with $J_z = 1/2$. Note that the HH and LH transition at a

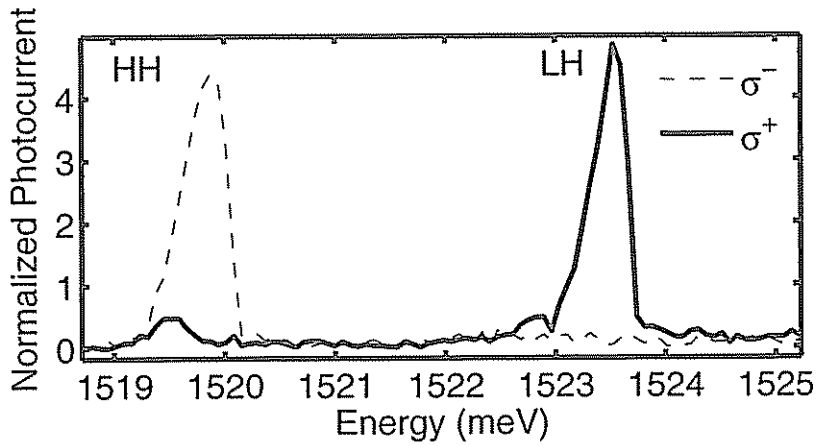

Figure 2.9: Spectra at 75 mK including transitions for both heavy hole (HH) and light hole (LH). Only LLL transitions are shown. The field is $B = 3.5$ T. At $V_g = -0.55$ V, the estimated filling factor is $\nu = 0.98$. In this situation the 2DES must be mostly spin polarized. As a result, the dominant transition should be into the upper Zeeman level in the conduction band with $J_z = +1/2$. The transition into this level corresponds to different light polarizations $\sigma^{\pm}$, depending on whether the correspond to HH or LH transitions (see text). The sample is Bell1.

given light polarization probe different electronic Zeeman levels: a σ^+ photon tuned to the HH transition creates a valence hole with $J_z = 3/2$ and an electron with $S_z = -1/2$. When tuned to the LH transition it creates a valence hole with $J_z = 1/2$ and an electron with $S_z = 1/2$. In other words, for $B < 0$ the HH transition probes the electron lower Zeeman state $|\uparrow\rangle$, while the LH probes the upper Zeeman state $|\downarrow\rangle$. Similarly, for σ^- the HH and LH transitions create an electron in the $|\downarrow\rangle$ and $|\uparrow\rangle$ states, respectively.

2.6 Experimental setup

The experiments setup included a magnetic field B applied along the growth axis of the wafer and illuminated with a circularly polarized light.

At a first stage, measurements were done in liquid Helium temperatures in a cryogenic dewar. At a later stage, further experiments were done in a dilution fridge in order to explore the region of lower temperatures. Both setups are described next.

Optical fiber system immersed into a liquid helium dewar

In this setup, the sample was mounted inside a dewar with liquid ^{4}He at a temperature of 4.2 K. The light source was a tunable Titanium:Saphire laser, and the sample was illuminated through a thick plastic optical fiber going inside the dewar and through a circular polarizer. Changing the direction of the magnetic field is equivalent to change the direction of the circular polarization respect to the field, allowing us to selectively excite electrons to the conduction band at each spin state, according to selection rules.

It must be noted that during the construction of the setup, it was found that glass optical fibers present the effect that they keep a partial polarization of the light, even when the fibers are very wide and multi-mode. This was checked up to a core width of 0.6 mm. As a result, as light travels along the axis of the magnet towards the sample, the polarization of the light is rotated according to Kerr effect. This rotation depend on the magnetic field present. When this partially polarized light reached the polarizer that is located on top of the sample, the transmission power through the polarizer depends on the incident polarization. As a result, the incident power on the sample depends on the magnetic field. This effect was finally overcome by the use of plastic fibers, which totally destroy the polarization.

Dilution fridge with optical windows

In this setup, the sample was mounted on the cold finger of a dilution fridge with optical windows at a base temperature of 70 mK. The light source was a tunable dye laser, and the sample was illuminated with power densities of $\sim 5 \times 10^{-4}$ W/cm^2.

In this setup, reversing the polarization by inverting the magnetic field direction presented the difficulty that, in addition to the slow pace at which the field could be changed, ramping the field resulted in a significant heating of the system. The alternative consisted in illuminating through a liquid crystal circular polarizer. The circular polarization was reversed by changing the voltage applied to the liquid crystal cell, allowing us to selectively excite electrons to the conduction band at each spin state, according to selection rules.

Thermal anchoring of the sample was a main concern in this setup. In the usual optical experiments the sample is doubly anchored to the copper cold finger by (a) gluing the sample

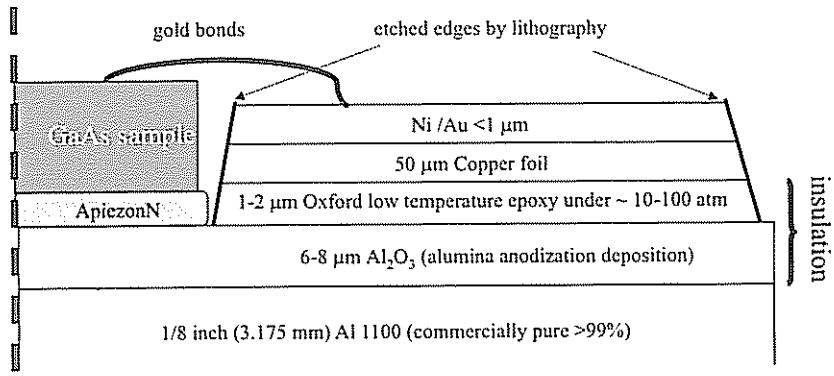

Figure 2.10: Scheme of the layered structure of the sample holder. The sketch shows a cross section of half of the structure, when cut along two perpendicular diameters. The drawing is not to scale. A thin insulation was formed around the aluminum body by alumina anodization deposition (oxidation of the surface). The alumina surface was polished to achieve micron sized roughness. Thermal conductive epoxy served to glue a copper foil to the holder, and provided further insulation. A thin layer of epoxy was achieved by applying high pressure. The copper foil and the epoxy layer were etched out in the region of the samples by lithographic techniques. This allowed gluing the samples by ApiezoN thermal conductive grease directly on the alumina layer and providing a better thermal contact to the sample. The electrical contacts in the sample were bonded to Au/Ni pads that were evaporated onto a copper foil. Thanks to Michael Rappaport for the fabrication.

to the cold finger by a thermal conducting grease, and (b) by bonding a gold wire from the sample to the cold finger. In this case, the sample needed to remain electrically insulated from the cold finger. Good thermal conduction is a property usually related to electrical conductors. This is much more true at the low dilution temperatures, where phonon thermal conduction vanishes as T^3. The approach used here was to have a layer of insulation as thin as possible, while avoiding electrical short-circuits. A scheme of the sample holder is shown in Fig. 2.10.

Chapter 3

The spectrum in perpendicular magnetic fields

3.1 The Landau fan in the absorption spectrum in magnetic fields

In this chapter we would like to present the results of the measurements and explain the features that were identified in the spectrum. Figure 3.1 presents a compilation of photocurrent measurements at constant $n_e = 2.2 \times 10^{11} cm^{-2}$ as B is varied between -9 T and $+9$ T [1]. The magnitude of the photocurrent is color-coded, with dark-red color indicating a strong signal (a vanishing signal is dark-blue). The absorption is strong when the photon energy is resonant with a transition.

By observing the evolution of the absorption lines (dashed lines) we note that in spite of the high density of the 2DES, the main features can be explained in terms of a single-particle picture where the electrons are regarded as non-interacting. In such a picture, in the presence of an external magnetic field, all energy bands quantize into discrete Landau levels (LL). As explained in section 1.2.2, the energy of each LL is proportional to B. Plotting the energies of

[1] We remind the reader that a negative field B corresponds to the σ^+ polarization, for which the HH transition is into the upper Zeeman level (see Fig. 2.8).

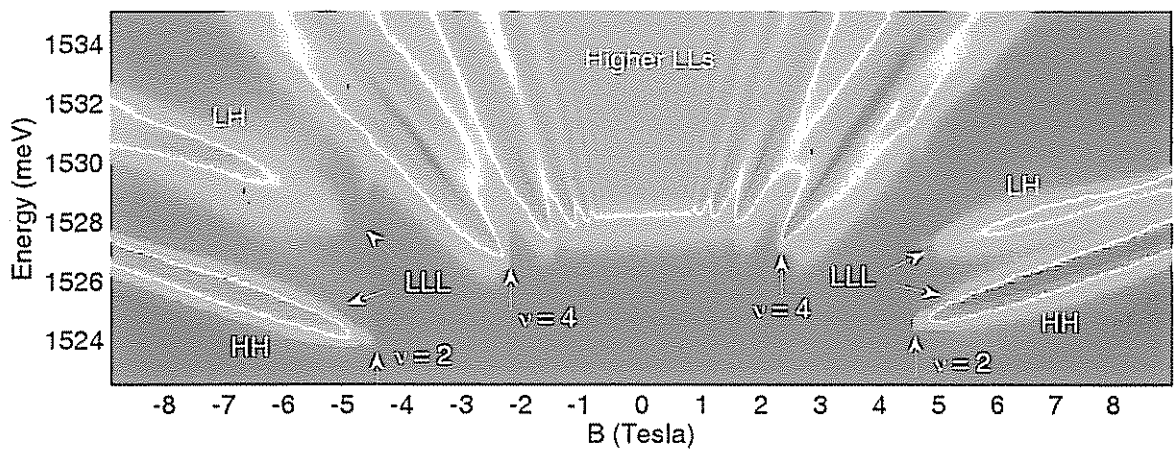

Figure 3.1: (color) Photocurrent spectra for for sample MBE7130 at 4.2 K, $n_e = 2.2 \times 10^{11} cm^{-2}$ and a light intensity of $I_L = 0.3$ mW/cm^2. $V_g = 0.5$ V. The Landau fan is well resolved (see the text). The dashed lines are guides for the eye.

the different Landau levels versus B results in what is called the 'Landau fan'.

Indeed, the characteristic Landau levels fan is well resolved even at low fields. The lowest energy line for both signs of B corresponds to an absorption process from the heavy-hole (HH) band into the lowest Landau level (LLL) in the conduction band. It has a sharp onset at $B_o = \pm 4.5$ T, corresponding to $\nu = 2$: below this magnetic field the LLL is full, so that no absorption is possible. This allows us to obtain n_e at each gate voltage, according to Eq. 2.1. Note also that higher LL present onsets of absorption at lower fields. For example, the LL with $n = 1$ presents an onset at $B = B_o/2 = 2.25$ T, corresponding to $\nu = 4$.

Parallel to absorption line of the LLL transition for the HH, there is a line corresponding to LLL transitions for the LH. This line is present in both negative and positive fields. While LH and HH bands in bulk are degenerate at $B = 0$ for optical active state (momentum $k = 0$), in a QW they split, with the LH being higher by about 3 meV for this QW width and barrier composition. The large energy difference between the LH line at $B > 0$ and $B < 0$ (Zeeman energy) is due to the large g-factor of the LH.

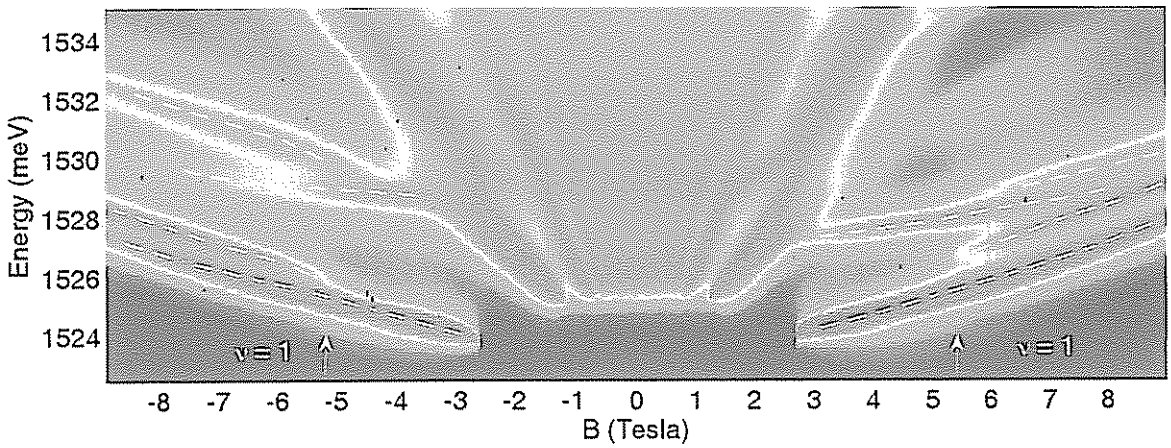

Figure 3.2: (color) Spectra as in Fig. 3.1, but with a lower $n_e = 1.3 \times 10^{11} cm^{-2}$ ($V_g = 0$ V). New absorption lines above each line in the LLL at $\nu = 1$. The onset field for this new lines corresponds to $\nu = 1$. Dashed lines are a guide to the eye.

3.2 Absorption around $\nu = 1$, onset of X-absorption

So far, the spectrum was described in terms of single-particle transitions, where only one transition was present for each LL, for each band (HH, LL), and for each light polarization, i.e. for each spin state. However, when we decreased the density in this sample, we found that the absorption peaks split and new peaks appear. Figure 3.2 shows a similar compilation of measurements to that of Fig. 3.1 for a density of $n_e = 1.3 \times 10^{11} cm^{-2}$. It is clear that while for low fields there is a single line for each single-particle allowed transition, as the field increases, each line splits into two, and new absorption lines appear above the previous ones. We observe that the onset field for this new lines corresponds to $\nu = 1$. This is observed more in detail in Fig. 3.3, were the spectra corresponding to the σ^+ polarization from 3.2 are plotted in three dimensions.

Figure 3.4 shows spectra at both polarizations at a density of $n_e = 1.7 \times 10^{11} cm^{-2}$ at the relatively high field of 8 T, so that $\nu < 1$. The new lines are particularly visible at the negative fields ($B < 0$) spectra, where the large HH-LH splitting allows us to easily resolve them. It is evident that the spectrum consists of four peaks at each light polarization. We denote the lowest peak of each split pair as T, and the higher one as X, with a subscript that identifies the

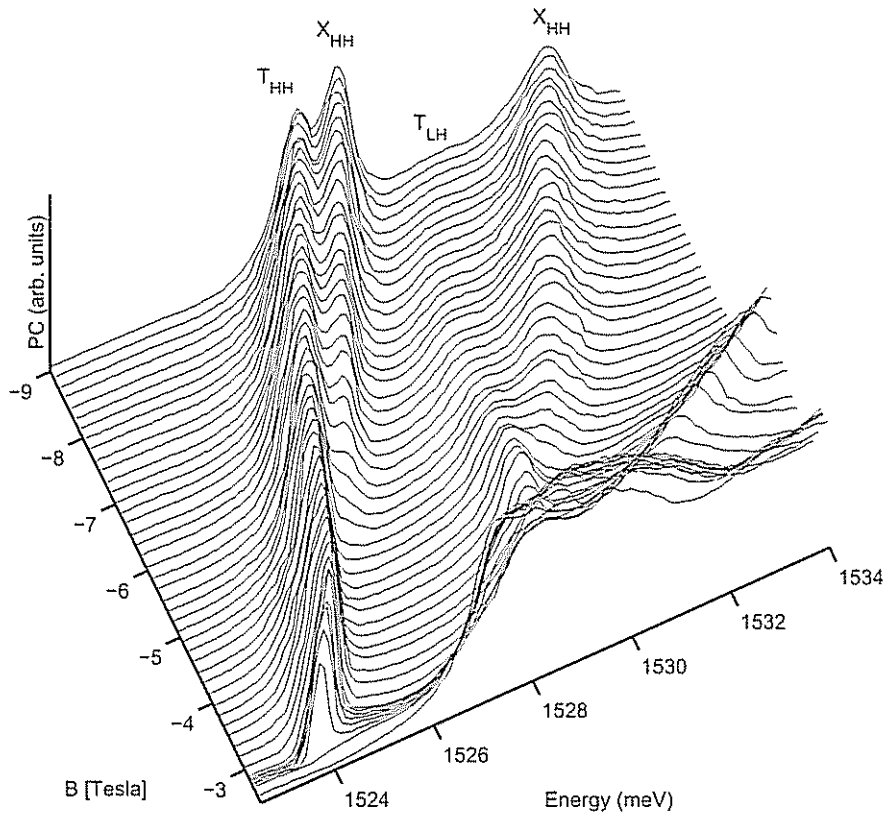

Figure 3.3: Photocurrent spectra in the σ^+ polarization. This figure shows part of the same data as in fig 3.2, but plotted in three dimensions.

band of the corresponding hole, namely heavy hole or light-hole. We shall later identify these peaks as hole-bound complexes.

The onset of the X-peak is observed in the evolution of the spectra with the magnetic field in other samples as well. Figure 3.5 shows the spectra evolution with the magnetic field for a different sample. It is very similar to that of Fig. 3.2. The onset for absorption for the T-peak at the LLL, corresponding to $\nu = 2$ can be seen very clearly. The white dashed line is a guide to the eye emphasizing the LLL lines for the HH and LH. It can be seen that when B is increased above $\nu = 1$, a new peak appears above each of the LLL lines for both HH, LH, at both polarizations.

In order to further establish that this is a filling-factor dependent effect, we were able to scan the filling factor by changing the density at constant magnetic field. Figure 3.6 shows the

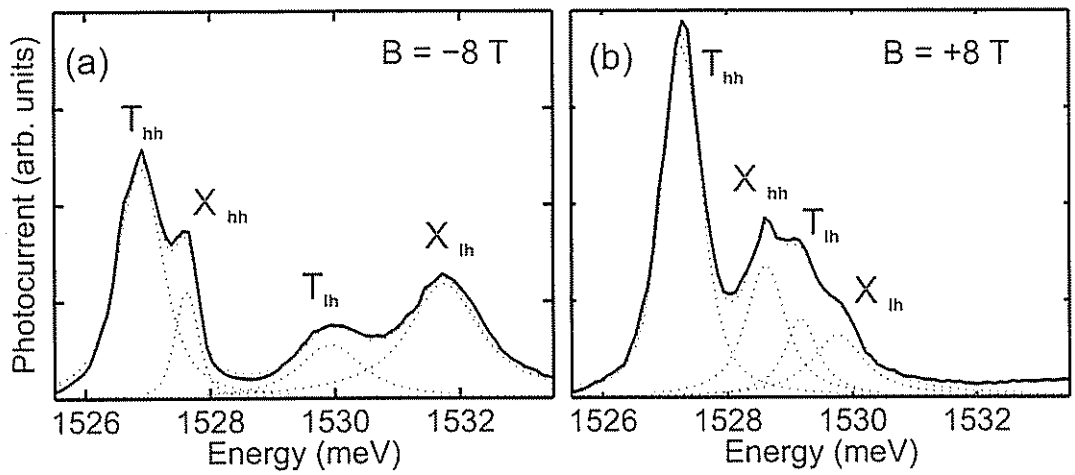

Figure 3.4: Spectra at both polarizations (solid line) for $\nu < 1$, where both the T and X peaks are present for heavy and light holes. The sample is MBE7130 at 4.2 K, and $n_e = 1.7 \times 10^{11}$ cm$^-2$. The dotted lines are fitted curves.

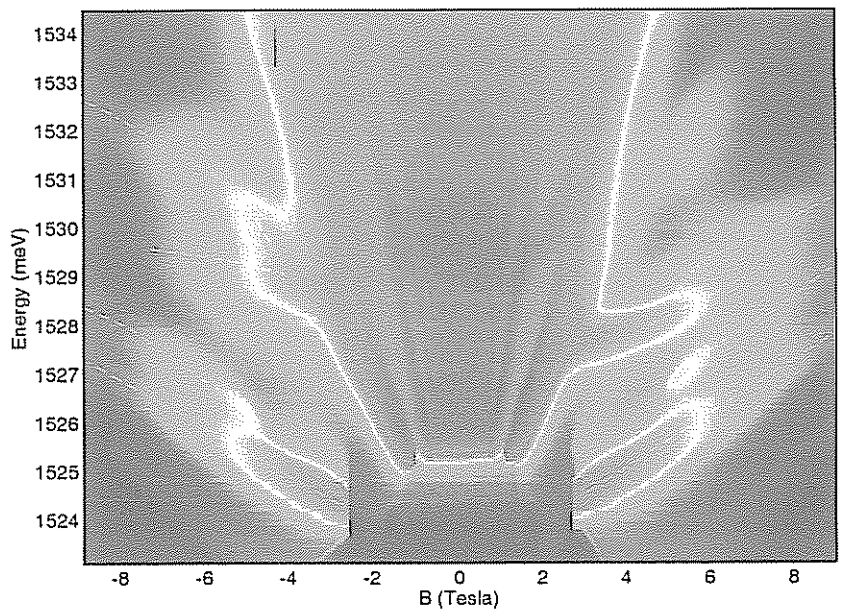

Figure 3.5: (color) Compilation of spectra at $n_e = 1.3 \times 10^{11}$ cm^{-2} for sample MBE7134 at 4.2 K. At low fields ($\nu > 1$), there is a single line for the LLL of each HH and LH at each polarization. At higher fields ($\nu > 1$), new absorption lines appear above each line. The dashed lines are guides to eye.

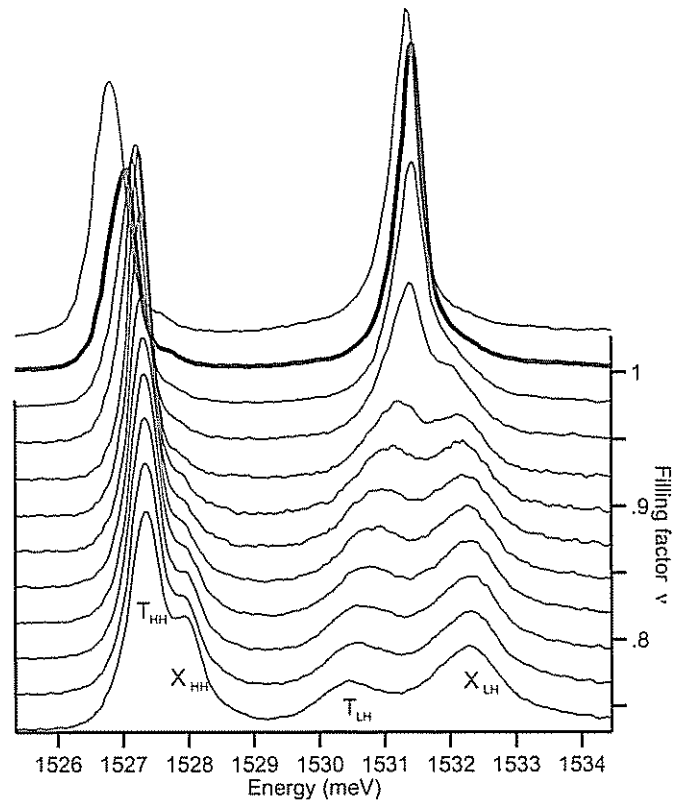

Figure 3.6: Evolution of the spectra of the exciton X and trion T as a function of the density at $B = 9$ T and $I_L = 3$ μW/cm^2. The temperature is 4.2 K and the sample is MBE7130. The subscript denotes the valence hole band (hh for heavy hole, lh for light hole). The $\nu = 1$ spectrum is emphasized by a thick line. It is seen that the X line abruptly appears below $\nu = 1$.

evolution of the photocurrent spectrum as n_e is is decreased below $\nu = 1$ at at constant $B = -9$ T. It is clearly seen that at $\nu = 1$ new satellite peaks, denoted by X_{HH} and X_{LH}, abruptly appear above the two lower energy peaks, T_{HH} and T_{LH}, and gain oscillator strength (OS) as the density is further reduced.

We repeated these measurements in several samples at various magnetic fields and electron densities and confirmed that this is indeed a filling-factor dependent phenomena that occurs at $\nu = 1$ for both HH and LH transitions and both light polarizations. Then sharp character of the onset of the X-peak can be clearly shown by plotting its oscillator strength OS versus filling factor as the field is varied at constant density. For this purpose we fitted the spectra, such as

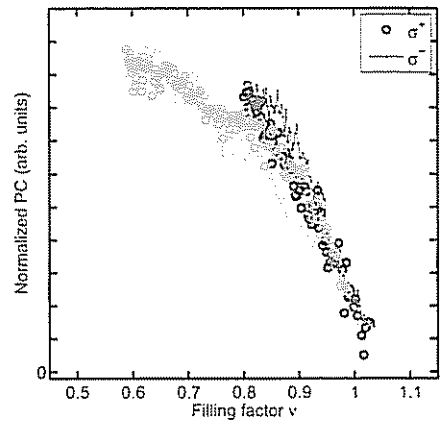

Figure 3.7: Oscillator strength (OS) of the X_{HH} absorption line, taken from the maxima of the fitted Voigt function, as function of the filling factor ν at 4K in sample MBE7130. ν is varied by scanning the magnetic field at two densities: $n_e = 1.3$ and 1.7×10^{11} cm^{-2} (grey and black color, respectively). Each density is plotted for both light polarizations (circles for σ^+ and dots connected by lines for σ^-). It is seen that the X line abruptly appears below $\nu = 1$, and that it is not much changed by the density or by the polarization. The four lines surprisingly seem to fall on each other. The normalization of the photocurrent (PC) is not arbitrary, but done following the procedure explained in Chapter 2.

those shown in Fig. 3.4 to the sum of four Voigt peaks [2]. In figure 3.7 we plot the maxima of the fitted X_{HH} peak for two different densities, $n_e = 1.3$ and 1.7×10^{11} cm^{-2} (grey and black color, respectively. Each density is plotted for both light polarizations (circles for σ^+ and dots connected by lines for σ^-). It is seen that the X line abruptly appears below $\nu = 1$, and that it is not much changed by the density or by the polarization. The four lines surprisingly seem to fall on each other. The normalization of the photocurrent (PC) is done following the procedure explained in Chapter 2.

[2]Voigt functions are the convolution of a Lorentzian and a gaussian peak. The rationale for this is that the Lorentzian corresponds to the homogenously broadened shape of an optical transition in an ideal, disorder free sample, and the gaussian corresponds to the inhomogeneous broadening.

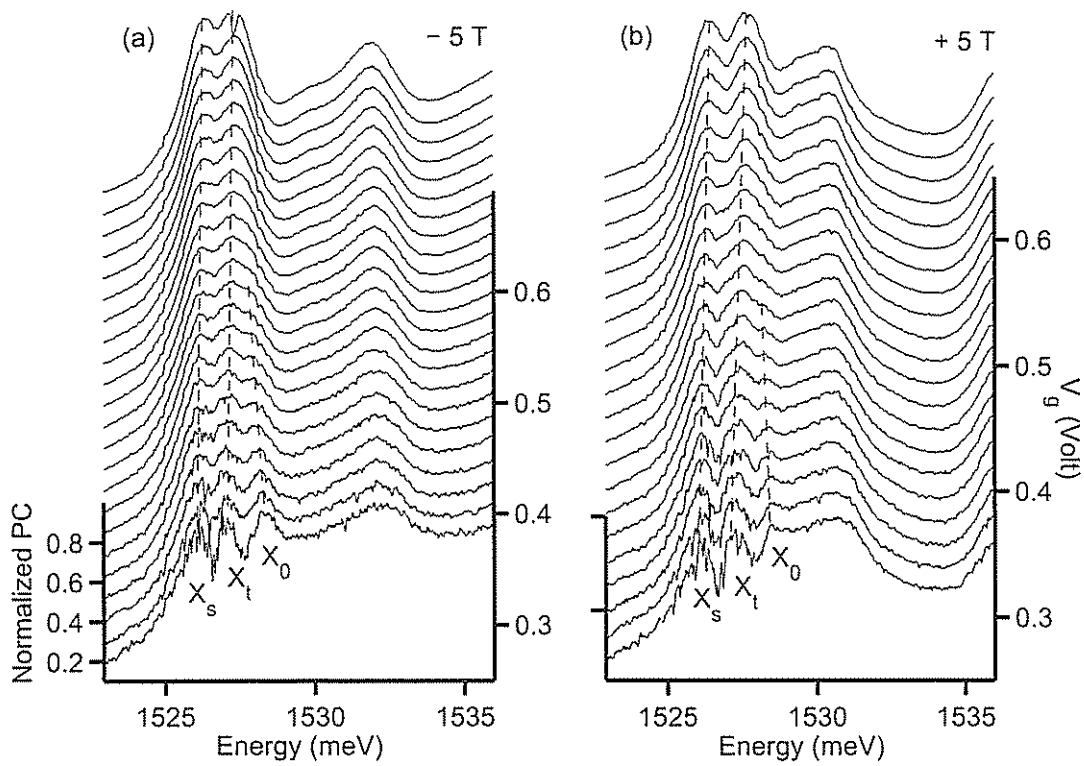

Figure 3.8: evolution of the spectrum as the gate voltage is decreased towards the dilute limit at a constant field of $B = 5$ T at both polarizations, at 4.2 K in sample MBE7134. At high V_g, the spectrum is characterized by the X and T peaks. It is seen that for the HH peaks, there is a continuous evolution towards the X_s and X_0 peaks, with the X_0 appearing at the lowest densities.

3.3 Identification of the hole-bound excitonic complexes in the absorption spectrum

To identify the nature of the peaks we followed their evolution with density. We found that as the electron density is decreased, for both HH and LH transitions the lower energy peak T evolves continuously into the singlet trion in the dilute limit, X_s, while the high energy peak X develops into the triplet trion, X_t, and the neutral exciton X_0. Figure 3.8 shows the evolution of the spectrum as the gate voltage is decreased towards the dilute limit at a constant field of $B = 5$ T at both polarizations. At high V_g, the spectrum is characterized by the X and T peaks , for both the HH and LH. It is seen that for the HH peaks, there is a continuous

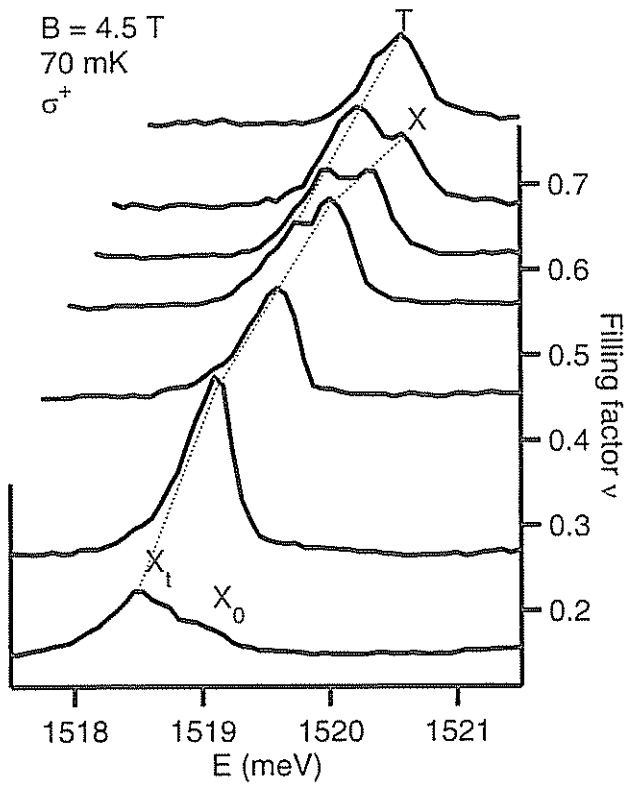

Figure 3.9: Spectrum evolution of the HH transition for the LLL as density is scanned towards the dilute limit at constant B. The X peak evolves into the triplet trion X_t in the dilute limit, where in addition a neutral exciton X_0 appears.

evolution towards the X_s and X_0 peaks, with the X_0 appearing at the lowest densities. A similar picture was found in a different sample at lower temperatures (Fig. 3.9), where as the density decreases, the T peak dissapears and the X_t dominates the spectrum. Further lowering of the densities result in the onset of the X_0-peak, as shown before.

These bound complexes X_s, X_t, X_0 were intensively studied in dilute 2DES during the last decade, and their identification is well established [Finkelstein *et al.*, 1995, Schüller *et al.*, 2003, Yusa *et al.*, 2000, 2001]. We note that such continuous evolution of the X and T peaks from the dilute limit to higher electron densities was observed in both photoluminescence and absorption measurements in the fractional quantum Hall regime [Schüller *et al.*, 2003, Yusa *et al.*, 2001].

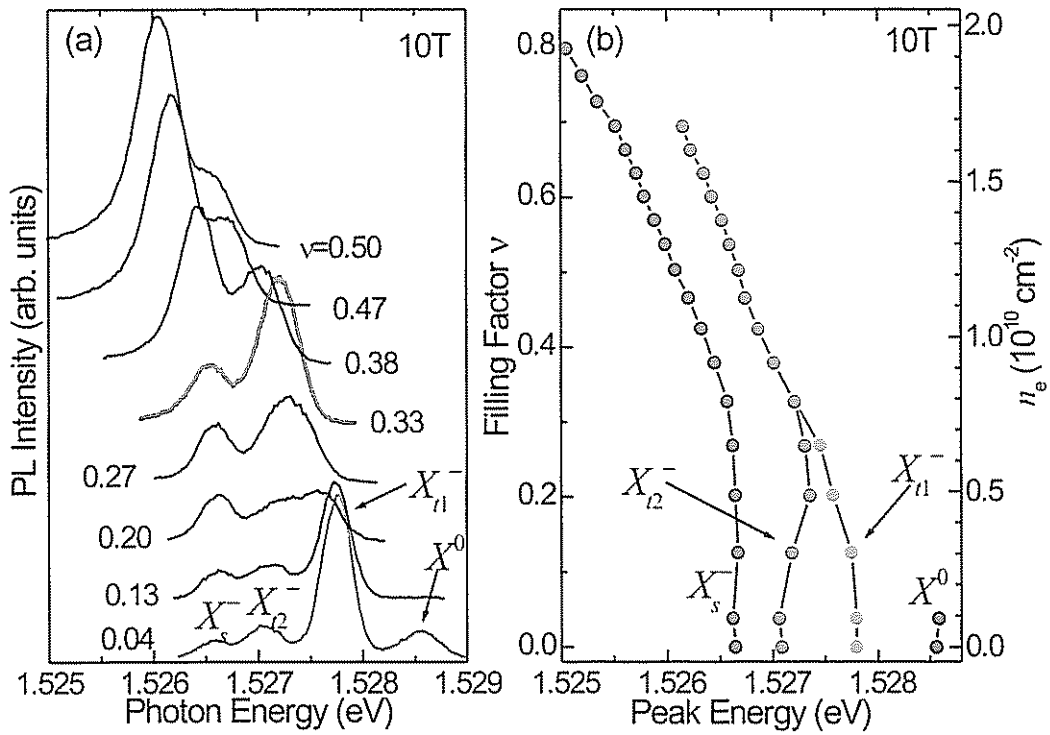

Figure 3.10: (color) Photoluminescence (PL) spectrum of the excitonic complexes evolution with the density at 20 mK. The neutral exciton, X_0, loses oscillator strength as the density is increased. The PL shows both the bright and dark triplet trions, X_{t1} and X_{t2}, and also the singlet trion X_s. (After [Yusa *et al.*, 2001]).

Figure 3.10 shows the results of [Yusa *et al.*, 2001] for the photoluminescence (PL) spectrum of the excitonic complexes evolution with the density. Both PL and absorption spectra show that the neutral exciton loses oscillator strength as the density is increased, a phenomenon usually attributed to screening. While the PL shows both the bright and dark triplets, X_{t1} and X_{t2}, our spectra shows only the bright one, in agreement with the absorption spectra obtained by [Schüller *et al.*, 2003], and confirming the 'dark' nature of the dark triplet.

In order to further confirm the excitonic nature of the peaks in the dilute limit, we followed the evolution of the peaks with magnetic field. Figure 3.11 shows the PC spectrum evolution of the HH LLL transition with the magnetic field. In addition to the singlet-like peak T, as B increases, the X peak gains oscillator strength. At higher fields, around $B = 4$ T, the line splits

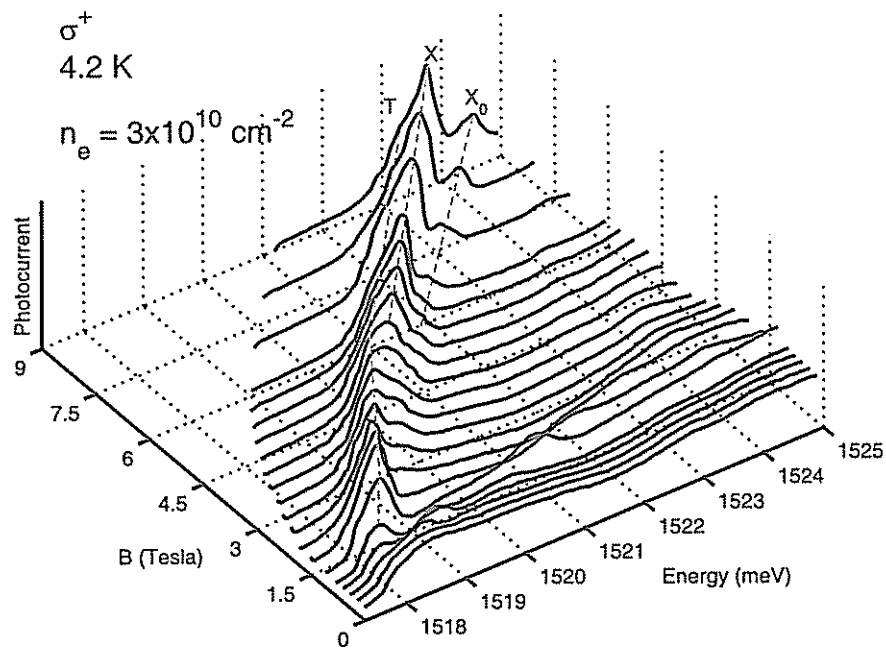

Figure 3.11: Spectrum evolution of the HH LLL transition in sample Bell1. In addition to the singlet-like peak T, as B increases, first there is an onset of the triplet-like X peak at $\nu = 1$. At higher fields, there is an onset of the neutral exciton peak X_0. The dashed lines are a guide to the eye.

and the neutral exciton peak, X_0, appears. This split occurs when the magnetic field is high enough for the triplet to have a finite binding energy. The dispersion of the energies versus the magnetic field, mainly at low fields, is not linear. The quadratic component is a manifestation of the excitonic nature of the complexes.

3.4 Hole-bound excitonic complexes in the absorption spectrum - the emerging picture

From the above results, we conclude that the lines that are observed around $\nu = 1$ are due to the formation of hole-bound excitonic states of a similar nature of those observed in the dilute limit. In this picture, the state excited in the T-transition is a singlet trion-like state. This state originates in the X_s state and its singlet nature is conserved as the density is increased. It must be noted that in the high densities at considered here, the actual states are not isolated from the surrounding electrons and the wavefunction of the hole has a finite overlap with many electrons. In this situation, the atomistic description of trion as a purely three-body state is insufficient. Therefore, the singlet trion-like state T should be described as a state with a high overlap between a valence hole and two electrons of opposite spin.

Similarly, the evolution with density shows that the X-peak has its origin in the triplet trion X_t-peak. In the X_t, one of the electrons is weakly bound. Due to this low binding energy of the triplet trion, it is energetically closer to a neutral exciton that to the singlet trion. Therefore, the X state should be described as a state where the hole is strongly overlapping with only one electron, and weakly overlapping with surrounding electrons from the 2DES. In this sense, the T state is more *trionic* than the X state, and that is why we denoted it by T. The notation chosen for the X state stresses its similarity with the neutral exciton.

From these measurements emerges a picture, schematized in figure 3.12, where absorption into the lowest Landau level for $1 < \nu < 2$ consists of a single peak, the singlet-like excitonic complex T. For $\nu < 1$, both T and a higher energy peak, X, is present. At higher B and low enough n_e (usually $<\sim 3 \times 10^{10}$ cm^{-2}), the X peak further splits into the triplet trion X_t and the neutral exciton X_0 [3]. For $\nu > 2$, the LLL is full and the absorption is quenched due to Pauli principle. PL emission is nevertheless possible, and the energy dispersion Landau-level-like (linear with B) due to screening of the hole potential and the breakdown of the hidden

[3]While for higher n_e, the onset of X_0 tends to happen at higher B, we were unable to find a systematic behavior as the parameters n_e, B and ν at which the onset takes place seem to change with light polarization, temperature and V_g, and between samples. Further measurements and careful analysis in the future might be able to reveal the underlying mechanism for the $X_0 - X_t$ splitting.

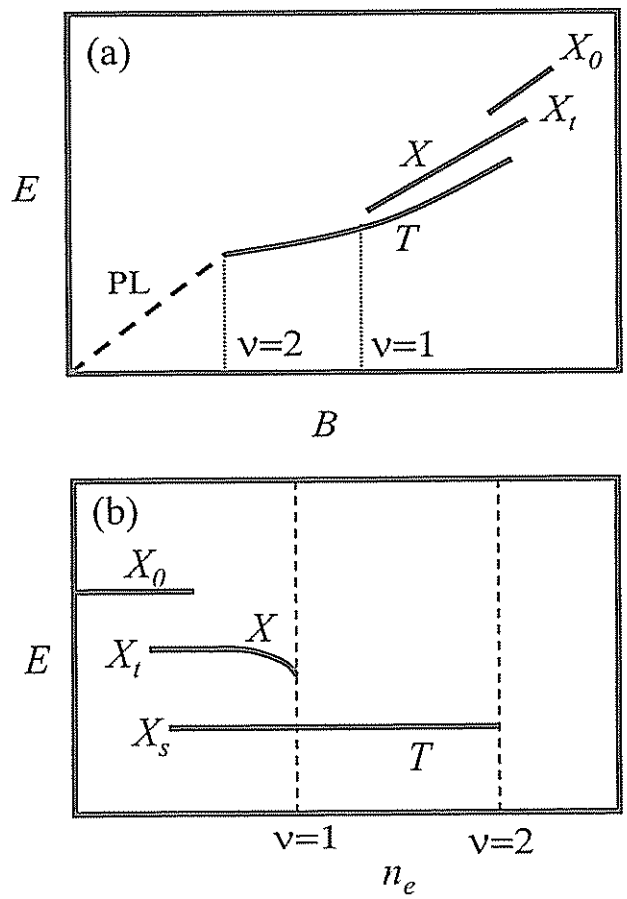

Figure 3.12: Scheme of the evolution of the hole-bound complexes in absorption (solid line) with the magnetic field, B, and the 2DES density, n_e. For $\nu < 1$, a single line, T, dominates the spectrum. For $\nu > 1$, the X-line appears at a higher energy. At low enough densities and higher B, the X_0 may appear. For $\nu > 2$, absorption is impossible because the lowest Landau level is full. The photoluminecence line (dashed) is known to change its dispersion at $\nu = 2$ from Landau-level like (linear in B) to excitonic-like (with quadratic term).

symmetry mechanism [4].

[4] See section 1.2.2

Chapter 4

The spectrum around $\nu = 1$: the Skyrmion regime

4.1 The oscillators strength around $\nu = 1$

In Chapter 1 we have discussed the effect of the polarization in the dichroism of the absorption. In figure 1.1 and 1.2 it was shown that the absorption into the lower Zeeman level, i.e. the $\uparrow$-absorption, is quenched at $\nu = 1$ due to the the abrupt spin-polarization of the 2DES. This effect, in conjuction with the observed increase in absorption into the upper Zeeman level, $\downarrow$-absorption, at $\nu = 1$, was mentioned as an early evidence for Skyrmions. Indeed, this effect was observed in our measurements as well. Figure 4.1 shows a compilation of measurement similar to that of Fig. 3.1, but in a different sample and at the colder temperature of 1.9 K. The onset of the LLL at $\nu = 2$ is clearly seen, and marked with an arrow. In addition to this onset, it is observed that for $B < 0$, corresponding to $\downarrow$-absorption for LH transitions, the signal abruptly increases at the fields corresponding to $\nu = 1$ (see upper left dashed circle). This is also concurrent with a minimum of the signal at $\nu = 1$ for $B > 0$, corresponding to $\uparrow$-absorption (see right dashed circle). The effect is less stark in the HH line. For the HH there there is a clear minimum at $\nu = 1$ for $B < 0$, corresponding to to $\uparrow$-absorption (see lower left

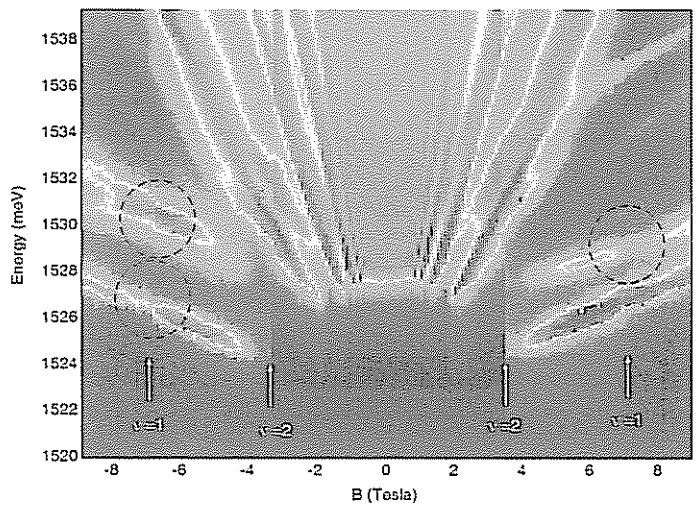

Figure 4.1: (color) Spectra at 1.9 K for sample CBE 1057, color coded as in fig 3.1. The maxima and minima in the absorption at $\nu = 1$ are pointed out by dashed circles (see text).

dashed circle), but the counterpart maximum for $B > 0$ is missing [1].

In order to confirm that this is indeed a filling factor dependent phenomena, we repeated the measurements in Fig. 4.1 for different 2DES densities, namely, different values of V_g. The results are shown in Fig. 4.2. The lower density is plotted in the upper-left corner, and it is increased along the first column towards the bottom of the figure. The density is further increased along the second column, from the top to the bottom. It is observed that onset of the LLL at $\nu = 2$ indeed migrates to higher fields, signaling the increase in the density. In addition, with the exception of the first two plots of very low density, we observe maxima and minima such as those marked by the dashed circles in 4.1, and they also migrate toward higher fields as the density increases, confirming that this is a filling factor phenomenon occurring at $\nu = 1$.

[1] The sharpness of these maxima and minima at $\nu = 1$ shows sensitivity to temperature, sample, 2DES density and hole band (LH and HH). The sensitivity to temperature is readily understood as reflecting the sensitivity of the spin-polarization, $\mathcal{P}$. The sensitivity on sample and density could be due to sensitivity of $\mathcal{P}$ to the disorder present. At higher density this disorder is better screened, and thus the features at $\nu = 1$ become sharper. The dependence on the hole band is not understood. We conjecture that the wavefunction of HH-bound complexes would involve larger components of higher Landau level orbitals due its smaller cyclotron energy. As a result, the OS of the HH and LH transitions are a result of the interplay of two factors. One factor is the 2DES state, and its manifestation in $\mathcal{P}$. This factor is shared by both LL and HH transitions. The second factor is the nature of the excitonic complexes and the role of the Coulomb interactions. This second factor may be different.

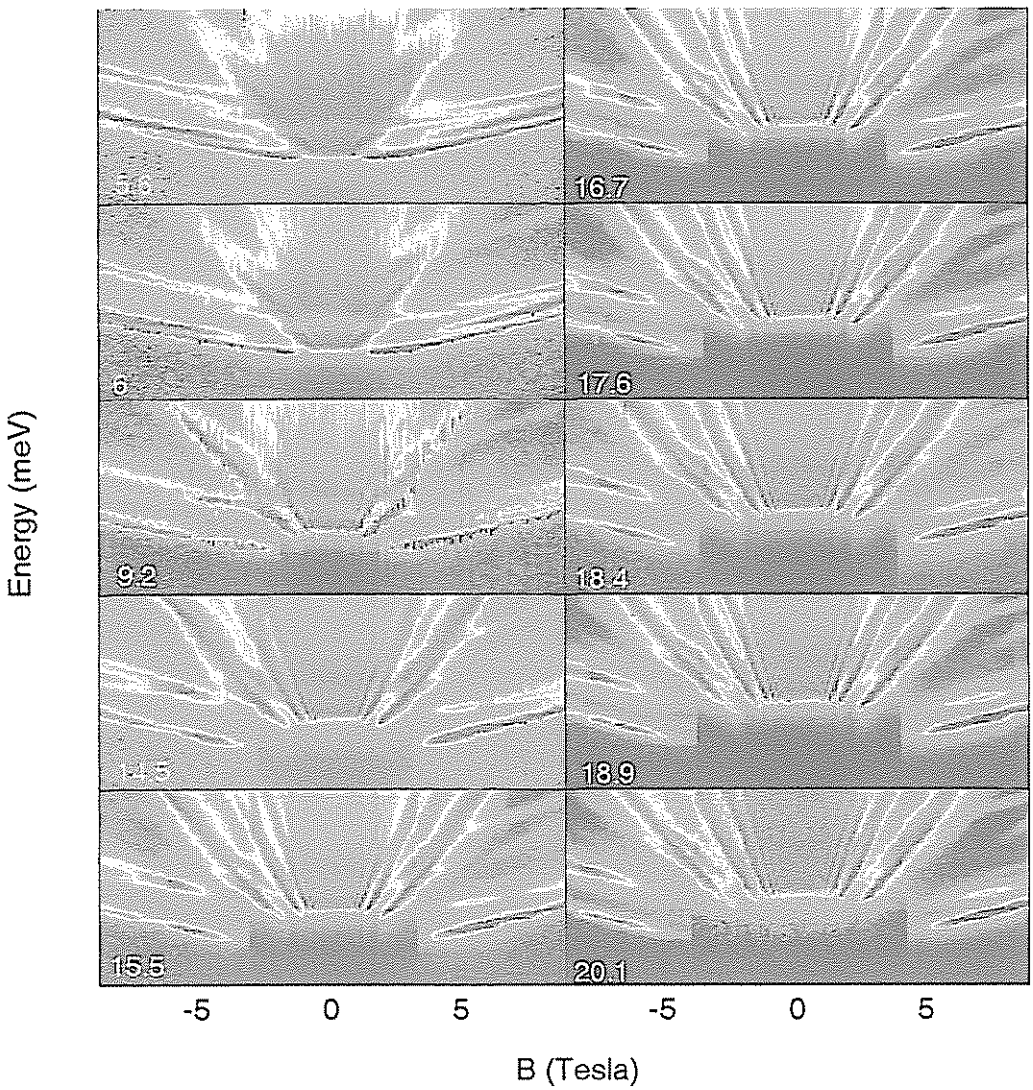

Figure 4.2: (color) Spectra at 1.9 K (as in figure 4.1) for different gate voltages,V_g, from 0 to 0.9 V in steps of 0.1 V. The density is indicated in the figure in units of 10^{10} cm^{-2}.

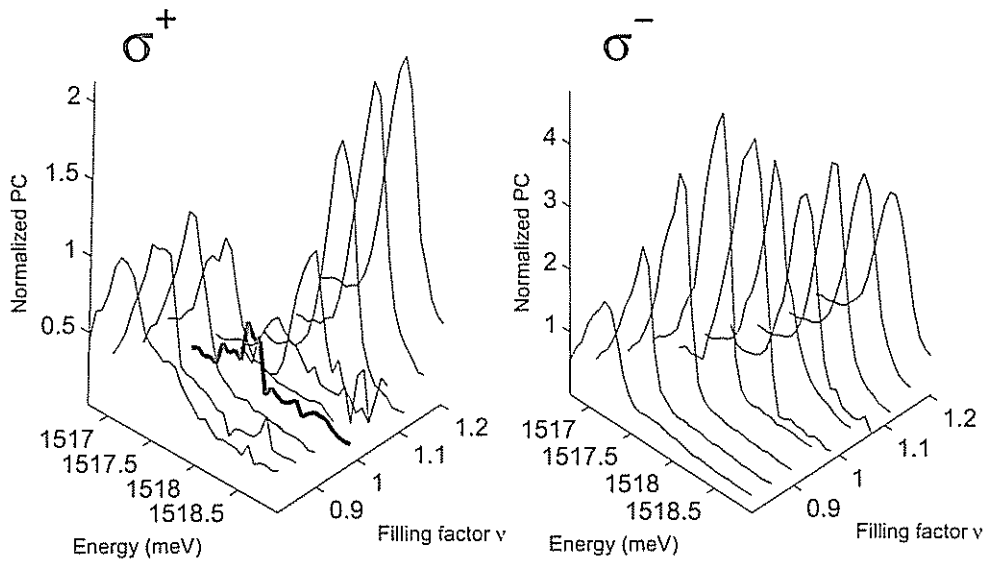

Figure 4.3: Photocurrent spectra of the LLL HH transition at 70 mK in sample Bell1 as n_e is scanned at a constant density field $B = 2.5$ T at both polarizations. At $\nu = 1$, we observe the familiar quenching of the and $\uparrow$-absorption (σ^+) and a strengthening of the $\downarrow$-absoprtion (σ^-).

Figure 4.3 shows spectra of the LL HH transition at both polarizations for a different sample at 70 mK, at constant $B = 2.5$ T as n_e is scanned around $\nu = 1$. Again, we find a strong absorption at $\nu = 1$ for $\downarrow$-absorption (σ^-), corresponding to a quenched absorption for $\uparrow$-absorption (σ^+).

Although the phenomenon of maxima and minima in absorption at $\nu = 1$ can be understood in terms of single particle transitions, as explained in Chapter 1, we have shown in Chapter 2 that hole-bound complexes are formed, and we wish to give an explanation in terms of this complexes. For this purpose, we would like to plot the OS of the T-peak at both polarization. The OS is taken as the area under the peak. In most of the cases, the X partially overlaps the T peak and thus there is need to fit the spectra, such as those in Fig. 3.4, to the sum of two Voigt peaks, and obtain the OS of the T-peak as the integral under the fitted peak.

Figure 4.4 shows the evolution of the OS of the $T_\uparrow$ and $T_\downarrow$ peaks, corresponding to the $\uparrow$ and $\downarrow$-absorption respectively, for LH transitions as B is scanned at constant n_e at 4.2 K. We observe the familiar peak and dip for $T_\downarrow$ and $T_\uparrow$, respectively. A similar result can be obtained

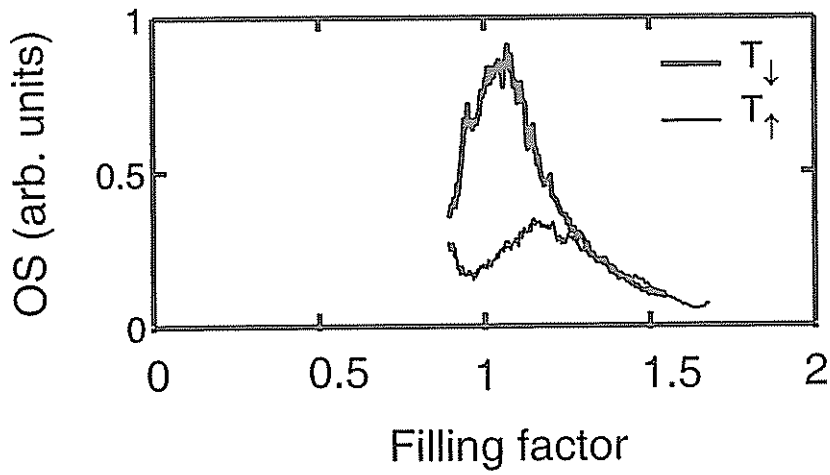

Figure 4.4: The OS of the $T_\uparrow$ and $T_\downarrow$ LH transition at 4.2 K in sample MBE7130 as B is scanned at a constant density $n_e = 1.8 \times 10^{11}$ cm^{-2}. We observe the familiar peak and dip for $T_\downarrow$ and $T_\uparrow$, respectively.

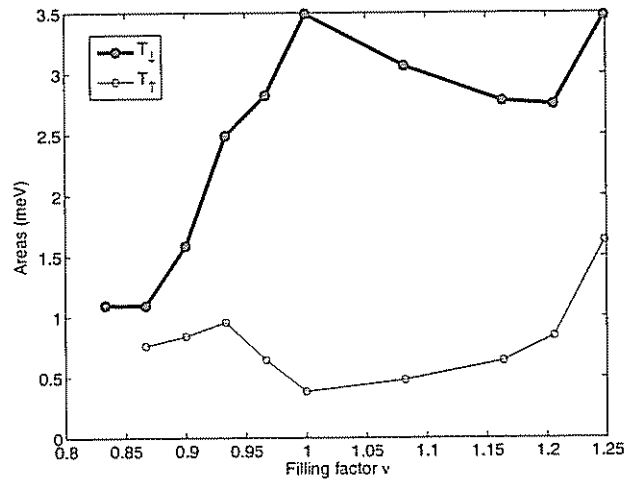

Figure 4.5: The OS of the $T_\uparrow$ and $T_\downarrow$ HH transition at 70 mK in sample Bell1 as n_e is scanned at a constant density field $B = 3.5$ T. We observe the familiar peak and dip for $T_\downarrow$ and $T_\uparrow$, respectively.

for the HH in the dilution fridge. Figure 4.5 shows the evolution of the OS of the $T_\downarrow$ and $T_\uparrow$ for HH transitions at 70 mK as n_e is scanned at constant $B = 3.5$ T. In what follows we present a model in order to account for the evolution of the OS of the T and X-peaks around $\nu = 1$.

4.2 Cooper and Chklovskii states

Cooper and Chklovskii [Cooper and Chklovskii, 1997] presented a theoretical model that was aimed to explain the emission spectrum spectrum around $\nu = 1$. We would like to explain how their work, with some adaptions, is applicable to interpreting the absorption spectrum.

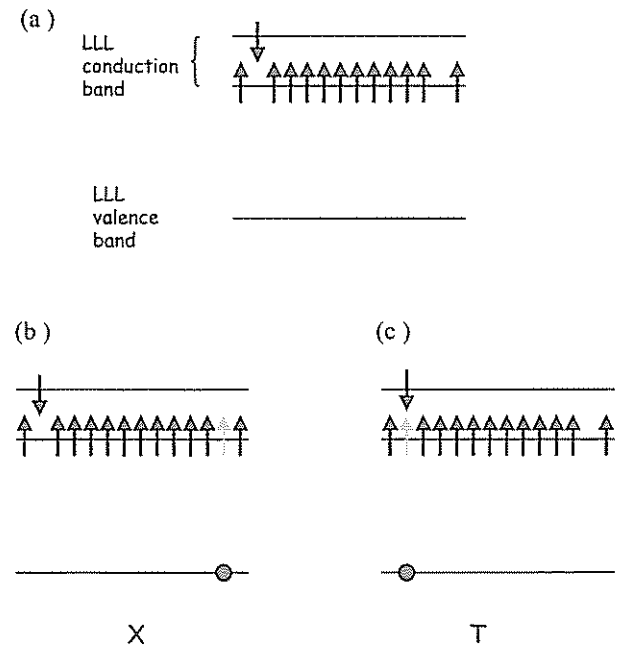

Figure 4.6: (a) Scheme for an hypothetical Fock initial state. This can also represent one term when the true ground state is expressed as a linear combinations of Fock states. The arrows represent electrons occupying orbitals in the lowest Landau level in the conduction band in the corresponding Zeeman level, according to the direction of the arrow. (b,c) two possible Fock final states upon absorption of a photon circularly polarized such that the photoexcited electron, denoted by a light-grey arrow, is created in the lower Zeeman level. The valence hole is shown as a full circle. In the X state, the electron-hole pair is created at infinite distance from the flipped spin, namely, the spin-wave of momentum $k = 0$ ($SW(k = 0)$). In the T state, the photoexcited electron fills-up the quasi-hole involved in $SW(k = 0)$. The difference in energy is discussed in the text.

Consider an hypothetical Fock initial state before absorption that occurs at $\nu = 1 - \epsilon$ as schematized in Fig. 4.6(a). The arrows represent electrons occupying different Landau orbitals in the corresponding Zeeman levels in lowest Landau level (LLL). An incident circularly polarized photon creates a valence hole and an electron in an available orbital in the lowest

Zeeman level. Two different final states are possible, depending on the orbital where the electron-valence hole pair is created. They are schematized in Fig. 4.6(a) and (b) and are labeled X and T, respectively. The valence hole is denoted by a full circle, and the photoexcited electron, by a light-grey arrow. The states X and T correspond to what the authors call in [Cooper and Chklovskii, 1997] 'free-hole' and 'exciton' states, respectively [2].

According to Ref. [Cooper and Chklovskii, 1997], the two final states X and T differ in energy. The difference in energy is estimated as follows. The X state is characterized by a free-hole, namely, a vacancy in the valence band that is surrounded by an homogenous density of electrons filling the lower Zeeman level. In addition to this free-hole, an electron with flipped spin, namely, a *spin-wave* of momentum $k = 0$, $SW(k = 0)$ [Kallin and Halperin, 1984] is present. The energy of a $SW(k = 0)$, assumed to be at an infinite distance from the valence hole, is equal to the bare Zeeman energy $E_z = g\mu_B B$, where $g = 0.44$ is the Lande factor in GaAs and μ_B is Bohr magneton. On the other hand, the T state is characterized by a spin wave of infinite momentum, $SW(k = \infty)$, namely an electron that flipped its spin and is physically removed at infinite distance from the *quasi-hole* left behind in the lower Zeeman level. The $SW(k = \infty)$ is higher in energy than $SW(k = 0)$ by an amount E_{SW} that is equal to the binding energy between the electron and the quasi-hole. Nevertheless, in the T state the valence hole binds to the spin-flipped electron to form an exciton in an homogenous background of electrons a filling the lower Zeeman level (excluding the quasi-hole). This lowers the energy with respect to the free-hole state by the exciton binding energy, E_B. As a result, the difference in energy between the X and T states is given by

[2] There are some differences between the X and T states schematized in figure 4.6 and the actual 'free-hole' and 'exciton' states considered in [Cooper and Chklovskii, 1997]). Since they authors were interested in PL, this two states were regarded as two possible initial states before recombination, and hence including a valence hole. At low temperatures, only one of this states would be present (the lower in energy). Each of this states led to a different final state upon recombination, which is would not be the ground state of the 2DES. For the absorption process, we needed to consider two states including a valence hole that could be connected by an optical transition from the same initial ground state. Therefore, we introduced an extra quasi-hole int the T state that wasn't present in the original 'exciton state'. It is assumed that the quasi-hole would negligibly interact with the exciton. Such requirement will be reflected later in the proposed wavefunction, with the crude assumption that it doesn't interact unless it completely overlaps the exciton, in which case we revert to the X state.

$$E_T - E_X = E_{SW} - E_B \tag{4.1}$$

To determine which state is lower in energy is equivalent to determine if the $\downarrow$-electron can bind more tightly to a quasi-hole or to a valence hole. In the limit of infinite magnetic field, namely within the lowest Landau approximation, and in the strict two-dimensional limit, the answer is that both energies are equal. The envelope wavefunction describing Landau orbitals are the same for all bands. If now the finite width of the QW is taken into account, the valence hole is slightly on a different plane than the electron and the quasi-hole and as a result, $E_{SW} > E_B$. In Ref. [Cooper and Chklovskii, 1997] it was shown that when coupling to the higher Landau levels is included perturbatively for both electrons and hole, the situation is reversed even in the presence of a finite width. Their estimate for the energy difference for usual parameters, such as width of QW and magnitude of the magnetic field, $E_T - E_X \sim -0.5$ meV. This reflects the fact that the electron can bind better to the hole because by having a wavefunction with higher Landau level components.

It must be noted that in the regime where the magnetic field is high enough so that the cyclotron energy is much larger than the binding energies of the excitons and trions, a small component in a high Landau level might have a large influence on these binding energies. As a result, there is no contradiction in treating the inter-Landau level coupling as a small correction to the oscillator strength in spite of its strong effect on the position of the peaks in the spectrum from the energy point of view.

4.3 Modelling the absorption processes

In this section, we will base on the schematic description of the two Cooper and Chklovskii states presented above in order to describe the absorption process and present a quantitative model.

According to the Fermi Golden Rule, the rate of absorption is proportional to the square of the dipole matrix element between the initial state $|i\rangle$ prior to absorption, and the final state

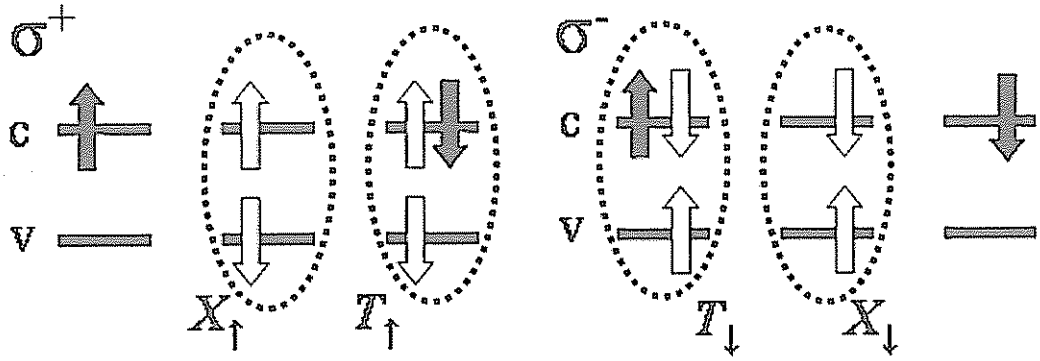

Figure 4.7: Scheme for the absorption processes. The horizontal lines represent spatially localized Landau orbitals in the conduction (c) and valence (v) band. The black arrows represent the electrons existing in the ground prior to absorption and their corresponding spins. The white arrows represent the photo-created electron-hole pairs. The scheme represents a process where the initial state consists of a Fock state of two electrons in different orbitals and with opposite spin. The subscripts correspond to the the spin of the photoexcited electron: in $X_\uparrow$ and $T_\uparrow$-process, an $\uparrow$ electron is created, and similarly of the $\downarrow$ subscript. Two final states are possible in each polarization, depending on the overlap between the photoexcited electron-hole and the preexisting electrons. In the X process, the final state is Fock state where the electron-hole pair are created in empty orbitals. In the T-process, the electron-hole pair is created in a spacial orbital fully overlapping an existing electron. In a correlated state at zero temperature, the wavefunctions of the initial and final states can be expressed as a superposition of such Fock states. In order for each of this terms to contribute to the transition matrix element, the electrons from the ground state do not change their spins nor its orbital during the absorption process, which is instantaneous.

$|f_s\rangle$, where s is the spin of the photocreated electron, depending on the light polarization. In the envelope approximation, the total dipole moment is a constant characterizing the bands involved in the transition times the optical operator matrix element in Eq. 1.4, i.e.

$$I_{f_s} \propto |\langle f_s| \sum_\alpha h^\dagger_{\alpha,-s} c^\dagger_{\alpha,s} |i\rangle|^2, \tag{4.2}$$

where $h^\dagger_{\alpha,s}$ and $c^\dagger_{\alpha,s}$ create a valence hole and a conduction electron, respectively, in state $\phi_{\alpha,s}$, and the sum is over a complete basis. It is evident that to obtain the oscillator strength of each final state f_s there is need to know the exact wavefunction by diagonalizing the interacting Hamiltonian.

Due to the great complexity of the problem, and taking into account our knowledge of the nature of the X and T peaks, we formulate a model based on the following conjecture: the known neutral exciton and singlet trion states evolve upon increasing the 2DES density into two bound complexes, X and T, that correspond to the Cooper and Chklovskii states described above. Both may be created in an absorption process, depending on the energy of the photon. The X complex is created only in orbitals which are *empty in both spin states*, while T is created only in orbitals in which *one electron is already present*. This conjecture preserves the nature of the bound complexes as in the dilute limit, and in particular - the singlet character of T [Whittaker and Shields, 1997]. These absorption processes are schematically summarized in Fig. 4.7 (the graphical representation is slightly different than in Fig. 4.6, see caption).

In order to use this picture in a quantitative model, we need to formulate a final wavefunction for each of the four absorption processes corresponding to X and T and transitions at each light polarization. We construct the wavefunctions such that they fulfill the following conditions and simplifying assumptions:

- In order for each of this terms to contribute to the transition matrix element, the electrons from the ground state do not change their spins nor their orbital during the absorption process, which is instantaneous. Therefore we limit ourselves to consider final states (that are expected to yield a large matrix elements) of the form (up to normalization factors) $|f_s) = \sum_\alpha h^\dagger_{\alpha,-s} c^\dagger_{\alpha,s} \hat{P}_\alpha |i\rangle$, where $\hat{P}_\alpha$ is a projection operator setting the conditions on the initial state for the f_s-absorption process. This operator needs to be defined for each final state X and T in a way consistent with the processes described in Fig. 4.7. We stress that when inserting the the above expression for the final wavefunction in Eq. 4.2, it is made explicit that optical absorption probes the ground state by both probing the *occupation* of the orbitals and their *spacial correlations*.

- We restrict ourselves to the LLL approximation. This amounts to set $\hat{P}_\alpha = 0$ for any state $|\alpha\rangle$ that is not in the LLL.

- In order for the T state to have a hole-bound singlet excitonic complex character, the projector operators $\hat{P}_\alpha$ need to be chosen such that there is a large spacial overlap be-

tween the photoexcited electron-hole pair and an existing electron with opposite spin. A simplifying assumption is to assume that interactions are of short range, and neglect interactions except that of 'nearest neighbors'. Specifically, we will require that there the three particles are fully overlapping. This is accomplished by choosing the projection to be the occupation number operator of the overlapping orbital with opposite spin, namely, $\hat{P}_{k,s} \equiv \hat{n}_{k,-s}$. Here k is the quantum number labeling the single particle spacial orbital $\phi_{k,s}(x)$ in the LLL with spin s, and $\hat{n}_{k,-s} \equiv c^{\dagger}_{k,-s}c_{k,-s}$ is its occupation number operator.

- In X state, we recquire there is a weak overlap between the photoexcited electron-hole pair and an existing electrons. This would allow the X state to preserve its nature as a state where the second electron is weakly bound (as in the triplet states) or not bound at all (as in the neutral exciton). Similarly to the case of the T states, we assume short range interactions and use the 'nearest neighbor' approximation. We assume that only an electron in fully overlapping orbital would be strongly bound to the valence hole, and hence effectively 'screen' the X state. Therefore we will require that in the X state, all orbitals overlapping with the photoexcited electron-hole pair are empty. This is accomplished by choosing the projection to be 1 minus the occupation number operator of the overlapping orbital with opposite spin, namely, $\hat{P}_{k,s} = 1 - \hat{n}_{k,-s}$. This choice of the projection operator also ensures that the X state evolves in the limit of zero density to the neutral exciton wavefunction (in the LLL approximation), namely, $|X_0\rangle = \sum_m h^{\dagger}_{m,-s}c^{\dagger}_{m,s}|0\rangle$.

- Note that the model is formulated in a general basis labeled by α (which includes the quantum numbers k, s) and its accuracy would also depend on the basis chosen [3]. As will be seen later, the calculations are greatly simplified by choosing the the basis of Landau orbitals in the symmetric gauge $\phi_{m,s}(x)$, where m is the angular momentum quantum number [4].

Following the above considerations, we postulate following final states for X and T-absorption:

[3] The basis chosen is appropriate to the extent that the wavefunctions are spacially localized, and the Coulomb interaction between two particles occupying the same spacial orbital is considerably stronger that the interaction between particles in different orbitals.

[4] This amounts to setting $k = m$.

$$
\begin{aligned}
|X_{\downarrow}\rangle &= \sum_{m=0}^{N_\phi - 1} h^{\dagger}_{m,\uparrow} c^{\dagger}_{m,\downarrow} c_{m,\uparrow} c^{\dagger}_{m,\uparrow} \; |\psi\rangle, \\
|T_{\downarrow}\rangle &= \sum_{m=0}^{N_\phi - 1} h^{\dagger}_{m,\uparrow} c^{\dagger}_{m,\downarrow} c^{\dagger}_{m,\uparrow} c_{m,\uparrow} \; |\psi\rangle,
\end{aligned}
\tag{4.3}
$$

where $|\psi\rangle$ is the state of the 2DES prior to absorption. In this expressions, each term includes the product of four operators. The first two operators correspond to the creation of an electron-hole pair. The last two operators constitute the projection operator $\hat{P}_\alpha$ discussed above. Given that $|\psi\rangle$ can be in general expressed as a superposition of Fock states, the projection operator operates on each term yielding 0 or 1. In the T state, it yields 0 for all terms where the created electron-hole pair do not overlap with an existing electron in opposite spin, effectively projecting $|\psi\rangle$ to a subspace where this overlap is full. In the X state, it projects the $|\psi\rangle$ state to a subspace where such overlap is small. For completeness, we write analogous expressions for the opposite polarization:

$$
\begin{aligned}
|X_{\uparrow}\rangle &= \sum_{m=0}^{N_\phi - 1} h^{\dagger}_{m,\downarrow} c^{\dagger}_{m,\uparrow} c_{m,\uparrow} c^{\dagger}_{m,\downarrow} \; |\psi\rangle, \\
|T_{\uparrow}\rangle &= \sum_{m=0}^{N_\phi - 1} h^{\dagger}_{m,\downarrow} c^{\dagger}_{m,\uparrow} c^{\dagger}_{m,\downarrow} c_{m,\downarrow} \; |\psi\rangle,
\end{aligned}
\tag{4.4}
$$

From Eqs. 4.2, it is clear than an explicit expression is needed for both the initial and final states. In what follows, we discuss the wavefunctions for the initial state.

4.4 The ground state of the 2DES

Let us now formulate the initial wavefunction for filling factors around $\nu = 1$. Following Ref. [Fertig *et al.*, 1994] we write the initial state at zero temperature at $\nu = 1$ as

$$|\psi_0\rangle = \prod_{m=0}^{N_\phi - 1} c_{m,\uparrow}|0\rangle. \tag{4.5}$$

The wave function of the 2DES at $\nu = 1 - \epsilon$ containing a single anti-Skyrmion, $\psi_-\rangle$, and the wavefunction at $\nu = 1 + \epsilon$ containing a single Skyrmion, $\psi_+\rangle$, are written as

$$\begin{aligned} |\psi_-\rangle &= \prod_{m=0}^{N_\phi - 1} (u_m c^\dagger_{m,\downarrow} + v_m c^\dagger_{m+1,\uparrow})|0\rangle, \\ |\psi_+\rangle &= \prod_{m=0}^{N_\phi - 1} (-u_m c^\dagger_{m+1,\downarrow} + v_m c^\dagger_{m,\uparrow}) c^\dagger_{0,\downarrow}|0\rangle, \end{aligned} \tag{4.6}$$

with $|u_m|^2 + |v_m|^2 = 1$ and $u_m \to 0$ as $m \to \infty$[5]. In order to understand the structure of the wavefunction, consider the expression for $\psi_-\rangle$ when setting $u_m = 0$ and $v_m = 1$ for all m. The result is a fully spin polarized Fock state, differing from the state at $\nu = 1$ only by a quasi-hole at $m = 0$. In the symmetric gauge, an orbital correspond to a radial distribution peaked at an annulus whose radius grow with m. In particular, the $m = 0$ quasi-hole is in gaussian orbital localized at the origin of coordinates. As explained in Chapter 1, such a state is not energetically favorable. A lower energy state is accomplished by letting the electrons surrounding the quasihole rotate their spin and simultaneously getting closer to the origin. This is accomplished by letting the u_m coefficients at low m, corresponding to orbitals close to the origin, to be finite. The condition that orbitals far away from the origin, namely large m, are not affected and their u_m coefficients vanish. The result is a radial distribution of spin. A similar description applies to the $\psi_+\rangle$ wavefunction, where the electrons shift away from the extra spin at $m = 0$ as u_m is increased.

[5]The expressions are written using the symmetric gauge basis. This is the reason of our choice of this basis in the formulation of the the wavefunctions for the final states.

4.5 Model for the oscillator strength of hole-bound complexes in the presence of Skyrmions

Using the above expression for the initial state, and the expressions for the OS and for the initial and final states from the previous section [Eqs. 4.2, 4.3, 4.4 and 4.6], and disregarding the matrix elements w_α associated with the bands, it is possible to straightforwardly to show [6] that the OS can be written explicitly for the four absorption peak lines as

$$\begin{aligned} I_{X_{\downarrow,\uparrow}} &= N_a\left(|v_0|^2 + \sum |u_{m-1}|^2|v_m|^2\right) + \\ &+ N_s\left(\sum |v_{m-1}|^2|u_m|^2\right), \\ I_{T_\downarrow} &= N_\phi - (N_s + N_a)\left(1 + \sum |u_{m-1}|^2|v_m|^2 + |u_m|^2\right), \\ I_{T_\uparrow} &= (N_s + N_a)\left(|u_0|^2 + \sum |u_{m-1}|^2|u_m|^2\right), \end{aligned} \tag{4.7}$$

where all sums are over m from $m = 1$ to $m = N_\phi - 1$, and N_s and N_a are the number of Skyrmions and anti-Skyrmions, respectively. Equation (4.7) allows us to calculate the OS dependence on ν at zero temperature, where $N_s = N_\phi(\nu - 1)$, $N_a = 0$ for $\nu > 1$ and $N_s = 0$, $N_a = N_\phi(1 - \nu)$ for $\nu < 1$.

It should be noted that the wavefunctions of the initial states in Eq. 4.6 were given only for filling factors departing from 1 only by a single flux quantum. We assume that for larger departures from $\nu = 1$, there exists a dilute gas of noninteracting Skyrmions. This puts a limitation on the range of validity of the model, although this limit is not well understood. In section 5 we will briefly discuss the issue from a phenomenological point of view.

We can obtain insight on what the u_m coefficients might be by comparing the model predictions with the experimental OS of T and X. Figure 4.8b shows the calculated OS of the T peak at both polarizations, obtained for two initial states: an initial Skyrmionic state (solid lines), and a non-interacting Fock state which minimizes the Zeeman energy only (dashed lines), which can be referred to as the 'zero-size' Skyrmion.

[6] Details of the caluclations are given in appendix B.

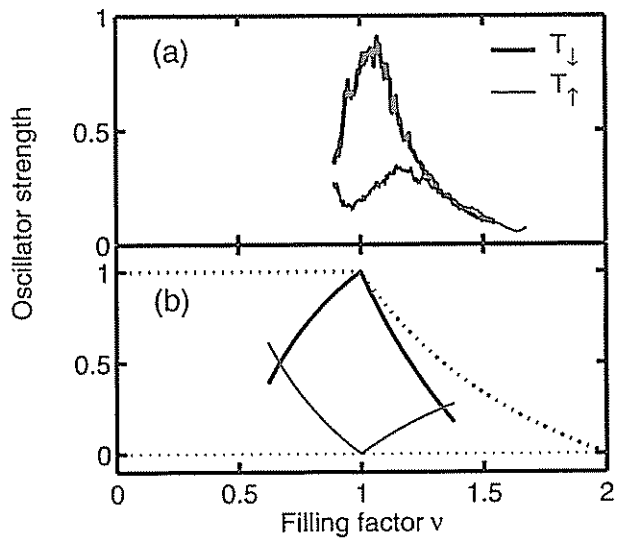

Figure 4.8: (a) The oscillator strength of T_{lh} for both polarizations at constant $n_e = 1.8 \times 10^{11}$ cm^{-2}. (b) The calculated values of $|M_{T,\downarrow}|^2$ and $|M_{T,\downarrow}|^2$ with $u_m = \delta_{m,0}$ as B is scanned. The dotted line corresponds to free electron picture ($u_m = 0$). The values of I are normalized by dividing by $N_\phi|_{\nu=1}$.

The 'zero-size' Skyrmion state was obtained by setting all $u_m = 0$, as discussed previously. In such a state, $T_\uparrow$ peak is predicted to vanish for all ν's above and below 1. The vanishing for $\nu > 1$ is easily understood by noting that the electrons minimize the Zeeman energy by completely filling the lowest Zeeman level, and absorption is impossible for any transition into this level, wether excitonic or single-particle transition, due to the Pauli principle. The vanishing of the OS of the $T_\uparrow$ for $\nu < 1$ is understood by noting that in this regime, the 'zero-size' Skyrmion state is fully polarized and there are no electrons in $\downarrow$-states to be bound by the photocreated electron-hole pair.

The predictions for the $T_\downarrow$ in the 'zero-size' Skyrmion state are understood as follows. For $\nu > 1$, there is no shortage of $\uparrow$-electrons to pair with the photoexcited electron, and thus the only limitation is the available phase space, namely, the number of empty orbitals in the upper Zeeman level. In this respect, this is the same evolution that would be expected in the single particle model of optical transitions described in section 1.2.3: as ν increases above 1, the number of available orbitals decreases and so does the OS. Below $\nu = 1$, it is seen that the OS

remains constant. This is understood by noting that the initial states were carefully defined as to include a constant number of electrons, and the change in filling factor is introduced as a change in the degeneracy of the LL. This was done to reproduce an experimental setup in which ν is scanned by changing the magnetic field at constant density. For $\nu < 1$, all the electrons are $\uparrow$-states and available to be bound, and therefore the OS of $T_\uparrow$ is limited only by the number of these electrons, and thus is constant [7].

Evidently, the behavior of the T-absorption cannot be explained by a single-particle picture where all $u_m = 0$. On the other hand, if we assume that the ground state includes a small but finite-size Skyrmion with at least $u_0 \neq 0$, the model reproduces the experimental findings qualitatively. The solid lines shown in Fig. 4.8b were obtained by assuming a small Skyrmion where we allow only one coefficient to be nonzero. For simplicity we set $u_m = \delta_{m,0}$. This small Skyrmion is enough to reproduce qualitatively the peak and dip in the evolution of the OS of the $T_\downarrow$ and $T_\uparrow$, respectively. The asymmetry in the slope and curvature of the lines around $\nu = 1$ reflects the fact that the degeneracy of the LLL is being changed as ν is scanned by changing the field. This change is neither linear in ν nor symmetric around $\nu = 1$.

Assuming a larger Skyrmion, namely one in which several u_m coefficients are allowed to be large, would result in a sharper peak and sharper dip in the of the $T_\downarrow$ and $T_\uparrow$. Due to the many approximations and simplifications included in the present model, it would not be meaningful to fit the u_m parameters to reproduce the measurement quantitatively. Therefore it will suffice to say that a from a qualititative comparison, the conclusion from the analysis of the T-absorption is that the results cannot be explained within by a 'zero-sized' Skyrmion ground state, and it requires the presence of some finite size spin texture.

In spite of the above, further information on the Skyrmion size can be inferred from an analysis of the X-absorption. Indeed, the behavior of the X-absorption, which vanishes for $\nu > 1$, sets an upper bound for the Skyrmion size. It follows from Eq. (4.7) that the X-absorption is strongly asymmetric with respect to $\nu = 1$. In order to explain the observed vanishing of the OS for $\nu > 1$ one has to assume that $u_m \approx 0$ for $m \geq 1$. This implies that only

[7] Our can be easily modified to reproduce a measurement in which ν is tuned by scanning n_e at constant field. In this case the OS of the $T_\uparrow$ would decrease linearly at both sides $\nu = 1$ to vanish at $\nu = 0$ and at $\nu = 2$. Although the result would look like a peak at $\nu = 1$, such peak is relatively blunt and cannot account to the sharp peaks observed.

electrons at $m = 0$ and 1 contribute significantly to the Skyrmion.

This result follows from the assumption that the exciton is formed in orbitals where both spin states are empty, implicitly allowing the nearest neighboring orbitals to be occupied [Eq. (4.6)]. If one requires that these orbitals are also unoccupied, the upper bound on the Skyrmion size will be higher. Thus, the actual number of electrons involved in a Skyrmion may be larger than two, but of this order of magnitude. The conclusion is that only a few electron orbitals participate in the Skyrmion texture.

In conclusion, the present model manages to account for the presence of two peaks in the spectrum and explains in a consistent way the behavior of the OS both peaks in terms of an initial ground state consisting of small-sized Skyrmions.

4.6 The dependence of the energy on the filling factor

Remarkably, the energy of the T-peak and its width exhibit a symmetry around $\nu = 1$. Figure 4.9(a) shows the energies of the X_{LH} and T_{LH} for absorption into the upper Zeeman level ($B < 0$) as a function of ν. Here n_e is varied at constant magnetic field. It is seen that the T energy is maximal at $\nu = 1$ and drops symmetrically at both sides. Similarly, we show in Fig. 4.9(b) the full width at half maximum of the T_{LH} peak in the same polarization. It is clearly seen that the width is minimal at $\nu = 1$ and rises symmetrically at both sides. These observations are another manifestation of the electron-hole symmetry of the Skyrmionic ground state [8]. A quantitative treatment of this behavior is, however, beyond the scope of this work.

[8] Such a behavior was also observed in the evolution with the magnetic field, where the energy of the T_{LH} for $B < 0$ showed a kink at $\nu = 1$. We note that the HH we obtained mixed results. Indeed the energy of the T_{HH} did not show any feature at $\nu = 1$. Nevertheless, the energy splitting $X - T$ for the HH at $B > 0$ (absorption into the upper Zeeman) did increased as ν decreased as in the $LH, B < 0$ case. None of this occurs for absorption into the lower Zeeman for LH nor HH, where the energies and widths do not show any filling factor sensitivity, namely, the $X - T$ energy splitting is relatively constant and the energies and widths do not show kinks at $\nu = 1$.

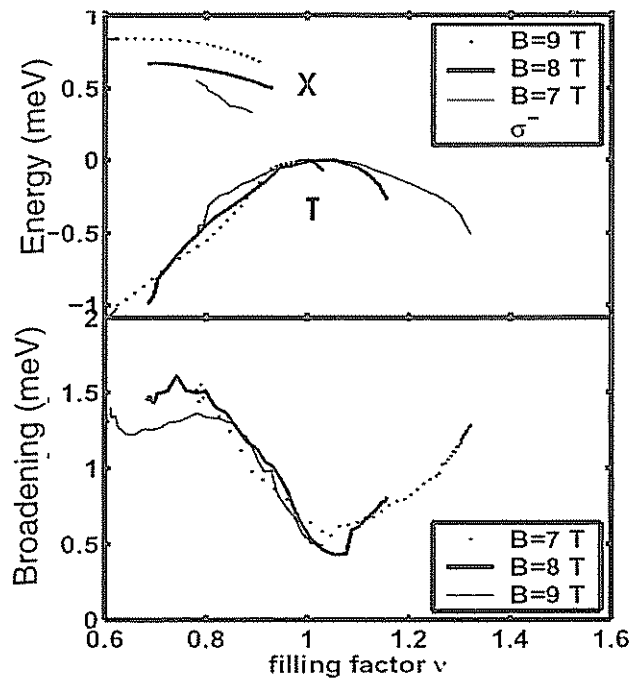

Figure 4.9: (a) The energies of the X and T peaks corresponding to LH transitions into the upper Zeeman level (corresponding to negative B according to the convention in the text) as n_e is varied at constant B, at 4.2 K for sample MBE7130. For clarity, at each magnetic field the energy corresponding to the T peak at $\nu = 1$ is substracted. This procedure effectively removes the single-particle magnetic energy. (b) Full width at half maximum of the T peak for LH transitions. Notice the symmetry of the energy and width around $\nu = 1$.

Chapter 5

The spin polarization at low temperatures

5.1 Spectra at dilution temperatures

We would like to open the chapter with a simple prediction that arises from the discussion so far. If indeed the T state is of a singlet character, and the absorption process does not include second order spin-flip processes, then we would predicted that at low temperatures and low filling factors (far from the Skyrmion regime), in a regime where the 2DES is spin polarized, the T-state should be observed only in one polarization, namely, the polarization corresponding to $T_{\downarrow}$ transitions. As a result, in this regime, for $B < 0$ the HH transitions should include only one peak, $X_{\uparrow}$, while for $B > 0$ both the $T_{\downarrow}$ and $X_{\downarrow}$ should be present. This prediction should be robust and not depending on the exact details in the formulation of the model, such as the choice of basis, the effective range of the interaction and the number of neighboring orbitals included in the range. This prediction is confirmed in Fig. 5.1, where the $T_{\uparrow}$ peak is absence for both HH and LH. Thus, the dichroism of the T-peak could be used as a sensitive probe of the spin polarization.

The change on the spectrum due to the increased degree of spin polarization as the tempera-

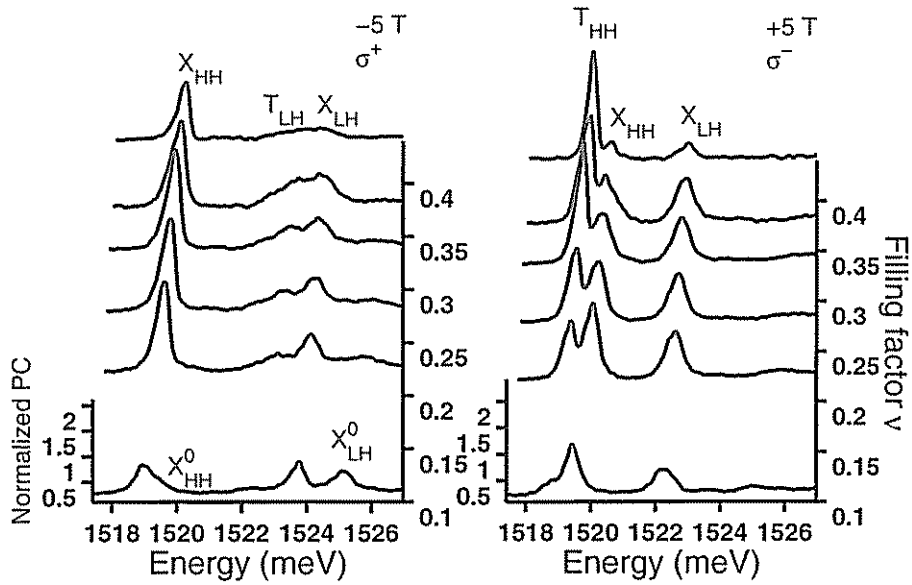

Figure 5.1: Spectra at both polarizations at 70 mK and a constant magnetic field of 5 T in sample Bell1. The T-peak is present only for absorption into the upper Zeeman for both HH and LH. This is a manifestation of the spin-polarization of the 2DES. At the lowest densities, an additional high energy peak appears, X^0, appears for both HH and LH. We attribute it to the neutral exciton

ture is lowered can be nicely seen in our measurements. Figures 5.2a and 5.2b show photocurrent spectra at the σ^+ light polarization that correspond to transitions from the heavy-hole band to the $|\uparrow\rangle$ states in the conduction band at two magnetic fields (solid lines). The left and right spectra are measured at 3.5 and 7 T, respectively. The electron density was tuned by the back gate such as to keep ν approximately constant near 1/3. The spectra are shown for two temperatures, 1.7 K and 70 mK. It is seen that the $T_\uparrow$ peak, which dominates the low field spectrum at 1.7 K completely disappears as the sample is cooled to 70 mK. A similar behavior is seen at the high field spectra. At 1.7 K the 2DES is not spin-polarized and hence there are electrons occupying $|\downarrow\rangle$ states, and they can pair with the photocreated $\uparrow$-electron giving rise to the $T_\uparrow$ peak. The absence of the $T_\uparrow$ peak at low temperatures implies that the 2DES in fully spin polarized at $\nu = 1/3$, i.e $\mathcal{P} = 1$. This description is confirmed by the fact that in

the σ^- polarization, which corresponds to transitions to $|\downarrow\rangle$ states, the T_1 peak persists at low temperatures (Fig. 5.2b, dashed line).

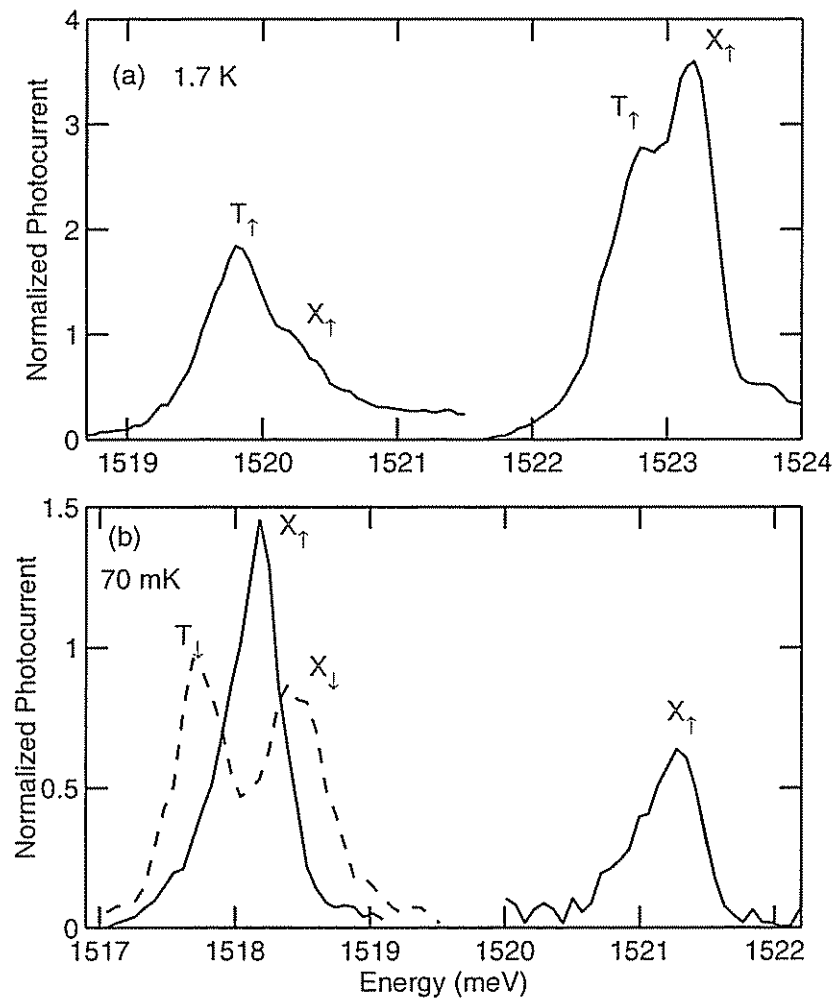

Figure 5.2: Photocurrent spectra at the σ^+ light polarization at $\nu \sim 1/3$ for $3B = 3.5$ and 7 T, shown at left and right, respectively, at two different temperatures: (a) at 1.7 K, and (b) 70 mK.(upper scheme) Schematic mechanism for the T, and X peaks. In the σ^+ light polarization, the $T_\uparrow$- peak is due to photocreated $\uparrow$-electrons (white arrows) pair with $\downarrow$-electrons from the 2DES (black arrows), and similarly for the $T_\downarrow$-peak. As the the 2DES cools down, it becomes spin polarized the $T_\uparrow$ peak disappears.

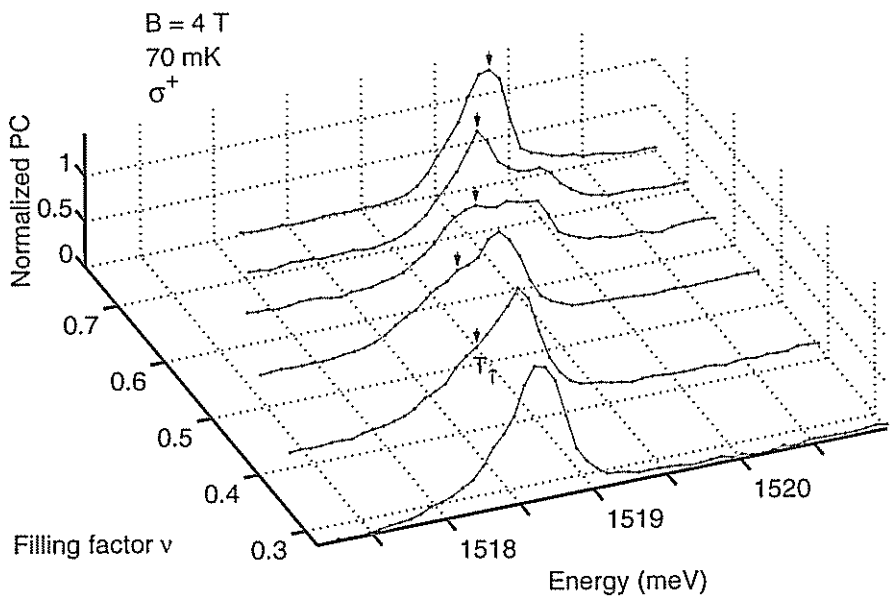

Figure 5.3: Photocurrent spectra at the σ^+ light polarization at constant $B = 4$ T versus ν as n_e is scanned. As ν increases, the $T_\uparrow$-peak, marked by the arrows, appears and increases.

Let us turn into examining the dependence of the polarization on the filling factor at low temperatures. Figure 5.3 shows the σ^+ spectra at 70 mK and constant magnetic field, $B = 4$ T, for $0.3 \lesssim \nu \lesssim 0.7$. We find that as ν increase the $T_\uparrow$ peak gradually appears and gains strength. Since the $T_\uparrow$ peak is associated with binding to an electron at the upper Zeeman level, the observed behavior indicates that the 2DES undergoes a depolarization. In particular, it is seen that around $\nu = 2/3$ the $T_\uparrow$ peak is well developed. A similar behavior is observed over a relatively broad magnetic field range. Figure 5.4 shows spectra taken near $\nu = 2/3$ at several magnetic field between 3 and 5 T. It is seen that the $T_\uparrow$ peak appears in all spectra, and becomes the dominant one as the field increases.

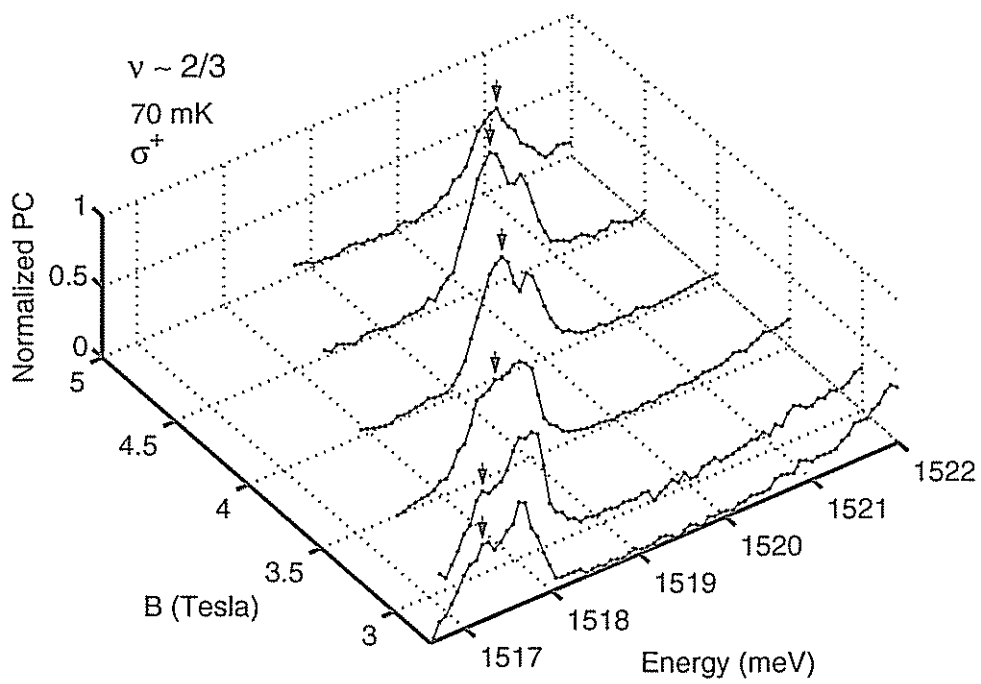

Figure 5.4: Photocurrent spectra at the σ^+ light polarization at $\nu \sim 2/3$ T versus B. The T_1-peak, marked by the arrows, is present throughout the range, and increases with B.

5.2 The trion dichroism

Much information can be obtained from an analysis of the dichroism of the trion absorption line. The dichroism is defined as

$$\mathcal{D} = \frac{I_{T_\uparrow} - I_{T_\downarrow}}{I_{T_\uparrow} + I_{T_\downarrow}} \tag{5.1}$$

It is a complex task to accurately relate the dichroism results to the absolute polarization. Nevertheless, an argument can be made to see they are both closely related. In order to make a quantitative analysis of the spin polarization, there is need for a model relating the OS to $\mathcal{P}$. We shall again base the analysis on the absorption mechanisms schematized in Fig. 4.7, in a previous chapter. In this case, there is difficulty in predicting the OS of the absorption because the wavefunction is not known in general, and in the cases that there is an available trial wavefunction, as in the case of Laughlin wavefunction for $\nu = 1/3$ [Laughlin, 1983], it is not known how to express it in terms of single electron operators. On the other hand, we don't intend to predict the result of the OS, but to infer information from it. Therefore we proceed as follows:

Since the photo-created electron needs to pair with an opposite spin, we assume that the OS of each T peak, $I_{T_{\uparrow(\downarrow)}}$, is proportional to the number of unpaired electrons with opposite spin, i.e.

$$I_{T_\downarrow} = C f_\downarrow N_\downarrow = C f_\downarrow N_e \frac{1}{2}(1 - \mathcal{P}) \tag{5.2}$$

$$I_{T_\uparrow} = C f_\uparrow N_\uparrow = C f_\uparrow N_e \frac{1}{2}(1 + \mathcal{P}). \tag{5.3}$$

Here $N_{\downarrow(\uparrow)}$ is the number of $\downarrow$ ($\uparrow$) - electrons, $\mathcal{P} \equiv (N_\downarrow - N_\uparrow)/N_e$, and C is an unknown constant, which includes the normalization factor I_0. The factor $f_{\downarrow(\uparrow)}$ is the fraction of $\downarrow$ ($\uparrow$) - electrons that are *unpaired*, i.e. that occupy orbitals where the state of opposite spin is empty. In an uncorrelated gas in the LLL approximation, this factors are proportional to the single-particle phase space available, i.e. $f_\downarrow = 1 - N_\uparrow/N_\phi$. In a strongly correlated 2DES, the

Coulomb repulsion tends to minimize the number of paired electrons. Therefore, for $\nu \leq 1$, we shall assume that in the ground state all the electrons are unpaired, i.e. $f_{\downarrow,(\uparrow)} = 1$. We stress that this model does not restrict the trion wavefunction to be in the lowest LL. Using Eq. 5.2 the spin polarization for $\nu \leq 1$ can then be expressed as

$$\mathcal{P} = \frac{I_{T_\uparrow} - I_{T_\downarrow}}{I_{T_\uparrow} + I_{T_\downarrow}} \tag{5.4}$$

Note that in this expression the constant C cancels out, and hence also the normalization factor I_0. This cancelation holds also when C varies with B and ν. This simple model interprets that the dichroism is identical to the spin polarization. We stress that this approach neglects the effect of valence band mixing [1].

For $\nu \geq 1$, the assumption that all electrons are unpaired does not hold, and we shall assume that the number of doubly occupied orbitals is minimal and equals to $N_e - N_\phi$. Thus, $f_\downarrow = [N_\downarrow - (N_e - N_\phi)]/N_\downarrow$ and similarly for $f_\uparrow$. From Eq. 5.2 we obtain that the expression for $\mathcal{P}$ for $\nu \geq 1$ is as in Eq. 5.4 but multiplied by $(2-\nu)/\nu$. This argument can be better explained with the help of the scheme in Fig. 5.5. The scheme shows different configurations of electrons in the initial state in the conduction band (no valence holes).To see the effect of the electron correlations, we express the f factors in Eq. 5.2 in terms of the number of doubly occupied orbitals N_d as $f_\downarrow = (N_\downarrow - N_d)/N_\downarrow$, and similarly for $f_\uparrow$. In a strongly correlated 2DES, the Coulomb repulsion minimizes N_d. For $\nu \leq 1$, Pauli principle does not restrict the minimal N_d, and it vanishes ($N_d^{min} = 0$). Near any electron, an electron with the opposite spin can be photocreated without being forbidden by the Pauli principle, and thus $f_{\downarrow(\uparrow)} = 1$. For $\nu > 1$, N_d cannot vanish: the minimal value that N_d can assume is $N_d^{min} = N_e - N_\phi$. N_d^{min} can also be expressed as $N_d^{min} = N_\phi(\nu - 1)$. Using Eq. 5.2 with the assumption that N_d assumes the minimal value possible at each value of ν, i.e. $N_d = N_d^{min}$, the spin polarization then can be expressed as

[1] In magnetic field, the different spin of the HH levels mix in different degree with the LH band and the strength transition is different. In such cases the C factors for $T_\uparrow$ and $T_\downarrow$ would be different and would not cancel. For a more accurate model, there is need to know the relation between the coefficients. The evolution of the mixing with magnetic field is also specific for each QW structure and should be done numerically (as for example in [Duque *et al.*, 2004]). Published work shows the calculated energies but not the coefficients or oscillator strengths. An exception is [G. Bauer and T. Ando, Phys. Rev. B 38 6015 (1988), Fig. 21], which shows in that the OS of a HH-exciton (Γ_{7g}) is almost the same for both polarizations $\sigma^{\pm}$ for a 100 Å QW.

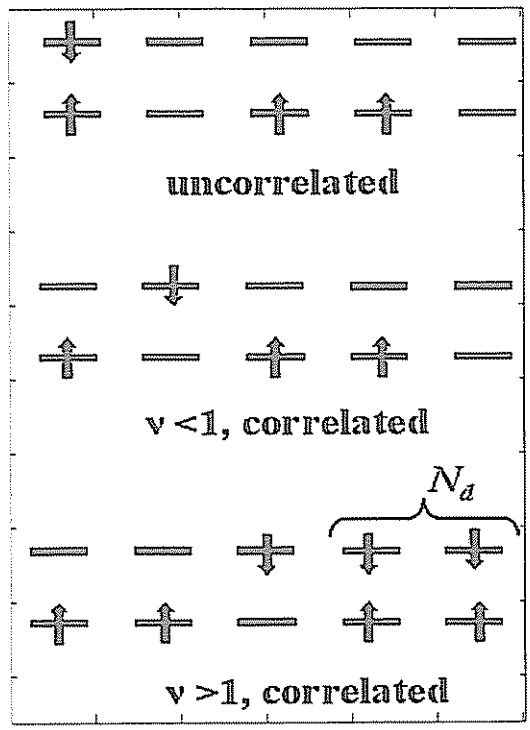

Figure 5.5: This diagram illustrates the meaning of the correlations. We schematize different configurations of electrons in the initial state (no valence holes). Each segment represents an orbital in the conduction band. In an incorrelated 2DES, orbitals can be doubly occupied with electrons at both spins. In a correlated 2DES, as long as $\nu < 1$ this double occupation can be avoided. For $\nu > 1$, there is minimum number of doubly occupied orbitals N_d.

$$\mathcal{P} = \alpha \frac{I_{T_\uparrow} - I_{T_\downarrow}}{I_{T_\uparrow} + I_{T_\downarrow}} \tag{5.5}$$

where $\alpha = 1$ for $\nu \leq 1$, and $\alpha = (2 - \nu)/\nu$ for $\nu \geq 1$.

It can be seen from Eq. 5.2 that $I_{T_{\uparrow(\downarrow)}}$ depend linearly on N_e, hence both T peaks are expected to increase with n_e. This behavior is best observed in Fig. 5.4, where the rise of the $T_\uparrow$ between different fields at constant ν is due to the increased electron density. It can be seen also that $I_{T_\uparrow} + I_{T_\downarrow} = CN_e$. Thus, an alternative way of getting the polarization is to estimate the constant C from the slope of $I_{T_\uparrow} + I_{T_\downarrow}$ versus n_e, and then calculate $\mathcal{P}$ by

$\mathcal{P} = 1 - 2I_{T_\uparrow}/(n_e C)$. The results for $\mathcal{P}$ are qualitatively similar to those obtained from Eq. 5.5.

The oscillator strengths $I_{T_{\uparrow,\downarrow}}$ are proportional to the area under the T peaks. Hence, they are obtained (up to a multiplication constant) by fitting each spectrum to a sum of two Gaussians. Figure 5.6a shows the area of $T_\uparrow$ and $T_\downarrow$ as a function of ν at $B = 2.75$ T. It is seen that the $T_\uparrow$ peak is finite throughout the range $\nu \gtrsim 1/3$ and exhibits a dip at $\nu = 1$, where there is a maximum in $T_\downarrow$. The overall rise in the two signals is due to the increased electron density.

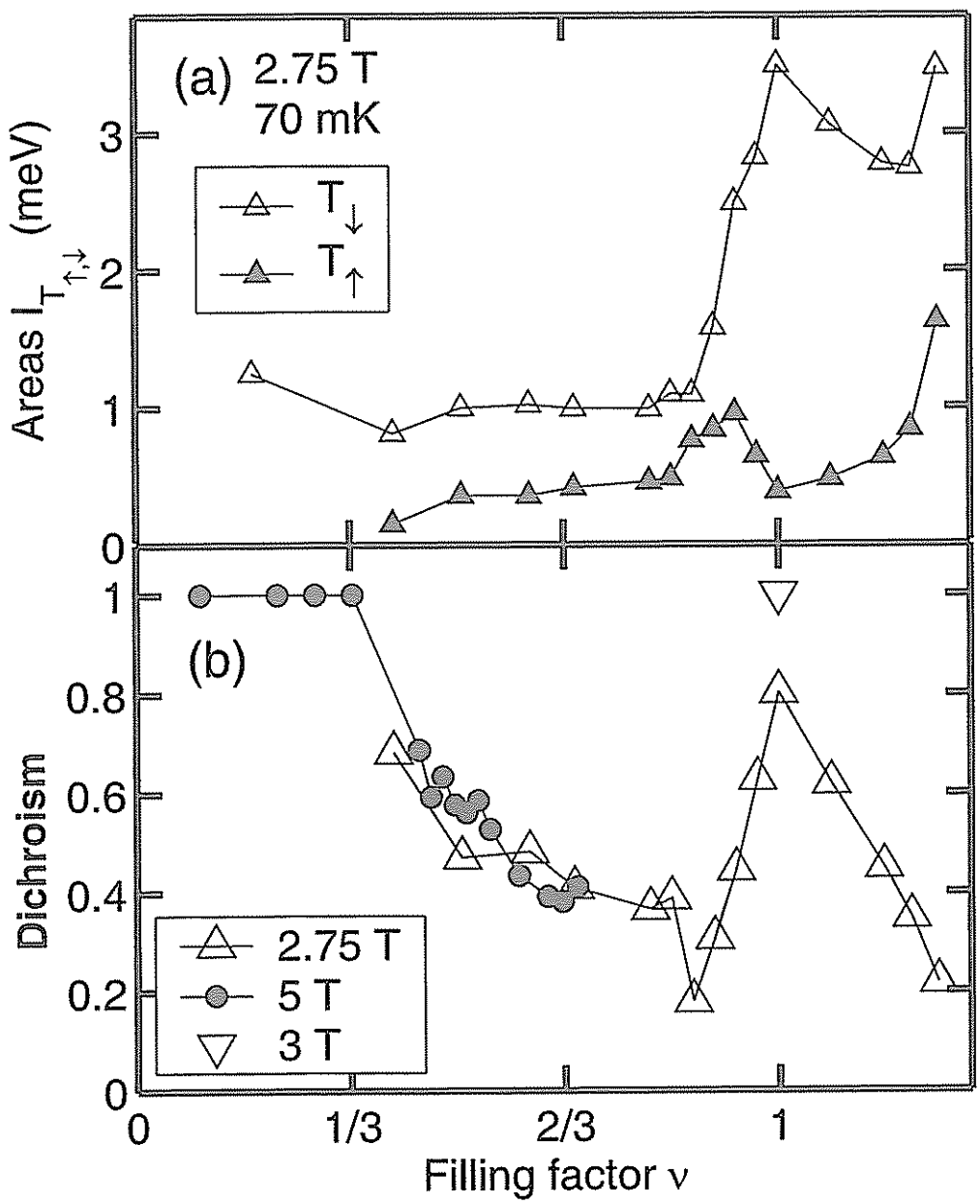

Figure 5.6: (a) The oscillator strength (OS) of the trion for the heavy hole at 70 mK versus filling factor ν as the density N_e is varied at constant magnetic field $B = 2.75T$, at both polarizations. (inset) The sum of the OS of $T_\uparrow$ and $T_\downarrow$ versus N_e. (b) The trion dichroism, $\mathcal{D}$, versus ν at constant B. For $\nu > 1$, the data shown is $\mathcal{D}$ multiplied by the factor α (see Eq. 5.5).

5.3 Discussion

The resulting spin polarization, using Eq. 5.4, is shown in Fig. 5.6b for two magnetic fields, 2.75 and 5 T. The observed depolarization around $\nu = 1$ is well studied and can be attributed at these low fields to Skyrmion formation [Fertig *et al.*, 1994, Sondhi *et al.*, 1993]. We notice, however, that the 2DES appears to be not fully polarized at $\nu = 1$. It could be attributed to an uncertainty in the density and the sharpness of the depolarization peak. Indeed, in a similar measurement at $B = 3$ T we found that $\mathcal{P}_{\nu=1} = 1$. As ν decreases below $\nu \approx 0.8$ there is a sharp increase in polarization followed by an intermediate range around $\nu = 2/3$, where the 2DES exhibits a more gradual re-polarization. As ν approaches 1/3 the increase in $\mathcal{P}$ is becomes again sharp, resulting in a fully polarized 2DES at low ν. We conduct these measurements at several magnetic fields in the range 2.75 - 6 T. We find that this pattern of the behavior of the polarization in the intermediate range is similar throughout the range. The filling factor at which the minimum of $\mathcal{P}$ occurs moves to lower ν's with increasing magnetic field, but the second step is always at $\nu \approx 1/3$. To investigate the polarization at $\nu = 2/3$, we plot $\mathcal{P}$ as a function of B as n_e was adjusted to keep ν constant (Fig 5.7). The field range at which we could achieve $\nu = 2/3$ and obtain well resolved excitonic peaks is between 2.75 to 5 T. We find that the 2DES is partially polarized throughout this magnetic field range, with $\mathcal{P}$ $\sim 1/2$.

A partially polarized phase at $\nu = 2/3$ was found in several other experiments. Photoluminescence measurements in heterojunctions, which investigated the transition from $\mathcal{P} = 0$ to $\mathcal{P} = 1$ at this filling factor, revealed a plateau of constant $\mathcal{P} = 1/2$ within the transition region, extending over a narrow magnetic field range of $\delta B = 0.3$ T around ~ 2 T [Kukushkin *et al.*, 1999]. A broader plateau of partial polarization at $\nu = 2/3$ was found in NMR measurements in QW's [Freytag *et al.*, 2002, 2001]. The plateau was found to extend for at least $\delta B \sim 1$ T, with $\mathcal{P} \sim 3/4$. An insight into the origin of the partially polarized phase was provided by recent spectroscopic NMR measurements, who showed that there is an inhomogeneous mixture of fully polarized and fully unpolarized regions at $\nu = 2/3$ [Stern *et al.*, 2004]. The relative weights of these regions could not be quantitatively determined in that experiment. Another evidence

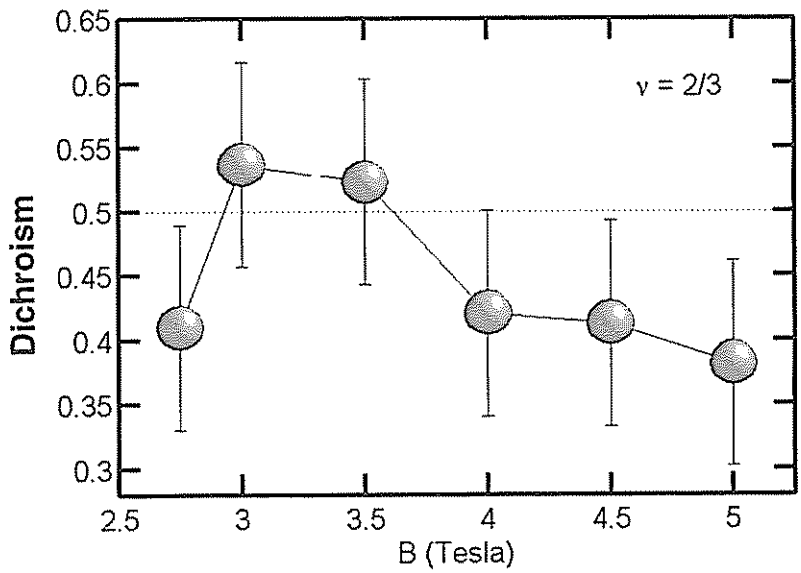

Figure 5.7: The trion dichroism at constant $\nu = 2/3$ as the magnetic field is varied. The dotted line is the theoretical value predicted for $\mathcal{P}$ for a plateau of constant partial spin-polarization.

for such inhomogeneous mixture was provided by the observation of the breaking in the selection rules for phonon excitation [Schulze-Wischeler *et al.*, 2004], and also by the observation of hystheresis in the spin phase transitions [Smet *et al.*, 2001].

The occurrence of a partially polarized phase at $\nu = 2/3$ is of considerable theoretical interest [Mariani *et al.*, 2002, Murthy, 2000, Vyborny and Pfannkuche, 2004]. One suggested explanation for this effect is the formation of a periodic array of polarized and unpolarized domains induced by the periodicity of the GaAs crystal, giving rise to an average $\mathcal{P} = 1/2$ over a relatively broad magnetic field range [Murthy, 2000]. An alternative model explains it in terms of the residual interaction between CF's [Mariani *et al.*, 2002]. This model predicts a plateau of $\mathcal{P} = 1/2$ within a narrow magnetic field range of $\delta B \sim 0.2$ T, in good agreement with the photoluminescence measurements [Kukushkin *et al.*, 1999].

We find that the partially polarized phase is stable over a broad range of at least $\delta B = 2.25$ T. This range is an order of magnitude larger than that found in Ref. [Kukushkin *et al.*, 1999], and it shows that the pattially polarized phase reaches into lower fields than has been previously found in NMR measurements [Freytag *et al.*, 2001]. We note that the experiment of Ref. [Kukushkin *et al.*, 1999] was conducted in a heterojunction, where the magnetic field at which the the critical field, B_c, at which the 2DES becomes fully polarized, is rather low. In QW's the Coulomb interactions at a given n_e and ν are larger, and thus critical field is expected to be larger and to increase with decreasing width. Results from NMR in QWs show that for widths of 30 nm and 25 nm QW, $B_c = 6.7$ T and 8.9 T respectively [Freytag *et al.*, 2001]. In our sample, a 20 nm QW, B_c is expected to be even larger. The trend is schematized in figure 5.8.

The estimate of Ref. [Mariani *et al.*, 2002] on δB in a homogeneous system gives a significantly narrower range than our observation. This suggests that the depolarized phase in our experiment consists of inhomogeneous mixture of polarized and unpolarized regions [Murthy, 2000].

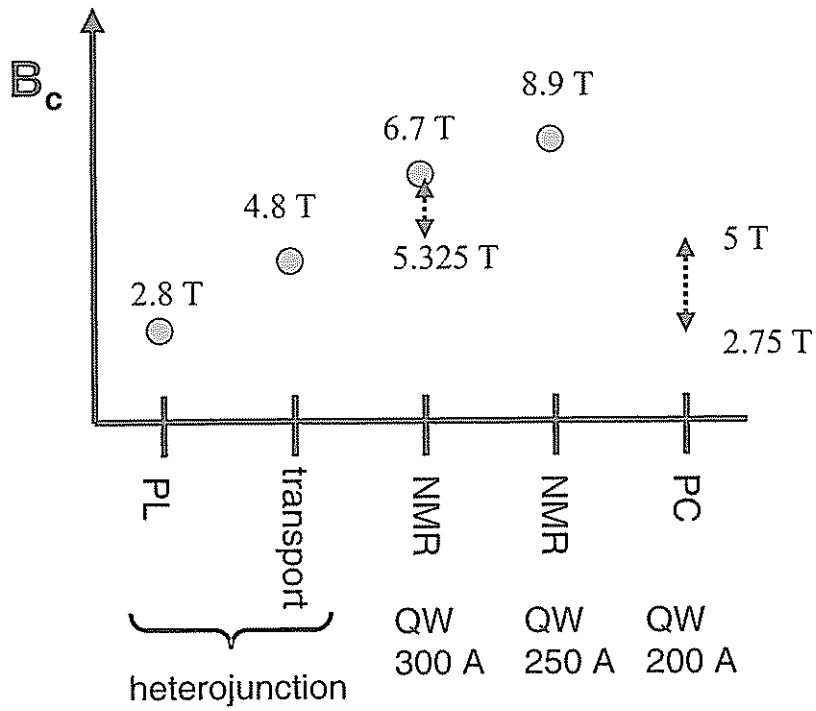

Figure 5.8: Results for the critical field B_c (circles) at which the 2DES becomes fully spin-polarized in PL measurements [Kukushkin *et al.*, 1999], transport [Smet *et al.*, 2001] and NMR [Freytag *et al.*, 2001]. The dashed arrow shows the range of fields over a partially polarized phase was found in NMR and this work (PC). In heterojunction, the 2DES effective width is usually larger than in QWs. As the width of the 2DES decreases, the Coulomb interaction is stronger and B_c is expected to increase. Our PC results indicate that the partially polarized phase extend over surprisingly low fields. According to the trend shown in the figure, it is expected that in the relatively thin QW of this work, there should be a transition at field higher than the range explored.

Appendix A

Samples structure

Several designs for the barrier layer and the back-gate were implemented. The designs of the barrier included simple barriers with constant Al content $x = 0.3$, and also superlattices and bilayer-type grading of the Al component. The back-gate consisted of a think layer of heavily doped Si-$Al_xGa_{1-x}As$ grown on top of the insulating GaAs substrate. The Al composition used included $x = 0$ to $x = 0.1$. The purpose of the Al in the barrier was to increase its band-gap. In this way, light at wavelengths near the onset of the absorption in the QW would not be absorbed in the gate. This, in turn, served two purposes: (a) when measuring the photoluminescence (PL) spectrum of the well, this avoids a superposition of PL coming from the gate; (b) when measuring photocurrent, to validate the assumption that the photocurrent signal comes from the absorption in the well only. Interestingly, even when using a GaAs back-gate, the background signal below the QW absorption edge was negligible, making this precaution not really necessary.

I include here the structure of some of the samples that were used in this research. All samples were grown on insulating GaAs substrate. Layers are given in order from the surface to substrate, and widths are in Angstroms.

Sample: **CBE1057**

Grower: Hadas Shtrikman

100	GaAs	(cap)
100	$Al_{0.33}Ga_{0.67}As$	
70	GaAs (Si:5e18 cm^{-3})	(doping sheet)
580	$Al_{0.33}Ga_{0.67}As$	(spacer)
200	GaAs	(QW)
5200	$Al_{0.33}Ga_{0.67}As$	(total barrier length = 5200 A)
9000	$Al_{0.10}Ga_{0.90}As$ (Si:5e18 cm^{-3})	(gate)
600	$Al_{0.10}Ga_{0.90}As$	
	25 $Al_{0.33}Ga_{0.67}As$ /	
	25 GaAs	x 20 superlattice (SL)
2000	GaAs	(buffer)

Sample: **MBE7130**

Grower: Vladimir Umansky

200	GaAs (Si: 3e18 cm^{-3})	(cap)
20	AlAs	(stop layer)
180	GaAs	
20	AlAs	(stop layer)
20	GaAs	
200	$Al_{0.32}Ga_{0.68}As$	
	Si	(delta doping sheet)
650	$Al_{0.32}Ga_{0.68}As$	(spacer)
200	GaAs	(QW)
11.2	GaAs	
200	$Al_{0.32}Ga_{0.68}As$	(total barrier length = 3900 A)
	50 GaAs /	
	60 $Al_{0.40}Ga_{0.60}As$ /	
	50 AlAs	x 30 SL
70	GaAs	
6000	GaAs (Si: 1.5e18 cm^{-3})	(gate)
500	GaAs	(buffer)

	Sample: **MBE7134**	
	Grower: Vladimir Umansky	
30	GaAs	(cap)
20	AlAs	(stop layer)
25	GaAs	
140	$Al_{0.33}Ga_{0.67}As$	
	Si	(delta doping sheet)
100	$Al_{0.33}Ga_{0.67}As$	
600	$Al_{0.33}Ga_{0.67}As$	(spacer)
200	GaAs	(QW)
11.2	GaAs	
200	$Al_{0.33}Ga_{0.67}As$	(total barrier length = 3900 A)
	50 GaAs /	
	60 $Al_{0.33}Ga_{0.67}As$	x 30 SL
400	$Al_{0.10}Ga_{0.90}As$	
	30 GaAs (Si: 1.8e18 cm^{-3}) /	
	400 $Al_{0.10}Ga_{0.90}As$ (Si: 1.6e18 cm^{-3})	x 30 SL (gate)
500	GaAs	(buffer)

Sample: **Bell1**

Grower: Loren Pfeiffer (May 21, 2004)

100	GaAs	(cap)
1000	$Al_{0.124}Ga_{0.876}As$	
	Si	(delta doping sheet)
500	$Al_{0.124}Ga_{0.876}As$	(spacer)
200	GaAs	(QW)
100	$Al_{0.124}Ga_{0.876}As$	(total barrier length = 16760 A)
30	GaAs	
200	$Al_{0.124}Ga_{0.876}As$	
2000	$Al_{0.124}Ga_{0.876}As \Rightarrow Al_{0.323}Ga_{0.677}As$	bilayer grading (50 x 40 A)
	30 GaAs /	
	200 $Al_{0.382}Ga_{0.618}As$	x 65 SL
	30 GaAs (Si) /	
	200 $Al_{0.382}Ga_{0.618}As$ (Si)	x 25 SL (gate)
2000	GaAs	(buffer)

Appendix B

Absorption in the Skyrmion regime

Here we present the details of the calculations involved in the model for absorption in the Skyrmion regime.

B.1 Skyrmion model

The wavefunctions of angular momentum m in the lowest Landau Level (LL) ($n = 0$) in the symmetric gauge are

$$\psi_m(z) = \frac{1}{\sqrt{2\pi l^2 2^m m!}} \left(\frac{z}{l}\right)^m e^{-\frac{|z|^2}{4l^2}} \qquad \text{where} \qquad z = x + iy. \tag{B.1}$$

where $m = 0, ..., N_\phi - 1$, and N_ϕ is the degeneracy of the LL.

The ground state at zero temperature of the two dimensional electron gas (2DEG) at $\nu = 1, 1^-, 1^+$, are a fully polarized state, a Skyrmion and and anti-Skyrmion respectively, and given by [Fertig *et al.*, 1997]:

$$
\begin{aligned}
|1\rangle &= \prod_{m=0}^{N_\phi-1} b_m^\dagger |0\rangle \\
|1^-\rangle &= \prod_{m=0}^{N_\phi-2} (u_m a_m^\dagger + v_m b_{m+1}^\dagger)|0\rangle \\
|1^+\rangle &= \prod_{m=-1}^{N_\phi-1} (-u_m a_{m+1}^\dagger + v_m b_m^\dagger)|0\rangle, \text{ with } \; v_{-1} = u_{N_\phi-1} = 0
\end{aligned}
\tag{B.2}
$$

where $b_m^\dagger$ and $a_m^\dagger$ are the creating operators of an electron in the state ψ_m in the lower $|\uparrow\rangle$ and upper $|\downarrow\rangle$ Zeeman level respectively, and $|u_m|^2 + |v_m|^2 = 1$.

We give below for each state $|\nu\rangle$ the expectancy values $\langle a_m^\dagger a_m\rangle$, $\langle b_m^\dagger b_m\rangle$. Details of the calculation are in section B.4. Note that the following identities hold for all the cases:

$$\langle a_m a_m^\dagger\rangle = 1 - \langle a_m^\dagger a_m\rangle \tag{B.3}$$

$$\langle b_m b_m^\dagger\rangle = 1 - \langle b_m^\dagger b_m\rangle \tag{B.4}$$

$$\langle a_m^\dagger b_m\rangle = \langle a_m b_m^\dagger\rangle = 0 \tag{B.5}$$

$$\langle a_m^\dagger a_m b_{m'}^\dagger b_{m'}\rangle = \langle a_m^\dagger a_m\rangle\langle b_{m'}^\dagger b_{m'}\rangle - |\langle a_m^\dagger b_{m'}\rangle|^2. \tag{B.6}$$

For the $|1\rangle$ state we have:

$$\langle b_m^\dagger b_m\rangle = 1 \tag{B.7}$$

$$\langle a_m^\dagger a_m\rangle = \langle a_m^\dagger b_{m'}\rangle = \langle a_m b_{m'}^\dagger\rangle = 0 \tag{B.8}$$

For the $|1^-\rangle$ state we have:

$$\langle b_m^\dagger b_m\rangle = |v_{m-1}|^2 = \frac{2m}{\lambda^2 + 2m} \tag{B.9}$$

$$\langle a_m^\dagger a_m \rangle = |u_m|^2 = \frac{\lambda^2}{\lambda^2 + 2(m+1)} \tag{B.10}$$

$$\langle a_m^\dagger b_{m'} \rangle = u_m^* v_m \delta_{m,m'-1}, \tag{B.11}$$

where the explicit expressions have been obtained taking the coefficients from the Hartree-Fock solution of the hard-core model [MacDonald *et al.*, 1996].

For the $|1^+\rangle$ state we have:

$$\langle b_m^\dagger b_m \rangle = |v_m|^2 = \frac{2(m+1)}{\lambda^2 + 2(m+1)} \tag{B.12}$$

$$\langle a_m^\dagger a_m \rangle = |u_{m-1}|^2 = \frac{\lambda^2}{\lambda^2 + 2m} \tag{B.13}$$

$$\langle a_m^\dagger b_{m'} \rangle = -u_{m-1}^* v_{m'} \delta_{m,m'+1} \tag{B.14}$$

It should be kept in mind that the hard-core model suffers from the unphysical property that the u_m coefficients decay very slowly with m, implying that skyrmion extends effectively over all the space. We modify thus the 2DEG wavefunctions from Eq. (B.2) by assuming there is a cutoff value m_c so that for all values of $m > m_c$, $|u_m| = 0$ and $|u_m| = 1$. We find m_c by assuming a cutoff ratio R_c as follows.

$$\left(\frac{R_c}{l}\right)^2 = \langle m_c | \left(\frac{r}{l}\right)^2 | m_c \rangle = 2m_c \tag{B.15}$$

For $R_c = 10\ l = 100\ nm$ we have $m_c = 50$.

B.2 Exciton wavefunction

For the case of an electron - hole pair, the eigenfunctions can be expressed in the center of mass (CM) coordinates as [Knox, 1963]

$$\psi(r_e, r_h) = \frac{1}{L} e^{i\chi} e^{iK_{CM}\cdot R} \psi_{rel}(r), \tag{B.16}$$

where

$$\begin{aligned}
r &= r_e - r_h = (x, y) \\
R &= \mu_e r_e + \mu_h r_h = (X, Y) \\
\mu_{e(h)} &\equiv m_{e(h)}/(m_e + m_h) \qquad \text{(B.17)} \\
\left|\frac{\partial(r, R)}{\partial(r_e, r_h)}\right| &= (\mu_e \mu_h)^2 \qquad \text{(B.18)} \\
\chi &= -(e/\hbar c) A(r) \cdot R = (yX - xY)/(2l^2) \\
&= [(y_e - y_h)(\mu_e x_e + \mu_h x_h) - (x_e - x_h)(\mu_e y_e + \mu_h y_h)]/(2l^2) \\
&= [y_e x_h - x_e y_h]/(2l^2) = \mathrm{Im}(z_e z_h^*)/(2l^2)
\end{aligned}$$

Here K_{CM} is the CM momentum. In order to have the wavefunction normalized, the CM is confined to a box of size $L^2 >> l^2$. We are interested in optically active excitons for which $K_{CM} = 0$, and in the zero relative angular momentum. In the approximation of infinite magnetic field, where we can neglect Landau Level mixing, we have

$$\psi(r_e, r_h) \approx \frac{g_0}{L} e^{i\chi} \psi_0(r) = \frac{g_0 l}{L} \sqrt{2\pi} \sum_m \psi_m(z_e) \psi_m(z_h)^*, \tag{B.19}$$

where the last equality was obtained using the following mathematical relations:

$$\begin{aligned}
|z_e - z_h|^2 &= |z_e|^2 + |z_h|^2 - z_h z_e^* - z_e z_h^* \\
&= |z_e|^2 + |z_h|^2 - 2\mathrm{Re}(z_e z_h^*) \qquad \text{(B.20)}
\end{aligned}$$

$$
\begin{aligned}
e^{iX}\psi_m(z_e - z_h) &= \frac{1}{\sqrt{2\pi l^2 2^m m!}}\left(\frac{z_e - z_h}{l}\right)^m e^{-\frac{|z_e-z_h|^2 - 2i\mathrm{Im}(z_e z_h^*)}{4l^2}} \\
&= \frac{1}{\sqrt{2\pi l^2 2^m m!}}\left(\frac{z_e - z_h}{l}\right)^m e^{-\frac{|z_e|^2+|z_h|^2-2z_e z_h^*}{4l^2}} \\
&= \frac{1}{\sqrt{2\pi l^2 2^m m!}}\left(\frac{z_e - z_h}{l}\right)^m e^{-\frac{|z_e|^2+|z_h|^2}{4l^2}} \sum_n \frac{1}{2^n n!}\left(\frac{z_e}{l}\right)^n \left(\frac{z_h^*}{l}\right)^n \\
&= \sqrt{\frac{2\pi l^2}{2^m m!}}\left(\frac{z_e - z_h}{l}\right)^m \sum_n \psi_n(z_e)\psi_n(z_h)^*, \qquad \text{(B.21)}
\end{aligned}
$$

where all ψ_m functions were defined in Eq. (B.1) .

We calculate g_0 from the normalization condition:

$$
\begin{aligned}
|g_0|^{-2} &= \frac{1}{L^2}\int |\psi_0(r_e - r_h)|^2 dx_e dy_e dx_h dy_h \qquad \text{(B.22)} \\
|g_0|^{-2} &= \frac{1}{(\mu_e\mu_h)^2 L^2}\int |\psi_0(r)|^2 dx dy \int dX dY \qquad \text{(B.23)} \\
|g_0|^{-2} &= \frac{1}{(\mu_e\mu_h)^2}. \qquad \text{(B.24)}
\end{aligned}
$$

For completeness, we would like to write now the wavefunction of an exciton in an empty well $|X_{vac}\rangle$ in second quantization. We define the operator $h_m^\dagger$ as the operator that creates a hole in the wavefunction $\psi_m^h(z_h)$ which is defined as

$$
\psi_m^h(z_h) \equiv \psi_m(z_h)^*. \qquad \text{(B.25)}
$$

Thus

$$
|X_{vac}\rangle = N_X \sum_m h_m^\dagger a_m^\dagger |0\rangle \quad \text{where} \quad N_X \equiv \frac{g_0 l}{L}\sqrt{2\pi} \qquad \text{(B.26)}
$$

Then the absorption/recombination operator $\Re$ is

$$\Re = \sum_{m,m'} \int \psi_m(z)\psi^h_{m'}(z)dz\ a_m h_{m'} + h.c. = \sum_{m'} a_{m'}h_{m'} + h^\dagger_{m'}a^\dagger_{m'} \tag{B.27}$$

To see that this operator is correct, we show that for any state $\phi(z_e, z_h)$ the matrix of absorption in the operator representation gives the same result as in the space representation, i.e.:

$$\begin{aligned}
\phi(z_e, z_h) &\equiv \sum_{m,m'} c_{m,m'}\psi^h_m(z_h)\psi_{m'}(z_e) && \text{(B.28)}\\
|\phi\rangle &= \sum_{m,m'} c_{m,m'}h^\dagger_m a^\dagger_{m'}|0\rangle && \text{(B.29)}\\
M_\phi &= \langle 0|\Re|\phi\rangle = \sum_{m,m',m''} c_{m',m''}\langle 0|a_m h_m h^\dagger_{m'}a^\dagger_{m''}|0\rangle = \sum_m c_{m,m}
\end{aligned}$$

Now we show that we obtain the same result by the following expression

$$M_\phi = \int \delta(z_e - z_h)\phi(z_e, z_h)dz_e dz_h = \sum_{m,m'} c_{m,m'} \int \psi^h_m(z_e)\psi_{m'}(z_e)dz_e = \sum_m c_{m,m}$$

B.3 Absorption

Upon absorption of an electron-hole pair, we postulate that two final states may arise, depending of the energy of the photon. The one with higher energy $|X\rangle$ is postulated to arise when the electron is created into an orbital ψ_m which has both spins states empty, and is analog to the neutral exciton. The lower energy one $|X_s\rangle$ is created while simultaneously binding an electron with opposite spin from some orbital and is analog to the singlet charged exciton. Thus the final state wavefunctions corresponding to each initial state $|\nu\rangle$ are given by (more details in section B.5) :

$$|X,\sigma^+\rangle = N_X \sum_m h_m^\dagger a_m^\dagger b_m b_m^\dagger \, |\nu\rangle \tag{B.30}$$

$$|X,\sigma^-\rangle = N_X \sum_m h_m^\dagger b_m^\dagger a_m a_m^\dagger \, |\nu\rangle \tag{B.31}$$

$$N_X^{-2} = \sum_m (1-\langle a_m^\dagger a_m\rangle)(1-\langle b_m^\dagger b_m\rangle) \tag{B.32}$$

$$|X_s,\sigma^+\rangle = N_{X_s,\sigma^+} \sum_m h_m^\dagger a_m^\dagger b_m^\dagger b_m \, |\nu\rangle \tag{B.33}$$

$$N_{X_s,\sigma^+}^{-2} = \sum_m (1-\langle a_m^\dagger a_m\rangle)\langle b_m^\dagger b_m\rangle \tag{B.34}$$

$$|X_s,\sigma^-\rangle = N_{X_s,\sigma^-} \sum_m h_m^\dagger b_m^\dagger a_m^\dagger a_m \, |\nu\rangle \tag{B.35}$$

$$N_{X_s,\sigma^-}^{-2} = \sum_m (1-\langle b_m^\dagger b_m\rangle)\langle a_m^\dagger a_m\rangle, \tag{B.36}$$

where $\sigma^\pm$ is the circular polarization of the light that created the state.

The corresponding absorption matrix elements are given by

$$M_{\sigma^+} = \langle i| \sum_{m'} a_{m'} h_{m'} |f\rangle \tag{B.37}$$

$$M_{X,\sigma^+} = N_X \sum_{m',m} \langle\nu| a_{m'} h_{m'} h_m^\dagger a_m^\dagger b_m b_m^\dagger \, |\nu\rangle \tag{B.38}$$

$$= N_X \sum_m \langle\nu| a_m a_m^\dagger b_m b_m^\dagger \, |\nu\rangle \tag{B.39}$$

$$|M_{X,\sigma^\pm}|^2 = \sum_m (1-\langle a_m^\dagger a_m\rangle)(1-\langle b_m^\dagger b_m\rangle) \tag{B.40}$$

The probability of absorption of X does not depend on the polarization. Similarly we get

$$|M_{X_s,\sigma^+}|^2 = \sum_m (1-\langle a_m^\dagger a_m\rangle)\langle b_m^\dagger b_m\rangle$$

$$|M_{X_s,\sigma^-}|^2 = \sum_m (1-\langle b_m^\dagger b_m\rangle)\langle a_m^\dagger a_m\rangle$$

Replacing nto these expressions the initial state as the skyrmion/antiskyrmion states, we

have for X:

$$\begin{aligned}
|M_{X,\sigma^{\pm}}(\nu=1)|^2 &= 0 \\
|M_{X,\sigma^{\pm}}(\nu=1^{-})|^2 &= |v_0|^2 + \sum_{m=1}^{N_\phi-1} |u_{m-1}|^2|v_m|^2 \approx 1 + |v_0|^2|u_1|^2 \\
|M_{X,\sigma^{\pm}}(\nu=1^{+})|^2 &= \sum_{m=1}^{N_\phi-1} |v_{m-1}|^2|u_m|^2 \approx |v_0|^2|u_1|^2,
\end{aligned}$$

where the approximates expressions are neglecting $|u_m|$ with higher indexes. For X_s we have:

$$\begin{aligned}
|M_{X_s,\sigma^{-}}(\nu=1)|^2 &= 0 \\
|M_{X_s,\sigma^{-}}(\nu=1^{\pm})|^2 &= |u_0|^2 + \sum_{m=1}^{N_\phi-1} |u_{m-1}|^2|u_m|^2 \approx |u_0|^2(1+|u_1|^2) \\
|M_{X_s,\sigma^{+}}(\nu=0)|^2 &= N_\phi \\
|M_{X_s,\sigma^{+}}(\nu=1^{\pm})|^2 &= \sum_{m=1}^{N_\phi-1} |v_{m-1}|^2|v_m|^2 \\
&= N_\phi - \left(1 + \sum_{m=1}^{N_\phi-1} |u_{m-1}|^2(1-|u_m|^2) + |u_m|^2\right) \\
&\approx N_\phi - \left(1 + |u_0|^2|v_1|^2 + |u_1|^2\right)
\end{aligned}$$

At the filling factors around $\nu = 1$, the density of skyrmions (antiskyrmions) will be very small, and we assume they are non-interacting. Then we can write:

$$\begin{aligned}
|M_{X,\sigma^{\pm}}|^2 &= N_\phi \left\{ n_a \left(|v_0|^2 + \sum_{m=1}^{N_\phi-1} |u_{m-1}|^2|v_m|^2 \right) + n_s \left(\sum_{m=1}^{N_\phi-1} |v_{m-1}|^2|u_m|^2 \right) \right\} \\
&\approx N_\phi \left\{ n_a \left(1 + |v_0|^2|u_1|^2\right) + n_s|v_0|^2|u_1|^2 \right\} \\
|M_{X_s,\sigma^{-}}(\nu)|^2 &= N_\phi(n_s+n_a) \left(|u_0|^2 + \sum_{m=1}^{N_\phi-1} |u_{m-1}|^2|u_m|^2 \right) \approx N_\phi(n_s+n_a)|u_0|^2
\end{aligned}$$

$$
\begin{aligned}
|M_{X_s,\sigma^+}(\nu)|^2 &= N_\phi - N_\phi(n_s+n_a)\left(1+\sum_{m=1}^{N_\phi-1}|u_{m-1}|^2(1-|u_m|^2)+|u_m|^2\right) \\
&\approx N_\phi\left\{1-(n_s+n_a)\left(1+|u_0|^2\right)\right\},
\end{aligned}
$$

where n_s and n_a are the occupation number of Skyrmions and anti-Skyrmions respectively (the total numbers of quasiparticles are given by multiplying by N_ϕ). They fulfil $n_s - n_a = \nu - 1$, and at zero temperature they also fulfil $n_s + n_a = |\nu - 1|$.

B.4 Expectation values

We calculate $\langle\nu|a_m^\dagger a_m b_{m'}^\dagger b_{m'}|\nu\rangle$. We define $f^\nu_{m_1,m_2}$ is as follows:

$$
f^{1^-}_{m_1,m_2} = \prod_{m=0,m\neq m_1,m\neq m_2}^{N_\phi-2}(u_m a_m^\dagger + v_m b_{m+1}^\dagger) \tag{B.41}
$$

$$
f^{1^+}_{m_1,m_2} = \prod_{m=-1,m\neq m_1,m\neq m_2}^{N_\phi-1}(-u_m a_{m+1}^\dagger + v_m b_m^\dagger) \tag{B.42}
$$

Note the following properties of f^ν_m

$$
\langle 0|{f^\nu_m}^\dagger f^\nu_{m'}|0\rangle = \delta_{m,m'} \tag{B.43}
$$

$$
|1^-\rangle = (-1)^m(u_m a_m^\dagger + v_m b_{m+1}^\dagger)f_m^{1^-}|0\rangle \tag{B.44}
$$

$$
|1^+\rangle = (-1)^{m+1}(-u_m a_{m+1}^\dagger + v_m b_m^\dagger)f_m^{1^+}|0\rangle \tag{B.45}
$$

For $|1^-\rangle$ we have :

$$
\begin{aligned}
a_m|1^-\rangle &= (-1)^m a_m(u_m a_m^\dagger + v_m b_{m+1}^\dagger)f_m^{1^-}|0\rangle = (-1)^m u_m f_m^{1^-}|0\rangle \\
b_m|1^-\rangle &= (-1)^m b_m(u_{m-1}a_{m-1}^\dagger + v_{m-1}b_m^\dagger)f_{m-1}^{1^-}|0\rangle = (-1)^m v_{m-1}f_{m-1}^{1^-}|0\rangle
\end{aligned}
$$

$$
\begin{aligned}
a_m^\dagger|1^-\rangle &= (-1)^m v_m a_m^\dagger b_{m+1}^\dagger f_m^{1^-}|0\rangle \\
b_m^\dagger|1^-\rangle &= (-1)^m u_{m-1} b_m^\dagger a_{m-1}^\dagger f_{m-1}^{1^-}|0\rangle
\end{aligned}
$$

$$
\begin{aligned}
\langle 1^-|a_m^\dagger a_m|1^-\rangle &= |u_m|^2\langle 0|f_m^{1^-\dagger} f_m^{1^-}|0\rangle = |u_m|^2 \\
\langle 1^-|b_m^\dagger b_m|1^-\rangle &= |v_{m-1}|^2\langle 0|f_{m-1}^{1^-\dagger} f_{m-1}^{1^-}|0\rangle = |v_{m-1}|^2 \\
\langle 1^-|a_m^\dagger b_{m'}|1^-\rangle &= (-1)^{m+m'-1} u_m^* v_m \langle 0|f_m^{1^-\dagger} f_{m'-1}^{1^-}|0\rangle = u_m^* v_m \delta_{m,m'-1} \\
\langle 1^-|a_m b_{m'}^\dagger|1^-\rangle &= (-1)^{m+m'-1} u_{m'-1} v_m^* \langle 0|f_m^{1^-\dagger} b_{m+1} a_m b_{m'}^\dagger a_{m'-1}^\dagger f_{m'-1}^{1^-}|0\rangle = -u_m v_m^* \delta_{m,m'-1}
\end{aligned}
$$

$$
\begin{aligned}
\langle 1^-|a_m^\dagger a_m b_{m'}^\dagger b_{m'}|1^-\rangle &= (-1)^{m+m'-1} v_{m'-1} u_m^* \langle 0|f_m^{1^-\dagger} a_m b_{m'}^\dagger f_{m'-1}^{1^-}|0\rangle \\
&= (-1)^{m+m'-1}(-1)^{m+m'} v_{m'-1} u_m^* (1-\delta_{m,m'-1}) \times \\
&\times \langle 0|f_{m,m'-1}^{1^-\dagger}(u_{m'-1}^* a_{m'-1} + v_{m'-1}^* b_{m'}) a_m b_{m'}^\dagger (u_m a_m^\dagger + v_m b_{m+1}^\dagger) f_{m,m'-1}^{1^-}|0\rangle \\
&= -|v_{m'-1}|^2 |u_m|^2 (1-\delta_{m,m'-1})\langle 0|f_{m,m'-1}^{1^-\dagger} b_{m'} a_m b_{m'}^\dagger a_m^\dagger f_{m,m'-1}^{1^-}|0\rangle \\
&= |v_{m'-1}|^2 |u_m|^2 (1-\delta_{m,m'-1})
\end{aligned}
$$

For $|1^+\rangle$ we have :

$$
\begin{aligned}
a_m|1^+\rangle &= (-1)^{m+1} a_m(-u_{m-1}a_m^\dagger + v_{m-1}b_{m-1}^\dagger) f_{m-1}^{1^+}|0\rangle = u_{m-1} f_{m-1}^{1^+}|0\rangle \\
b_m|1^+\rangle &= (-1)^{m+1} b_m(-u_m a_{m+1}^\dagger + v_m b_m^\dagger) f_m^{1^+}|0\rangle = -v_m f_m^{1^+}|0\rangle \\
a_m^\dagger|1^+\rangle &= (-1)^{m+1} v_{m-1} a_m^\dagger b_{m-1}^\dagger f_{m-1}^{1^+}|0\rangle \\
b_m^\dagger|1^+\rangle &= -(-1)^{m+1} u_m b_m^\dagger a_{m+1}^\dagger f_m^{1^+}|0\rangle
\end{aligned}
$$

$$
\langle 1^+|a_m^\dagger a_m|1^+\rangle = |u_{m-1}|^2\langle 0|f_{m-1}^{1^+\dagger} f_{m-1}^{1^+}|0\rangle = |u_{m-1}|^2
$$

$$\begin{aligned}
\langle 1^+|b_m^\dagger b_m|1^+\rangle &= |v_m|^2\langle 0|f_m^{1^+\dagger}f_m^{1^+}|0\rangle = |v_m|^2\\
\langle 1^+|a_m^\dagger b_{m'}|1^+\rangle &= -(-1)^{m+m'+1}u_{m-1}^* v_{m'}\langle 0|f_{m-1}^{1^+\dagger}f_{m'}^{1^+}|0\rangle = -u_{m-1}^* v_{m'}\delta_{m,m'+1}\\
\langle 1^+|a_m b_{m'}^\dagger|1^+\rangle &= -(-1)^{m+m'+1}u_{m'}v_{m-1}^*\langle 0|f_{m-1}^{1^+\dagger}b_{m-1}a_m b_{m'}^\dagger a_{m'+1}^\dagger f_{m'}^{1^+}|0\rangle = +u_{m'}v_{m-1}^*\delta_{m,m'+1}
\end{aligned}$$

$$\begin{aligned}
\langle 1^+|a_m^\dagger a_m b_{m'}^\dagger b_{m'}|1^+\rangle &= -(-1)^{m+m'+1}v_{m'}u_{m-1}^*\langle 0|f_{m-1}^{1^+\dagger}a_m b_{m'}^\dagger f_{m'}^{1^+}|0\rangle\\
&= -(-1)^{m+m'+1}(-1)^{m+m'}v_{m'}u_{m-1}^*(1-\delta_{m,m'+1})\times\\
\times\langle 0| &\quad f_{m-1,m'}^{1^+\dagger}(-u_{m'}^*a_{m'+1}+v_{m'}^*b_{m'})a_m b_{m'}^\dagger(-u_{m-1}a_m^\dagger+v_{m-1}b_{m-1}^\dagger)f_{m-1,m'}^{1^+}|0\rangle\\
&= -|v_{m'}|^2|u_{m-1}|^2(1-\delta_{m,m'+1})\langle 0|f_{m-1,m'}^{1^+\dagger}b_{m'}a_m b_{m'}^\dagger a_m^\dagger f_{m-1,m'}^{1^+}|0\rangle\\
&= |v_{m'}|^2|u_{m-1}|^2(1-\delta_{m,m'+1})
\end{aligned}$$

B.5 Normalization

We calculate the normalization constants N_X and $N_{X_s,\sigma^\pm}$.

$$\begin{aligned}
N_X^{-2} &= N_X^{-2}\sum_m\langle X,\sigma^+|X,\sigma^+\rangle\\
&= \sum_{m,m'}\langle\nu|b_{m'}b_{m'}^\dagger a_{m'}h_{m'}h_m^\dagger a_m^\dagger b_m b_m^\dagger|\nu\rangle\\
&= \sum_m(1-\langle a_m^\dagger a_m\rangle)(1-\langle b_m^\dagger b_m\rangle)
\end{aligned}\tag{B.46}$$

$$\begin{aligned}
N_{X_s,\sigma^+}^{-2} &= N_{X_s}^{-2}\sum_m\langle X_s,\sigma^+|X_s,\sigma^+\rangle\\
&= \sum_{m,m'}\langle\nu|b_{m'}^\dagger b_{m'}a_{m'}h_{m'}h_m^\dagger a_m^\dagger b_m^\dagger b_m|\nu\rangle\\
&= \sum_m(1-\langle a_m^\dagger a_m\rangle)\langle b_m^\dagger b_m\rangle
\end{aligned}\tag{B.47}$$

For the other polarization, simply exchange the a_m and b_m operators.

The electron density in a given state $|\nu\rangle$ is

$$\rho_e(r) = \sum_m |\psi_m(r)|^2 \langle a_m^\dagger a_m + b_m^\dagger b_m \rangle \tag{B.48}$$

The hole density in the state $|X, \sigma^+\rangle$ is

$$\begin{aligned} \rho_h(r) &= \sum_m |\psi_m^h(r)|^2 \langle X, \sigma^+ | h_m^\dagger h_m | X, \sigma^+ \rangle \\ &= N_X^2 \sum_{m,m',m''} |\psi_m^h(r)|^2 \langle \nu | b_{m'} b_{m'}^\dagger a_{m'} h_{m'} h_m^\dagger h_m h_{m''}^\dagger a_{m''}^\dagger b_{m''} b_{m''}^\dagger | \nu \rangle \\ &= \frac{\sum_m |\psi_m^h(r)|^2 (1 - \langle a_m^\dagger a_m \rangle)(1 - \langle b_m^\dagger b_m \rangle)}{\sum_m (1 - \langle a_m^\dagger a_m \rangle)(1 - \langle b_m^\dagger b_m \rangle)}. \end{aligned} \tag{B.49}$$

Bibliography

Aifer, E. H., B. B. Goldberg, and D. A. Broido, 1996, Physical Review Letters **76**, 680.

Ashcroft, N. W., and N. D. Mermin, 1976, *Solid state physics* (Thomson Learning, Inc., U.S.A.).

Astakhov, G. V., V. P. Kochereshko, D. R. Yakovlev, W. Ossau, J. Nurnberger, W. Faschinger, and G. Landwehr, 2000, Physical Review B **62**, 10345.

Barrett, S. E., G. Dabbagh, L. N. Pfeiffer, K. W. West, and Z. Tycko, 1995, Physical Review Letters **74**, 5112.

Brey, L., and C. Tejedor, 2002, Physical Review B **66**, R41308.

Brum, J., and P. Hawrylak, 1997, Comments Cond. Matt. Phys. **18**, 135.

Cooper, N. R., and D. Chklovskii, 1997, Physical Review B **55**, 2436.

Dethlefsen, A. F., E. Mariani, H. P. Tranitz, W. Wegscheider, and R. J. Haug, 2005, arXiv:cond-mat/0508393 URL `http://lanl.arxiv.org/abs/cond-mat/0508393`.

Duque, C. A., Z. Barticevic, M. PAcheco, and L. E. Oliveira, 2004, phys. stat. sol. (b) **241**, 2434.

Dzyubenko, A. B., and Y. E. Lozovik, 1991, Journal of Physics A **24**, 414.

Eisenstein, J. P., H. L. Stormer, L. Pfeiffer, and K. W. West, 1989, Physical Review Letters **62**, 1540.

Esser, A., 2001, Ph.D. thesis, der Humboldt-Universität zu Berlin.

Fertig, H. A., L. Brey, R. Cote, and A. H. MacDonald, 1994, Physical Review B **50**, 11018.

Fertig, H. A., L. Brey, R. Ct, A. H. MacDonald, A. Karlhede, and S. L. Sondhi, 1997, Physical Review B **55**, 10671.

Finkelstein, G., H. Shtrikman, and I. Bar-Joseph, 1995, Physical Review Letters **74**, 976.

Finkelstein, G., H. Shtrikman, and I. Bar-Joseph, 1996a, Physical Review B **53**, R1709.

Finkelstein, G., H. Shtrikman, and I. Bar-Joseph, 1996b, Physical Review B **53**, 12593.

Finkelstein, G., H. Shtrikman, and I. Bar-Joseph, 1997, Physical Review B **56**, 10326.

Freytag, N., 2001, Ph.D. thesis, Université Joseph Fourier, Grenoble 1.

Freytag, N., M. Horvatic, C. Berthier, M. Shayegan, and L. P. Lévy, 2002, Physical Review Letters **89**, 246804.

Freytag, N., Y. Tokunaga, M. Horvatic, C. Berthier, M. Shayegan, and L. P. Lévy, 2001, Physical Review Letters **87**, 136801.

Gakhtman, D., E. Cohen, A. Ron, and L. N. Pfeiffer, 1996, Physical Review B **54**, 10320.

H. Westfahl, J., A. O. Caldeira, D. Baeriswy, and E. Miranda, 1998, Physical Review Letters **80**, 2953.

Hawrylak, P., 1991, Physical Review B **44**, 3821.

Horvatic, M., and C. Berthier, 2002, International Journal of Modern Physics B **16**, 3265.

Huard, V., R. T. Cox, K. Saminadayar, A. Arnoult, and S. Tatarenko, 2000, Physical Review Letters **84**, 187.

Huard, V., S. Lovisa, R. T. Cox, K. Saminadayar, M. Potemski, A. Arnoult, J. Cibert, S. Tatarenko, and A. Wasiela, 1998, Physica B **256**, 136.

Jain, J. K., 1989, Physical Review Letters **63**, 199.

Jain, J. K., 1990, Physical Review B **41**, 7653.

Jain, J. K., 1994, Science **266**, 1199.

Kallin, C., and B. I. Halperin, 1984, Physical Review B **30**, 5655.

Kamilla, R. K., X. G. Wu, and J. K. Jain, 1996, Solid State Communications **99**, 289.

Kheng, K., R. T. Cox, Y. M. d'Aubigne, K. S. F. Bassani, and S. Tatarenko, 1993, Physical Review Letters **71**, 1752.

von Klitzing, K., 1980, Physical Review B **21**, 3349.

Knox, R. S., 1963, *Theory of Excitons* (Academic Press, New York and London).

Kukushkin, I., J. H. Smet, K. von Klitzing, and K. Eberl, 2000, Physical Review Letters **85**, 3688.

Kukushkin, I. V., K. v. Klitzing, and K. Eberl, 1997a, Physical Review B **55**, 10607.

Kukushkin, I. V., K. v. Klitzing, and K. Eberl, 1997b, Physical Review B **60**, 2554.

Kukushkin, I. V., K. v. Klitzing, and K. Eberl, 1999, Physical Review Letters **82**, 3665.

Kukushkin, I. V., J. H. Smet, K. von Klitzing, and W. Wegscheider, 2002, Nature **415**, 409.

Laughlin, R. B., 1983, Physical Review Letters **50**, 1395.

Leadley, D. R., R. J. Nicholas, D. K. M. , A. N. Utjuzh, J. C. Portal, J. J. Harris, , and C. T. Foxon, 1997, Physical Review Letters **79**, 4246.

Lematre, A., C. Testelin, T. Wojtowicz, and G. Karczewski, 2000, Physical Review B **62**, 5059.

Lopez, A., and E. Fradkin, 1991, Physical Review B **44**, 5246.

Lovisa, S., R. T. Cox, N. Magnea, and K.Saminadayar, 1997, Physical Review B **56**, R12787.

MacDonald, A. H., H. A. Fertig, and L. Brey, 1996, Physical Review Letters **76**, 2153.

Mahan, G. D., 1967, Physical Review **153**, 882.

Manfra, M. J., E. H. Aifer, B. B. Goldberg, D. A. Broido, L. Pfeiffer, and K. West, 1996, Physical Review B **54**, R17327.

Mariani, E., N. Magnoli, F. Napoli, M. Sassetti, and B. Kramer, 2002, Physical Review B **66**, 241303(R).

Murthy, G., 2000, Physical Review Letters **84**, 350.

Nozieres, P., and C. de Dominicis, 1969, Physical Review **178**, 1097.

Palacios, J. J., D. Yoshioka, and A. H. MacDonald, 1996, Physical Review B **54**, R2296.

Pinczuk, A., J. Shah, R. C. Miller, A. C. Gossard, and W. Wiegmann, 1984, Solid State Communications **50**, 735.

Plochocka, P., 2005, unpublished .

Plochocka, P., P. Kossacki, W. Maslana, J. Cibert, S. Tatarenko, C. Radzewicz, and J. A. Gaj, 2004, Physical Review Letters **92**, 177402.

Rapaport, R., R. Harel, E. Cohen, A. Ron, E. Linder, and L. N. Pfeiffer, 2000, Physical Review Letters **84**, 1607, ; R. Rappaport, PhD thesis, Technion, Haifa, Israel. F.X. Bronold, Physical Review B 61:12620 (2000).

Rashba, E. I., and M. D. Sturge, 2000, Physical Review B **63**, 045305.

Sanvitto, D., D.M.Whittaker, A. J. Shields, M. Simmons, D. A. Ritchie, and M. Pepper, 2002, Physical Review Letters **89**, 246805.

Sarma, S. D., and A. Pinczuk, 1997, *Perspectives in Quantum Hall Effects: Novel Quantum Liquids in Low-Dimensional Semiconductor Structures* (Wileys, New York).

Schmeller, A., J. P. Eisenstein, L. N. Pfeiffer, and K. W. West, 1995, Physical Review Letters **75**, 4290.

Schüller, C., K. B. Broocks, P. Schröter, C. Heyn, D. Heitmann, M. Bichler, W. Wegscheider, V. M. Apalkov, and T. Chakraborty, 2004a, Physica E **22**, 131.

Schüller, C., K. B. Broocks, P. Schröter, C. Heyn, D. Heitmann, M. Bichler, W. Wegscheider, V. M. Apalkov, and T. Chakraborty, 2004b, Proceedings of the International Workshop Optical Properties of 2D Systems", Warsaw 2004 **106**, 341.

Schüller, C., K. B. Broocks, P. Schröter, C. Heyn, D. Heitmann, M. Bichler, W. Wegscheider, T. Chakraborty, and V. M. Apalkov, 2003, Physical Review Letters **91**(11), 116403 (pages 4), URL `http://link.aps.org/abstract/PRL/v91/e116403`.

Schulze-Wischeler, F., F. Hohls, U. Zeitler, D. Reuter, A. D. Wieck, and R. J. Haug, 2004, Physical Review Letters **93**, 26801.

Shields, A. J., M. Pepper, M. Y. Simmons, and D. A. Ritchie, 1995, Physical Review B **52**, 7841.

Skolnick, M. S., J. M. Rorison, K. J. Nash, D. J. Mowbray, P. R. Tapster, S. J. Bass, and A. D. Pitt, 1987, Physical Review Letters **58**, 2130.

Smet, J. H., R. A. Deutschmann, W. Wegscheider, G. Abstreiter, and K. von Klitzing, 2001, Physical Review Letters **86**, 2412.

Sondhi, S. L., A. Karlhede, S. A. Kivelson, and E. H. Rezayi, 1993, Physical Review Letters **47**, 16419.

Stern, O., N. Freytag, A. Fay, W. Dietsche, J. H. Smet, K. von Klitzing, D. Schuh, and W. Wegscheider, 2004, Physical Review B **70**, 75318.

Stormer, H. L., D. C. Tsui, and A. C. Gossard, 1999, Rev. Mod. Phys. **71**, 298.

Tsui, D. C., H. L. Stormer, and A. C. Gossard, 1982, Physical Review Letters **48**, 1559.

Vyborny, K., and D. Pfannkuche, 2004, International Journal of Modern Physics B **18**, 3871.

Whittaker, D. M., and A. J. Shields, 1997, Physical Review B **56**, 15185.

Wojs, A., and P. Hawrylak, 1995, Physical Review B **51**, 10880.

Wojs, A., J. J. Quinn, and P. Hawrylak, 2000, Physical Review B **62**, 4630, ; Physica (Amsterdam) 8E, 254 (2000).

Yakovlev, D. R., V. P. Kochereshko, R. A. Suris, H. Schenk, W. Ossau, A. Waag, G. Landwehr, P. C. M. Christianen, and J. C. Maan, 1997, Physical Review Letters **79**, 3974.

Yayon, Y., 2003, Ph.D. thesis, Weizmann Instititue of Science, Rehovot, Israel.

Yoon, H. W., M. D. Sturge, and L. N. Pfeiffer, 1997, Solid State Communications **104**, 287.

Yusa, G., H. Shtrikman, and I. Bar-Joseph, 2000, Physical Review B **62**, 15390.

Yusa, G., H. Shtrikman, and I. Bar-Joseph, 2001, Physical Review Letters **87**, 216402.

Publications

[1] J.Groshaus, V. Umansky, H. Shtrikman, Y. Levinson, and I. Bar-Joseph, *Absorption Spectrum Around $\nu = 1$: Evidence for a Small-Size Skyrmion*, Physical Review Letters **93**, 96802 (2004).

[2] J.Groshaus, V. Umansky, H. Shtrikman, Y. Levinson, and I. Bar-Joseph, *The absorption spectrum around $\nu = 1$: evidence for a small-size skyrmion*, CP772, Physics of Semiconductors: 27th International Conference on the Physics of Semiconductors ICPS-27, Flagstaff, Arizona, edited by José Menéndez and Chris C. Van de Wall, AIP, Part A, page 501 (2005).

Declaration

The thesis summarizes my independent efforts.